



NTNU – Trondheim
Norwegian University of
Science and Technology

Splitting as a Load Releasing Mechanism for a Floater in Ice

Sverre Haug Lindseth

Civil and Environmental Engineering

Submission date: June 2013

Supervisor: Sveinung Løset, BAT

Co-supervisor: Raed Lubbad, BAT
Wenjun Lu, BAT

Norwegian University of Science and Technology
Department of Civil and Transport Engineering



Oppgavens tittel: Splitting as a load releasing mechanism for a floater in ice (Splitting som lastavløsningsmekanisme for en flytende konstruksjon i is)	Dato: 03.06.2012
	Antall sider (inkl. bilag): 125
	Masteroppgave <input checked="" type="checkbox"/> Prosjektoppgave <input type="checkbox"/>
Navn: Stud.techn. Sverre Haug Lindseth	
Faglærer/veileder: Professor Sveinung Løset, Førsteamanuensis Raed Lubbad, Stipendiat Wenjun Lu	
Eventuelle eksterne faglige kontakter/veiledere: Ingen	

<p>Ekstrakt: Denne masteroppgaven består primært av tre deler: 1) Litteraturstudie av materialegenskapene til is, bruddmekanikk generelt og splitting spesielt; 2) Utledning av et robust kriterium for bestemmelse av hvor vidt et gitt isflak kun vil oppleve stivlegemebevegelse (ubrekkelig) under påkjenningene av en is-struktur kollisjon; 3) Validering av eksisterende lineærelastiske bruddmekaniske teorier (LEFM) for splitting av isflak ved bruk av kohesive elementer (CEM) i det kommersielt tilgjengelige elementmetodeprogrammet <i>Abaqus</i>.</p> <p>Litteraturstudiet viste utilstrekkeligheten i teori og fullskala materialtester for bruddmekanisk oppførsel av is. Særlig gjelder dette bruddseigheten (K_{IC}) og bruddenergiens frigivelseshastighet (G_c), og hvordan disse blir påvirket av en meget omdiskutert "størrelseeffekt" for de mekaniske egenskapene til is. Først når disse temaene er avklart vil splitting som lastavløsningsmekanisme kunne brukes for å optimalisere isbryting rundt, og design av, flytende offshorekonstruksjoner.</p> <p>Kriteriet for ubrekkelige isflak ble utledet ved en kombinasjon av analytiske formler for antatt frikoblede bevegelsesmoder og eksplisitt kollisjonsanalyse i <i>Abaqus</i>. Kunnskapen fra denne analysen ga ubrekkelige isflak for lengde (L) og istykkelse (h_{ice}) som oppfyller følgende krav $L < \sqrt{(130h_{ice}-11)}$.</p> <p>Ikkelineær bruddmekanisk elementanalyse viste konvergens mellom metoder for lineær og ikkelineær bruddmekanikk relatert til splitting av isflak, dersom konsistente verdier for K_{IC} og G_c ble brukt. Dette funnet muliggjør bruk av tidligere utviklede formler for LEFM for beregning av enkle kollisjonslaster for splitting, og bruken av CEM for mer kompliserte beregninger. Videre ble bruken av CEM for utforskning av dynamisk sprekkvekst under momentan splitting illustrert. Resultatene og funnene fra denne masteroppgaven representerer dermed et steg på veien mot implementering av splitting som lastavløsningsmekanisme i simuleringer og dimensjonering av flytende konstruksjoner under påkjenning av islaster.</p>
--

Stikkord:

1. Ismekanikk
2. Ubrekkelige isflak
3. Bruddmekanikk
4. Ikkelineær analyse med elementoden

Sverre Haug Lindseth
(sign.)

Abstract

This master thesis divided into three parts: 1) A literature review on available literature concerning ice, fracture mechanics and theories for splitting of ice floes; 2) The development of a robust criterion for determination of whether an ice floe would be subject to only rigid body motions (unbreakable) during an ice-structure impact scenario; 3) Validation of existing linear elastic fracture mechanics approaches towards splitting, by means of the *Cohesive Element Method* (CEM) in Abaqus.

The literature review of material properties of ice and splitting-related fracture mechanics highlighted the lack of theory, the insufficient amount of material tests and the general uncertainties related to fracture of ice. The most critical finding is the lack of full-scale tests of fracture toughness (K_{IC}) and fracture energy release rate (G_c). Ongoing disputes regarding the *size effect* in ice needs to be addressed in order to make trustworthy simulations of splitting. Only then can splitting as a load releasing mechanism be used for improving design of ice management and geometric relationships for a floater in ice.

Knowledge on which floes to treat as unbreakable is of great importance for the development of real-time numerical simulators for ship-ice interactions. A robust criterion for this purpose has been developed. The derivation of the criterion was the result of three different numerical simulations. Firstly, a framework based on analytical expressions for decoupling of the modes of motion for an ice floe was developed. Secondly, verification of the assumptions made in the decoupled model was performed by means of the commercial finite element software *Abaqus*. Lastly, an explicit ship-ice impact analysis proved inconsistency in the assumption of decoupled modes, whereafter conclusions were made that a floe with representative length and thickness (h_{ice}) of $L < \sqrt{(130h_{ice}-11)}$ safely could be treated as unbreakable.

Disregarding the uncertainties related to the material fracture parameters for ice, convergence between linear and nonlinear theory was found through consistent choice of K_{IC} and G_c . Proving convergence of linear and nonlinear theory by CEM, provides both the possibility to use LEFM as an upper bound for simple calculations of splitting load, and the comfort for using CEM to model more complex cases including crack initiation. Furthermore, the possibility of obtaining reasonable results for examination of the crack growth velocity during rapid propagation was illustrated. The results obtained in this thesis thereby represent progression towards implementation of splitting for simulation and design procedures. Further research on this topic is needed in order to facilitate the development of the enabling technology required for arctic offshore developments.

Keywords

Mechanics of ice, Unbreakable ice floes, Decoupled modes of response, Finite Element Method, Abaqus, Nonlinear elastic fracture mechanics, Cohesive Element Method

Preface

This thesis is the product of the master thesis course TKT4915 for MSc Computational Mechanics students at Department of Structural Engineering, the Norwegian University of Science and Technology (NTNU), spring 2013. The thesis was written in affiliation with the Sustainable Arctic Marine and Coastal Technology (SAMCoT) research group, one of the *Centres for Research-based Innovation (SFI)* appointed by the Research Council of Norway for the period of 2011-2019.

Writing the MSc thesis under the supervision of SAMCoT has been an enriching endeavour. All involved parts deserve honour for the professional, yet friendly, way I've been accommodated throughout the last year. Special thanks goes to my supervisors, Prof. Sveinung Løset, Assoc. Prof. Raed Lubbad and PhD cand. Wenjun Lu. Much of the foundation for the work performed in this thesis rests on the academic work of these outstanding individuals, and their research group as a whole, has produced. Their kind guidance has been of great importance to the final work of my master degree, as well as on the personal level.

Professor Sveinung Løset introduced me to the field of Arctic technology through his UNIS-course in Arctic Offshore Engineering, and I wouldn't have been writing this thesis if it hadn't been for his inspiring lectures. Further, the motivational factor provided by including me in his group of pioneering scientists within the field of Arctic technology is indisputable.

The effort Associate Professor Raed Lubbad put in providing me the confidence needed to take on the challenge of improving the criterion of unbreakable ice floes made a huge difference to my work. The discussions we had were always inspiring and gave me direction whenever I felt lost.

PhD candidate Wenjun Lu has been a true source of motivation and inspiration to me throughout my work. His expertise in finite element modelling, and his innovative way of rethinking the mechanics of ice, has provided high quality discussions that have been of substantial importance to the completion of this master thesis.

Although not part of the team of supervisors, acknowledgement also goes to Prof. Bjørn Skallerud for valuable discussions on fracture mechanics in general.

The “Masterkontrakt”, signed by both the student and the supervisor January 14. 2013, defined the scope of the thesis as follows:

“For marine operations in arctic waters, ice actions are of high importance in for the design criteria. The mode of failure of the ice decides to a large extent the imposed loads on a structure. Splitting is a failure mechanism that still is not well understood, but that could prove to be of importance to design of offshore structures accompanied by ice management. To examine the phenomenon of splitting as a load releasing mechanism the student shall:

- 1) Present an overview of relevant literature, including splitting in other materials than ice.*
- 2) Examine the influence the geometry of an ice floe has on the splitting phenomenon when interacting with a floating structure by means of the cohesive element method in Abaqus*
- 3) Examine the competing phenomenon between splitting and other failure mechanisms of ice for various ice floe geometries*
- 4) If time permits, the developed theory and software will be applied in a couple of case studies*

The work scope may prove to be larger than initially anticipated. Subject to approval from the supervisor, topics may be deleted from the list above or reduced in extent.”

Throughout the work, several meetings was held with the supervisors, and late February, there was a common agreement of making a side path, to devote considerable focus towards the development of a criterion for whether an ice floe should be considered breakable or unbreakable. Although not directly related to splitting, the main motivation for choosing the topic of this thesis was to contribute to the development of the numerical model for real-time simulation of ship-ice interaction described by Lubbad and Løset (2011). In order to properly implement splitting and other modes of failure in this model, a better criterion for identifying unbreakable ice floes would be a prerequisite. Consequently, less time was available for the cohesive element analyses of the phenomenon of splitting itself. Still, the obtained knowledge serves as a foundation for further studies that would enable splitting to be implemented in the real-time simulator or for other purposes.



Sverre Haug Lindseth
Trondheim, June 3. 2013

Table of contents

Abstract.....	iii
Preface.....	iv
Table of contents.....	vi
Table of figures.....	viii
Symbols.....	xii
1 Introduction.....	1
2 Ice – a diverse material.....	5
2.1 Definition.....	5
2.2 Formation and brine.....	5
2.3 Secondary ice.....	7
2.4 Constitutive relation.....	9
2.4.1 Young’s modulus.....	10
2.4.2 Poisson’s ratio.....	11
2.5 Density.....	11
2.6 Friction coefficients for ice.....	11
2.7 Indentation rate.....	12
2.8 Brittle versus ductile behaviour.....	13
2.9 Compressive, tensile and flexural strength.....	14
2.10 Chosen ice parameters.....	16
3 Ship-ice interaction process.....	17
3.1 Floaters in ice.....	17
3.1.1 Shape of hull.....	18
3.1.2 Velocity of impact.....	18
3.1.3 Icebreaking capabilities.....	19
3.2 Failure modes of ice.....	19
3.2.1 Crushing.....	19
3.2.2 Bending.....	20
3.2.3 Splitting.....	21
3.3 Simplification of interaction.....	21
4 Splitting as a load releasing mechanism – a literature review.....	23
4.1 Fracture mechanics as the basis for determination of splitting.....	23
4.1.1 Splitting in fracture mechanics.....	23
4.1.2 Principle of Linear Elastic Fracture Mechanics (LEFM).....	24
4.1.3 Fracture toughness.....	24
4.1.4 Nucleation and propagation.....	25
4.2 Upper bound theorem for plastic limit analysis of splitting.....	25
4.3 Cohesive method for splitting purposes.....	26
4.4 Splitting as a load releasing mechanism for ice.....	28
4.4.1 Nucleation and propagation of cracks in ice.....	29
4.4.2 Fracture toughness of ice.....	30
4.4.3 Compressive splitting of ice.....	32
4.4.4 Tensile splitting of rectangular ice floes.....	33
4.4.5 Tensile splitting of circular ice floes.....	36
4.4.6 Indentation speed dependence for splitting of ice.....	38
4.4.7 Cohesive zone method for splitting of ice floes.....	40
5 Breakdown structure for problem approach.....	43
6 A criterion to determine if an ice floe is breakable or unbreakable.....	45

6.1	Previous approaches.....	45
6.2	Decoupled approach by analytical expressions	46
6.2.1	Displacement by surge.....	49
6.2.2	Displacement by bending	51
6.2.3	Displacement by rotation	54
6.2.4	Comparison of results from the decoupled approach.....	60
6.2.5	Criterion based on decoupled events.....	63
6.3	Coupled approach in Abaqus.....	64
6.3.1	Semi-coupled approach through multiple loads	64
6.3.2	Coupled approach through ice-structure impact simulation.....	68
6.3.3	Comparison with theoretical 2D ice rotation module.....	70
6.4	Discussion and comparison of decoupled and coupled approach	72
6.5	Summary and proposed criterion	75
7	Splitting as a load releasing mechanism in ice	77
7.1	Model setup.....	77
7.2	Results and discussion	80
7.2.1	Geometric influence on the ice floe resistance towards splitting	80
7.2.2	Crack propagation and velocity	83
7.2.3	Suggested areas of improvements for the cohesive finite element model....	84
7.3	Conclusions	85
8	Summary, conclusions and recommendations for further work	87
8.1	Breakable or unbreakable ice floes.....	87
8.2	Splitting as a load releasing mechanism.....	87
9	References.....	89
9.1	Research papers and books.....	89
9.2	Pictures from other sources.....	94

Table of figures

Figure 1-1 Probability (%) for the presence of at least one undiscovered oil/gas field with recoverable resources greater than 50 MMBOE (Bird et al. 2008,USGS)	1
Figure 1-2 Decisive properties for calculation of ice actions (Løset, 2012c)	1
Figure 1-3 Ice breaker assisted tanker on dynamic positioning (Metrikin et al., 2012b/www.smsc.no)	2
Figure 2-1 Basal plane and c-axis orientation in ice Ih (Gillet-Chaulet et al. 2006)	5
Figure 2-2 Phase relation of sea ice, $S=34.3$ ppt (Assur, 1958)	6
Figure 2-3 Volumetric size and relations of ice Ih and NaCl crystallographic structure (Løset, 2012a).....	6
Figure 2-4 Microstructure in ice (Kovacs, 1997)	7
Figure 2-5 Schematic structure of first year ice (Schwarz and Weeks, 1977)	8
Figure 2-6 Fabric diagram for S1, S2 and S3 ice accordingly, showing C-axis orientation on half sphere	8
Figure 2-7 Strain versus time for pure ice when constant stress is applied. (Løset et al. 1998)	9
Figure 2-8 Elastic, delayed elastic, viscous (plastic) and fracture type grain deformation in polycrystalline ice (Sanderson 1988, 76).....	10
Figure 2-9 Plot of the density versus temperature for four different salinities for gas-free sea ice.....	11
Figure 2-10 The kinetic friction coefficient of fresh-water granular ice sliding across itself across a smooth interface (Kennedy et al., 2000)	12
Figure 2-11 Transition from ductile to brittle behaviour for ice under compression (Schulson, 1990).....	14
Figure 2-12 Grain size vs. strain rate for propagation (P) and nucleation (N) (Schulson and Duval 2009, p.223)	14
Figure 2-13 Tensile strength of sea ice by temperature (Schulson and Duval 2009, p.216)	15
Figure 2-14 Flexural strength of sea ice by brine volume (Schulson and Duval 2009, p.224)	15
Figure 3-1 Arctic floating structures	17
Figure 3-2 Oden Icebreaker seen from above (Prof. Martin Jakobsson, http://people.su.se/~mjako/).....	18
Figure 3-3 Dual Direction Icebreaking Shuttle Tanker Mikhail Ulnyanov (Aker Arctic) .	19
Figure 3-4 Failure modes for ice, after Sanderson (1988).....	19
Figure 3-5 Forces acting on ice sheet and development of the crushing height (v_h) and length (v_c)	19
Figure 3-6 Level-ice interaction with a sloping surface (Lubbad, 2011 (after Kotras et al. 1983))	20
Figure 3-7 The replacement of the semi-infinite plate model with the model of adjacent wedge-shaped beams resting on an elastic foundation (Lubbad and Løset, 2011)..	20
Figure 3-8 Simplification and measurement of ice floes	21
Figure 4-1 Crack propagation modes: Tensile, Sliding and Tearing mode (Schulson and Duval 2009, p.193)	23
Figure 4-2 The three phases of a cohesive crack (Barenblatt, 1959)	26
Figure 4-3 Crack tip models of Griffith, Dugdale and Barenblatt, after Geißler and Kaliske (2010)	26

Figure 4-4 Assumptions and notations of the cohesive zone model (Geißler and Kaliske, 2010)	27
Figure 4-5 Coexisting descriptions of a damage model-cohesive zone crack (Cuvilliez et al., 2012)).....	28
Figure 4-6 Tensile and compressive stress fields for radial crack analysis (Sanderson 1988, p.168)	28
Figure 4-7 Fracture toughness of ice as function of temperature (Schulson and Duval 2009, p.199)	30
Figure 4-8 Apparent fracture toughness as function of specimen size (Schulson 2012, results of Dempsey)	31
Figure 4-9 Variation of toughness with loading rate for columnar freshwater ice (Nixon and Weber, 1993)	31
Figure 4-10 Plain strain fracture toughness as function of porosity (Schulson and Duval 2009, p.202)	31
Figure 4-11 Brazilian test failure geometry and velocity fields, for circular and quadratic floes (Ralston, 1981).....	32
Figure 4-12 Radial cracks propagation model as described by Bhat (1988)	34
Figure 4-13 Results from Finite Element Analysis for crack tip stress intensity factors. Solid squares are based on tensile loading (F) only. Open squares also include the body force of Figure 4-12 b) (Bhat, 1988)	34
Figure 4-14 Finite element analysis mesh, load and boundary conditions used by Sodhi and Chin (1995)	35
Figure 4-15 Expected changes in failure modes as a function of aspect ratio changes (Bhat, 1988).....	36
Figure 4-16 Stress intensity factors for an edge crack in a circular floe (Bhat et al. 1991)	36
Figure 4-17 Tensile strength of freshwater granular ice at strain rate and (Schulson and Duval 2009, p.220)	39
Figure 4-18 Deducted stress-separation curve (Mulmule and Dempsey, 1998).....	40
Figure 4-19 Constructed stress-separation curves for various specimen sizes (Mulmule and Dempsey, 1999).....	40
Figure 4-20 Illustration of cohesive element results for infinite (left frames) and finite (right frames) ice floe simulations at the same instance of simulation time (Konuk et al., 2009a)	42
Figure 4-21 Cross triangle structured mesh pattern (Lu et al., 2012b).....	42
Figure 5-1 The processes that take place during the interaction between ship and ice. The major processes are modelled in the simulator. The minor processes are shown in grey colour. (Lubbad and Løset, 2011)	43
Figure 5-2 Breakdown structure for ice-structure interaction that show how splitting may be determined	44
Figure 6-1 Challenges considering development of a criterion for unbreakable floes	45
Figure 6-2 Solutions for when a floe, of $h_{ice}=1\text{m}$, can be considered unbreakable (after Hovland, 2012).....	46
Figure 6-3 Decoupled motions of movement for an ice floe interacting with a floating structure.....	46
Figure 6-4 Description of different modes of loading.....	47
Figure 6-5 Geometric relationship for conical loading.....	48
Figure 6-6 Forces acting on ice sheet and development of the crushing height (v_h) and length (v_c)	48

Figure 6-7 Negligible importance of drag and skin friction forces for development of floe velocity	50
Figure 6-8 Development of surge reactions of ice floe during ship-ice interaction for $h_{ice}=1\text{m}$	51
Figure 6-9 Simplified model of the ice floe bending process.....	52
Figure 6-10 Maximum stress for different floe sizes limited by end b of the floe lifting out of the water.....	54
Figure 6-11 Sketch of the turning floe in the normal section of the ship during the main phase of rotation. Length of floe (L) and ventilated length of floe (L_1) is shown (after Valanto, 2001)	55
Figure 6-12 Flowchart for calculation of the ship-ice contact force according to Eq 6-20 to Eq 6-26	58
Figure 6-13 Development of ship-ice contact force during rotation of an ice floe with Valanto's (2001) method. Force given per meter of floe width for a floe of $L=W=15\text{m}$, $h_{ice}=1\text{m}$, $\psi=45^\circ$	59
Figure 6-14 Limit case where equivalent maximum horizontal force for rotation equals that of bending	61
Figure 6-15 Abaqus verification stress plot for case limited by $y_{b,lim}=0.897\text{m}$, $F_v=45.85\text{kN/m}$. $L=10\text{m}$, $W=h_{ice}=1\text{m}$	62
Figure 6-16 Loading conditions for floe with semi-coupled loading in Abaqus	64
Figure 6-17 Flexural stresses for $L=W=6\text{m}$, $h_{ice}=1\text{m}$, at $y_b=y_{b,lim}$. Point of $\sigma_{f,max}$ indicated. Deflections are exaggerated.	65
Figure 6-18 Theoretical stresses in floe, for $h_{ice}=1\text{m}$. Point where the far end is lifted out of the water is indicated.....	65
Figure 6-19 Limited value of decoupled solutions in time domain	66
Figure 6-20 Time domain plots extracted from Abaqus model showing competition between modes of motion.....	67
Figure 6-21 Coupled ship-ice interaction model. The ship is modelled as a single degree of freedom instance with constant velocity (v_s) in surge (x -direction), while the floe is initially at rest.	68
Figure 6-22 Flexural stresses plotted for interaction scenario with $v_s=1.5\text{m/s}$, $L=W=10\text{m}$, $h_{ice}=1\text{m}$	69
Figure 6-23 Maximum deflection of ice floe during 3D model interaction scenario for $L=W=10\text{m}$, $h_{ice}=1\text{m}$	69
Figure 6-24 Competition between rotation and bending for ship-ice interaction in 3D model with $v_s=1.5\text{m/s}$	70
Figure 6-25 Maximum stress at the moment the far end of the floe lifts out of the water for $v_s=1.5\text{m/s}$	70
Figure 6-26 Moment distribution during the ice beam rotation process (Lu et al, 2013)	71
Figure 6-27 Load on cantilever part of floe lifted above the waterline (after Lu et al. (2013))	72
Figure 6-28 Limit stadium for secondary breaking of rotating floe of $L=W=7.3\text{m}$, $h_{ice}=0.5\text{m}$	73
Figure 6-29 Limit for unbreakable ice floes. All floes below the blue line could be considered unbreakable.....	73
Figure 6-30 Comparison of developed criterion with the other approaches present in the literature	74
Figure 6-31 Criterion for determination of unbreakable ice floes.....	75

Figure 7-1 Pressure loading on pre-cut crack surface.....	77
Figure 7-2 Hinges at far end of floe, $U_1=U_2=U_3=0$	77
Figure 7-3 Mesh for examination of splitting	77
Figure 7-4 Illustration of the cohesive traction-separation relationship for $G_c=15\text{J/m}^2$, $\sigma_t=300\text{ kPa}$ (δ -axis not in scale)	78
Figure 7-5 Relationship between the analysis applied force and corresponding Bhat (1988) impact force	78
Figure 7-6 Mesh dependency for the cohesive zone. Forces measured at nodes in the centre of the pre-cut crack. Performed with displacement controlled deformation with constant crack mouth opening velocity of 0.01 m/s on a floe of $L=W=10\text{ m}$, $h_{ice}=1\text{ m}$. Elements per meter given for both directions in the cohesive plane (square elements).....	79
Figure 7-7 Force evolution for displacement controlled deformation with crack mouth opening of 0.01 m/s. For $G_c=15\text{ J/m}$, $\sigma_t=300\text{ kPa}$	80
Figure 7-8 Varying mesh density for larger floes	81
Figure 7-9 Comparison between Bhat (1988) and the Cohesive Element Approach for compatible parameters	81
Figure 7-10 Comparison between the reported length-to-width ratio of Bhat (1988) and observations with CZM.....	82
Figure 7-11 Crack propagation illustrated by element degradation plot, for $P_{sc}=220\text{ kN}$, $L=W=10\text{m}$, $h_{ice}=1\text{m}$	83

Symbols

The following list states the unit and description of the symbols used in this thesis

Symbol	Unit	Description
a	m	Crack length (Figures from Bhat 1988, Bhat et al. 1991)
a^*	m	Oxygen-oxygen distance in the basal plane of the ice crystal
c	m	Crack length
c_d	m/s	Dilatational speed of sound in ice
C_d		Drag coefficient
C_s		Skin friction coefficient
d	m	Contact width (Sodhi and Chin, 1995)
d	mm	Platelet spacing or grain size in sea ice microstructure
d	m	Length of elevated part of floe during main rotation phase
E	N/m ²	Young's modulus
F	N	Normal-to-impact direction impact force (splitting force)
F	N	Normal-to-hull ship-ice contact force
F_v	N	Vertical force component
F_h	N	Horizontal force component
g	m/s ²	Acceleration of gravity
G_c	J/m ²	Fracture energy release rate
h_{ice}	m	Representative thickness of ice floe
I	m ⁴	Second moment of area
J_1		First stress invariant of the deviatoric stress tensor
J_2		Second stress invariant of the deviatoric stress tensor
k		Constant for strain rate-indentation pressure relationship
k	N/m ²	Foundation modulus of Winkler foundation for 2D beam
K		Drucker-Prager yield limit
K_{Ic}	Nm ^{-3/2}	Fracture toughness of ice
K_I	Nm ^{-3/2}	Stress intensity factor for mode I fracture
L_b	m	Breaking length for semi-infinite ice floes
L_0	m	Length of ventilated part of floe during initial rotation phase
L_1	m	Length of ventilated part of floe during main rotation phase
L	m	Representative length of ice floe
m_{ice}	kg	Mass of ice floe
m_{ship}	kg	Mass of ship
m		Drucker-Prager material parameter
M	Nm	Moment
P	N	Impact force resistance towards splitting (floe inertia included)
P^*	N	Impact force resistance towards splitting (floe inertia excluded)
r_s	m	Radius of impacting structure (radius of ship bow)
S	ppt	Salinity of seawater
u	m	Movement of ship in surge direction
\dot{u}	m/s	Velocity of ship in surge direction
\ddot{u}	m/s ²	Acceleration of ship in surge direction

U	J	Internal energy
v	mm/h	Growth velocity of sea ice
v_c	m	Movement-direction component of the crushed part of the floe
v_h	m	Thickness-direction component of the crushed part of the floe
v_{sl}	m/s	Sliding velocity during friction test
W	m	Representative width of ice floe
W_L	m	Nominal ice-structure contact width
y	m	Vertical deflection of ice floe
α		Drucker-Prager material parameter
γ_s	J/m ²	Energy required to create new surface
δ	µm	Crack opening distance (COD)
ε		Strain of ice specimen
$\dot{\varepsilon}$		Strain rate of ice specimen
η		Porosity
θ		Angular rotation of an ice floe
λ	m ⁻¹	Inverse of characteristic length of beam (Hetenyi, 1946)
μ		Steel-ice friction coefficient
μ_0		Ice-ice friction coefficient
ν		Poisson's ratio
ρ_i	kg/m ³	Density of sea ice
ρ_w	kg/m ³	Density of seawater
σ	N/m ²	Normal stress
σ_c	N/m ²	Compressive strength
σ_f	N/m ²	Flexural strength
σ_t	N/m ²	Tensile strength
σ_{coh}	MPa	Cohesive stress
τ	N/m ²	Shear stress
ψ		Inclination of ship hull
C3D10M		10-node modified quadratic tetrahedron
COH3D8		8-node three-dimensional cohesive element
C3D8R		8-node brick element with reduced integration and hourglass control

1 Introduction

The Arctic region, previously defined as the area north of the Polar circle, has the later years commonly been defined as the areas with expected Arctic conditions (SNL, 2013). For offshore operations, presence of sea ice could therefore serve as a definition.

The world demand for energy, and especially hydrocarbons has continuously gained momentum during the last decades. Expected to contain more than a quarter of the world's undiscovered oil and gas resources (Regjeringen, 2011), the Arctic has therefore been subject to steadily increasing interest among the worlds energy producing companies. There are several engineering aspects related to Arctic offshore development that need to be encountered in order to pursue these resources. The hostile Arctic climate drives the development of enabling technologies.

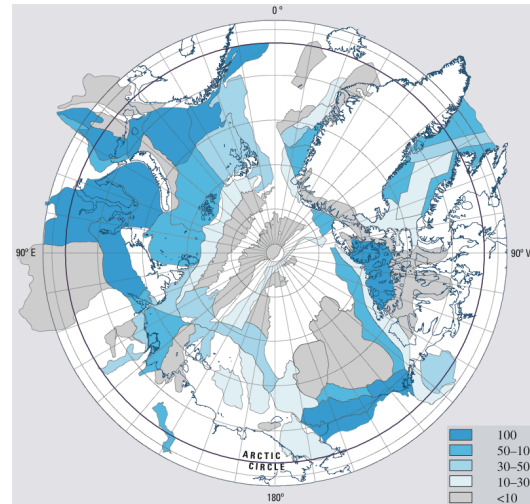


Figure 1-1 Probability (%) for the presence of at least one undiscovered oil/gas field with recoverable resources greater than 50 MMBOE (Bird et al. 2008,USGS)

Ice actions are among the most important aspects to consider when designing structures for operating in the Arctic regions. Figure 1-2 depicts an overview of the factors influencing the resulting actions ice could exert on a structure. Among the modes of failure that frequently are observed in nature, splitting is at present one of the least understood. Still, it's also expected to exert the lowest ice actions when all other parameters are equal (Løset et al. 2006, p.112). Improved understanding of this load releasing mechanism could therefore be of importance to further Arctic offshore development, especially when this knowledge is combined with both structural design and ice management.

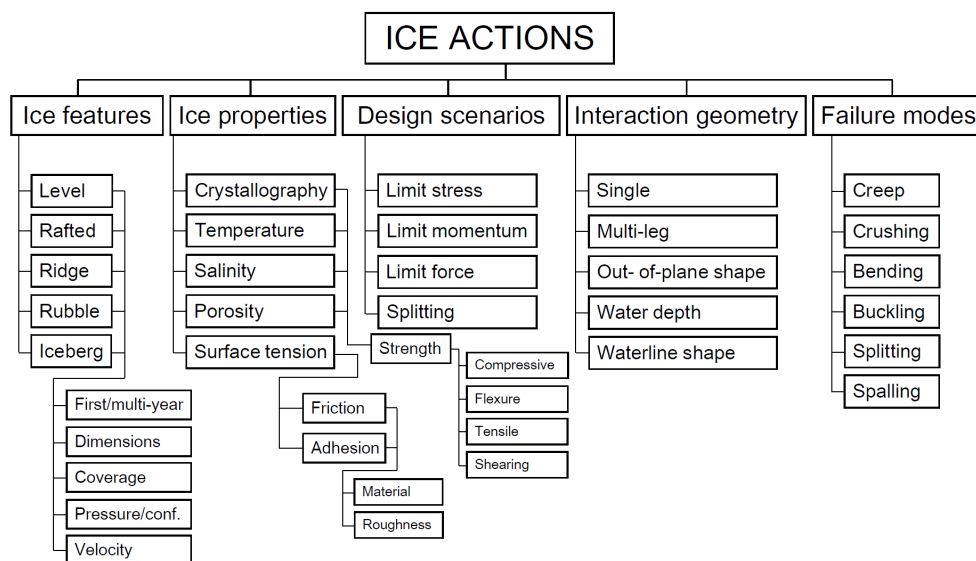


Figure 1-2 Decisive properties for calculation of ice actions (Løset, 2012c)

In order to facilitate Arctic offshore development, Lubbad and Løset (2011) developed a numerical model for real-time simulation of ship-ice interaction (Figure 1-3). This initial model, only encountered bending failure of the continuous ice cover and rigid body motion of the broken cusps and wedges (see Chapter 3). If developed to take account of the most important ice actions given in Figure 1-2, such model have its potential strengths in all following fields (Metrikin et al., 2012a):

- Quantifying risks of an offshore field operation
- Quantifying the effect of ice management for an Arctic offshore floater
- Support and decision making tool for on board operations
- Virtual training of personnel for Arctic offshore operations

The real-time simulator is divided in two sub-models: One large-scale model, treating hundreds or thousands of floes (all floes present) by means of rigid body motion; A small-scale model, treating the floes in the vicinity of the floater, which might need calculations of internal stresses in order to determine response of the floe. Research performed by Metrikin et al. (2012a) was done to identify what could be done to improve the simulator. For the second generation model they state that splitting is the mode in addition to bending that would be of interest to consider.



Figure 1-3 Ice breaker assisted tanker on dynamic positioning (Metrikin et al., 2012b/ www.smsc.no)

Disregarding the choice of obtaining intra-floe stresses, the computational expense calls for a robust criterion to determine whether a floe would only be subject to rigid body motion or if it would be subject to potential failure. Splitting, on the other hand, is one of the most intricate problems encountered when the goal is to determine actions from sea ice (Bhat, 1988). These two aspects will be treated in this master thesis in order to provide useful knowledge on splitting as a load releasing mechanism for a floater in ice. Due to the potential strengths of a fully developed numerical real-time simulator, all theory developed in this thesis have improvement of this model as its underlying goal.

Generally, the thesis is divided in two parts. The first chapters constitute a study of the relevant and available literature considering ice in general, ship-ice interactions, and splitting as a load releasing mechanism. In particular, Chapter 4 refers to task 1) in the predefined scope of the thesis. Chapter 2 and 3 are not directly linked to the scope but provide useful insight for the reader in order to build common understanding of floaters, ice and the terminology in general which is used in the other chapters. The latter Chapters 5, 6 and 7 provides the results, discussions and developed theory related to task 2) and 3) of the predefined scope. Due to the diversity of the topics treated in this thesis, there's not a separate chapter dedicated to discussion. Instead, the theory is discussed in their respective chapters.

Important to notice is that Chapters 2 and 4 to some extent are based on two individual project reports produced fall 2012 in the NTNU course TKT4511 (Lindseth, 2012a) and the UNIS course AT327 (Lindseth, 2012b). However, they are improved and completely reworked and to fit with the topic of this thesis. Several new aspects are also added.

The structure of the report is outlined below:

- Brief description of ice as a material, in order to support the following discussion
- Description of floaters in ice and ship-ice interaction scenarios
- Literature review of splitting as a load release mechanism, both in general and for ice in particular
- Breakdown structure for the distinct problem approach
- Development of a criterion for breakable and unbreakable ice floes
- Validation of previous linear approaches to splitting of level ice by means of nonlinear elastic fracture mechanics
- Conclusive remarks

2 Ice – a diverse material

Ice is a highly heterogenic material and its behaviour depends to a large extent on its structure and formation. In order to thoroughly understand and explain the physics of ice actions, proper understanding of what ice really is, is necessary. Extensive explanation of structure and formation of ice is out of the scope of this report, and only a brief introduction of the concepts most important for the discussion in the following chapters will be given. The literature, however, is rich of descriptions on the basics of ice. Reference is given to Sanderson (1988), Løset et al. (2006), Schulson and Duval (2009) and Timco and Weeks (2010) for more complete descriptions of ice.

2.1 Definition

Water in its solid state is usually referred to as ice. When transforming from liquid water to solid ice, the crystallographic structure may take different configurations due to the pressure and temperature conditions. Figure 2-1 shows the most common structure of ice present in nature – configuration Ih. This configuration has oxygen atoms forming parallel (basal) planes perpendicular to the hexagonal column structure. The axis perpendicular to the basal planes is often termed c-axis or optical axis, since this is the preferred direction for light to pass through the crystal.

By counting the number of hydrogen bonds that need to be broken in order to fracture the ice Ih-crystal, it's reasonable that fracture along a plane parallel to the basal plane would require less energy than for a plane normal to the basal plane. Hence, this nanostructure is the main source of anisotropy in ice. As will be shown, different orientation of crystals throughout the ice specimen will provide heterogeneous material properties on the micro scale.

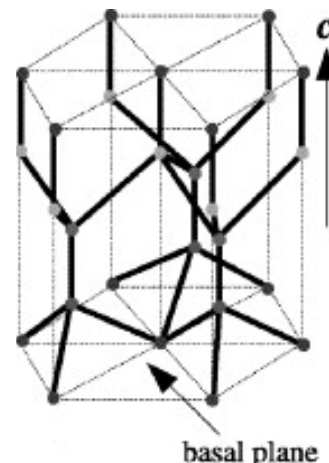


Figure 2-1 Basal plane and c-axis orientation in ice Ih
(Gillet-Chaulet et al. 2006)

2.2 Formation and brine

Ice present in the arctic oceans originates in essence either from seawater, precipitation or glaciers. The origin of the ice to a large extent decides its' mechanical properties. Glacier ice often is harder, more pure, and to a larger extent homogenous due to formation under high pressure over many years. Sea ice, on the other hand, is formed in a more complex way. Only sea ice will be treated in this thesis.

Arctic seawater, with a typical salinity of 35 ppt freezes at -1.9°C at atmospheric pressure (Figure 2-2). Hence, the ocean needs to both reach this temperature, and transport the necessary latent heat fusion, in order to accumulate sea ice. For calm seas, only the surface water needs to be super cooled in order to initiate growth of Ih ice crystals.

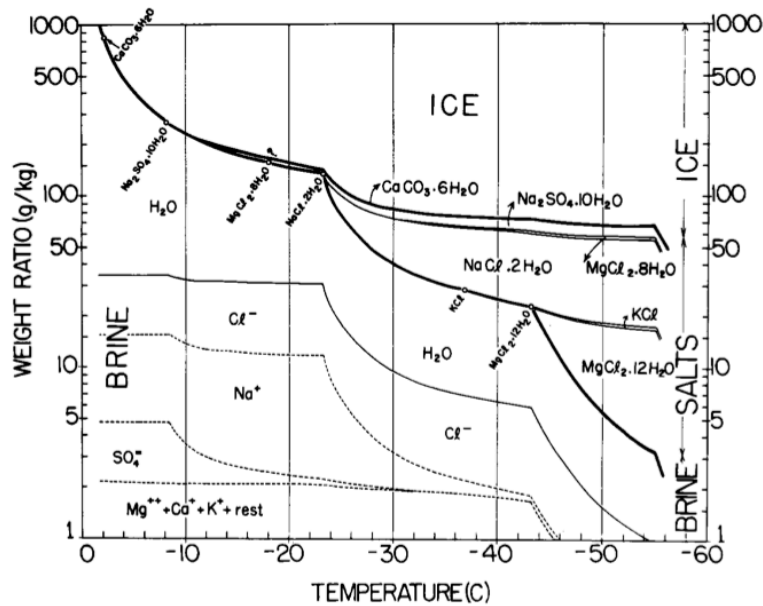


Figure 2-2 Phase relation of sea ice, S=34.3ppt (Assur, 1958)

The considerable amount of solute salt in seawater needs to be taken into account during the freezing process. Even though the crystallographic structure of ice Ih is less dense than that of liquid water, the same holds when NaCl transforms from solute ions to solid salt. The size difference therefore disqualifies any NaCl from being embedded within the ice crystals (Figure 2-3).

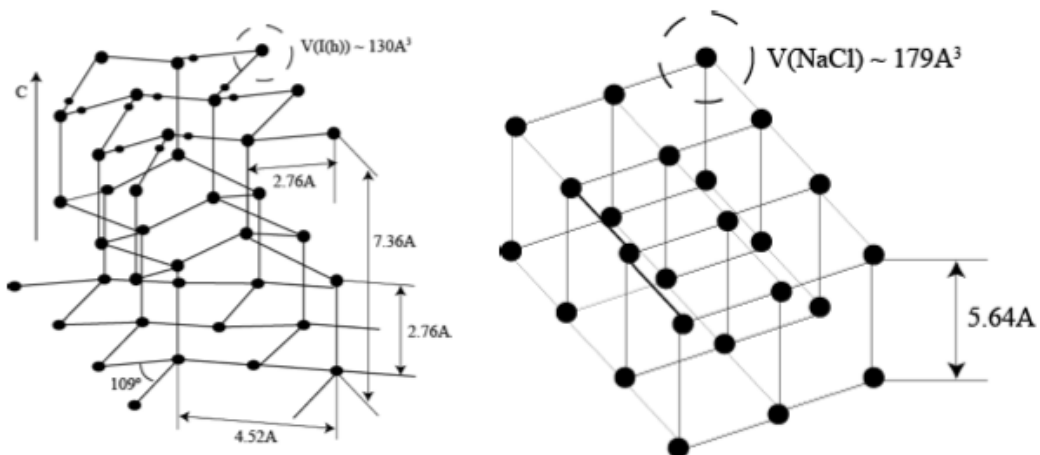
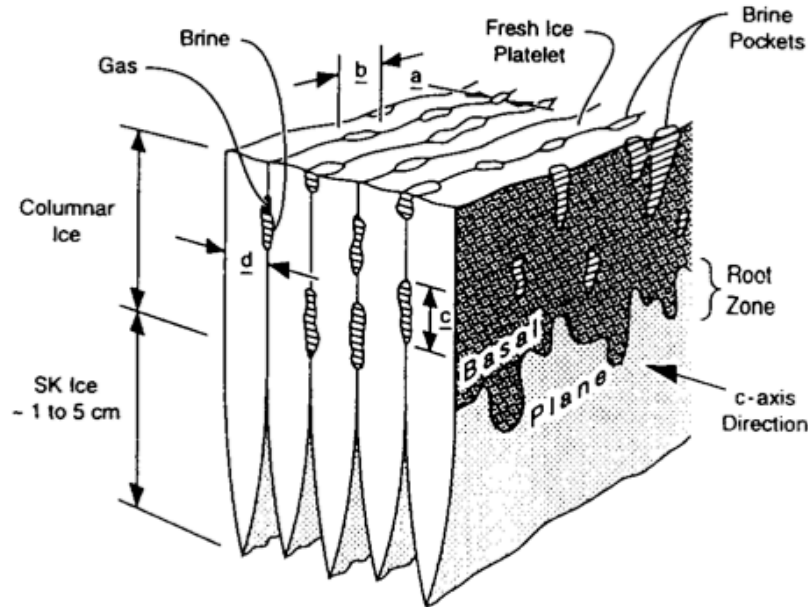


Figure 2-3 Volumetric size and relations of ice Ih and NaCl crystallographic structure (Løset, 2012a)

The salt in the seawater cannot be part of the ice Ih structure, and is therefore “squeezed” out of the crystals during formation of sea ice (Figure 2-4). This leads to the formation of small ice platelets, consisting of ice crystals with randomly orientated c-axis. As the amount of these platelets grow, they tend to bond together to form a highly saline slush called grease ice (Løset et al. 2006, p.53). Grease ice eventually forms a thin sheet of primary ice called *nilas*. Naturally, the orientation of the c-axis in this ice is randomly distributed.





- $a \leq b < c$
 a - 0.1 to 0.3 mm; b - 1 to $5 \times a$; $c > 5 \times a$
 d - 0.25 to 1.25 mm (avg 0.7)
-  Frozen Interface
 Seawater Interface

Figure 2-4 Microstructure in ice (Kovacs, 1997)

Collections of platelets constitute the grains in ice, independent of granular or columnar ice structure. The strength of these grains is dependent of the distance between the platelets (Løset lecture, 2012b). Difference in platelet distance is among the parameters that decide the grain size. Ice with smaller platelet distance has greater strength than the opposite. Hurdle (1986) showed that that the platelet spacing (d) is dependent on growth velocity (v), through the relationship shown in Eq 2-1. Hence, faster growing ice will be stronger than that of slower growth rate.

$$d_0 \sqrt{v} = \text{const} \quad \text{Eq 2-1}$$

Formation of the ice that constitutes the floes that interacts with floaters are of great importance to the load releasing mechanisms they exert. Brine channels and other flaws could create pathways for crack propagation or other features that increase the possibility of any of the other modes of failure as will be discussed in Chapter 3.

2.3 Secondary ice

If the temperature gradient allows, heat from the super cooled seawater just below the primary ice will be transported away. This is leading to further accumulation of ice (secondary ice), as the heat diffusion allows the water to turn to solid state. Since the ice crystals now form under the same sheet of ice, the tendency is that the c-axis of the secondary ice is more structured, as seen in Figure 2-5. In order to transfer as much latent fusion heat as possible from the cooled water, the bottom of the ice sheet is dendritically shaped (Schulson and Duval 2009, p.43).

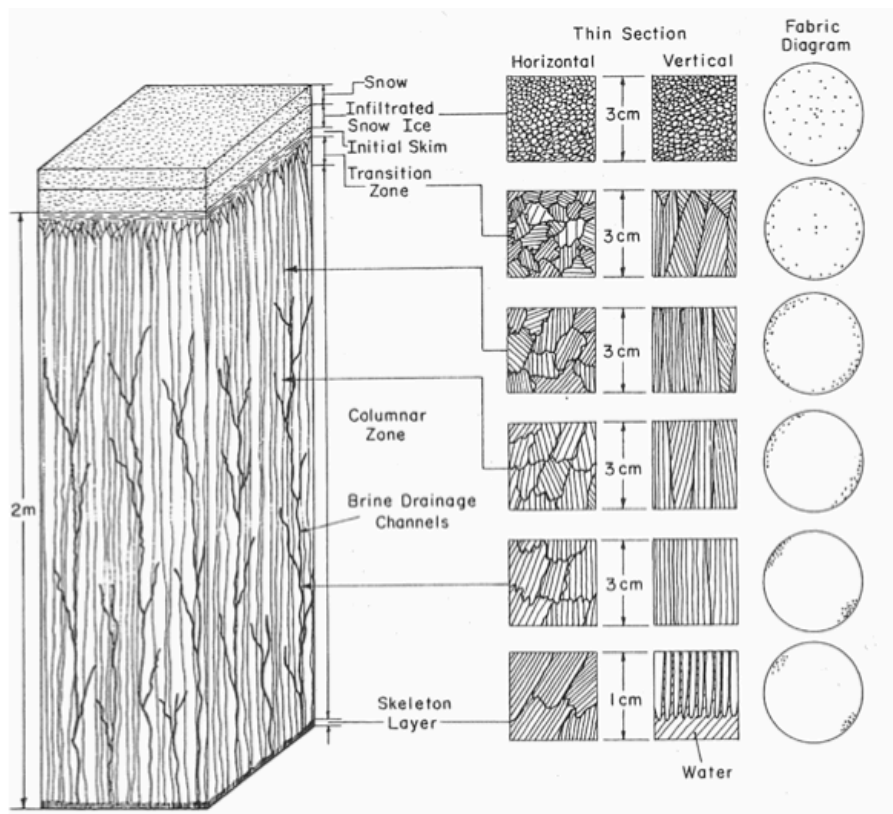


Figure 2-5 Schematic structure of first year ice (Schwarz and Weeks, 1977)

During the formation of secondary ice (not to be confused with second year ice), heat diffuse more easily parallel to the basal plane than to the c-axis, leading to a tendency of the c-axis of secondary ice formed in nature to be oriented in the horizontal plane. This ice is usually classified as S2 ice (Løset et al. 1998, p.22).

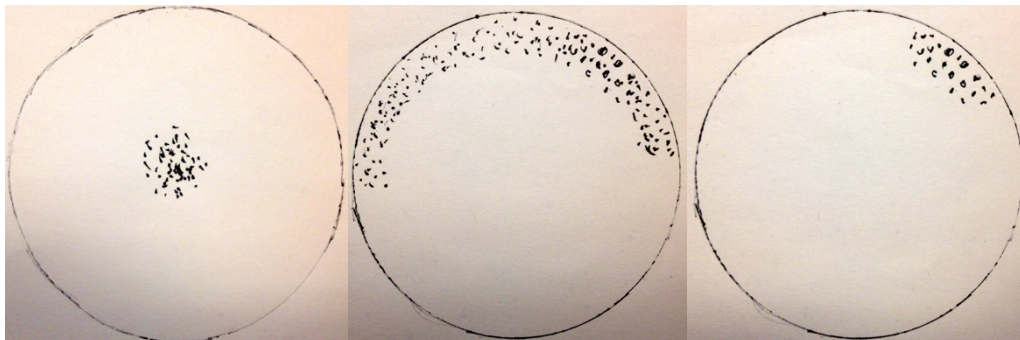


Figure 2-6 Fabric diagram for S1, S2 and S3 ice accordingly, showing C-axis orientation on half sphere

The other two main types of secondary ice, as shown in Figure 2-6, is termed S1 ice – for which the c-axis is vertically oriented – and S3 ice where the c-axis is oriented in the horizontal plane, but aligned in the same direction. Weeks and Ackley (1982) claim that ice formed under a stable ice cover tend to align in the direction of the ocean current at the water-ice boundary. The latter has been observed in Van Mijenfjorden at Svalbard, where the c-axis of the secondary ice is believed to have a tendency to be oriented aligned in the direction of the ocean current (Strub-Klein and Høyland, 2012).

Since the heat transfer necessary to freeze the seawater in the water-ice contact zone naturally increases with increased thickness of the ice above, it follows naturally that the platelet distance (d , see Figure 2-4) commonly is largest near the bottom of the ice

sheet. Large variations in air temperature or other parameters influencing the heat flux through the ice, during the growth period, may of course change this.

The potential difference in ice strength at top and bottom of the ice sheet would have consequences for the mechanical properties of the ice. One example of this would be the bending capacity upwards compared to bending capacity downwards, since ice don't have anything near the same capacity in tension as in compression (Section 2.9). Another consequence of this would be that the ice would have the possibility to fail in different modes through the same cross section.

2.4 Constitutive relation

Material behaviour properties of ice, and the understanding of the physics that governs ice, is a field where research still is making progress year by year. Although ice formation and structure is fairly well understood, as described in Section 2.2, the inhomogeneous character of ice found in the nature make it difficult to obtain material parameters in a consistent manner. There have even been academic disputes of whether the measured behaviour of ice under controlled circumstances in the laboratory is representative for large-scale ice behaviour in the field (Dempsey et al., 1999).

A common rheological model is the Burgers model (Figure 2-7 b)), which compromises the linear viscoelastic behaviour of the Maxwell model (spring and dashpot in series) and the Kelvin-Voigt model (spring and dashpot in parallel). Based on a generalized creep equation with the grain size effect incorporated, Sinha (1983) launched his now widely accepted model for continuum behaviour of polycrystalline ice. In his model, strain is predicted in terms of elastic (ϵ^e), delayed-elastic/recoverable (ϵ^d) and viscous permanent strains (ϵ^v). Thereby Sinha's model by definition is a Burgers model.

$$\epsilon^{tot} = \epsilon^e + \epsilon^d + \epsilon^v \tag{Eq 2-2}$$

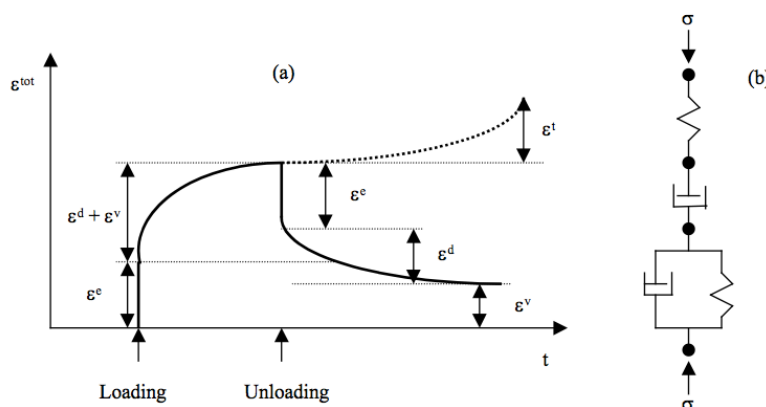


Figure 2-7 Strain versus time for pure ice when constant stress is applied. (Løset et al. 1998)

The physical phenomena constituting the total strain is described by atomic bond deformation, boundary deformation dislocation glide and dislocation pile-ups. These represent elastic deformation, delayed elastic strain, permanent viscous strain and crack formation accordingly (Figure 2-8). Any deformation of polycrystalline ice will be a combination of these modes. The model will not be described in detail here, but reference is made to the papers of Sinha (1978, 1983, 1989).

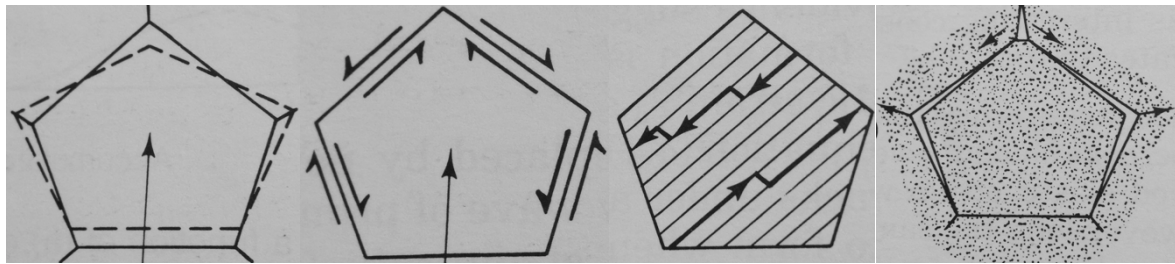


Figure 2-8 Elastic, delayed elastic, viscous (plastic) and fracture type grain deformation in polycrystalline ice (Sanderson 1988, 76)

Sinha (1983) intended his formula for conditions where grain boundary conditions were of minor importance and loading leading to voids and cracks did not disrupt the microstructure of the ice. It's therefore disputable whether this model is suitable when considering splitting of level ice floes. Further, the model is based on pure fresh water ice. Hence, brine and porosity is not taken into account.

Despite the obvious lacks, Timco and Weeks (2010) claim in their review of ice engineering properties that Sinha's model still is one of the most fulfilling. Thereby they implicitly conclude that rough simplifications of rheological models are necessary when modelling ice in engineering applications. The main disadvantage with a simplified approach, however, is the need for full-scale measurements in order to calibrate situation dependent empirical models. These empirical adjustments are in turn only valid for the exact same conditions as where they were derived.

In order to examine splitting as a load releasing mechanism for floaters in ice within the limited scope and time available for this master thesis, further simplifications will be made. In general, ice will be treated as a homogenous linear elastic material. Hence, constant Young's modulus and Poisson's ratio would apply in all directions. Taking into account the roughness of these simplifications, one need to bear in mind that the results obtained later in this report only can be treated as approximations to the problems considered. Further, only *effective* values are considered useful for further use, as will be evident in the following subsections.

2.4.1 Young's modulus

Schulson and Duval (2009, p.55) claim that the most accurate values for elastic stiffness and compliance constants available to this date is those obtained by Gammon et al. (1983), based on Brillouin spectroscopy. This choice of method provides what often is termed as the *real Young's modulus* for ice – in other words the likely value determined from the properties of the crystal lattice. As stated above, ice found in nature is nowhere near homogenous on the nanoscale level. Hence, the approach by spectroscopy only will give valuable results for pure freshwater ice made in the laboratory. Natural ice, as is relevant for further calculations in this thesis will have a significantly lower modulus than the 9.5 GPa (dependent of temperature and brine among other factors) found by Gammon et al. (1983) and accepted by Schulson and Duval (2009).

Tatinclaux and Hirayama (1982) examined elastic properties for several cantilever beam tests by applying analytic expressions for "beams on elastic foundation" on the load-displacement data previously obtained by others. By this approach they found Young's modulus for ice to be somewhere in the range of 0.24 GPa to 2.23 GPa, by

different regression analysis techniques. They recognize that their results indicate that this approach only may be used for comparison between different types of ice when the same test method is used. In practical terms this also imply that the numerical value of their results only are valid for the same type of ice loaded at the same strain rate as given. If loaded in a manner comparable to the process of bending when a ship advances in level ice, the numerical values might also be useful for other purposes than comparison.

Although there's a large discrepancy between the values suggested by Tatinclaux and Hirayama (1982) and Gammon et al. (1983), they are also given on different basis. For the use in this thesis, the first is more relevant than the latter. However, a value of 3 GPa is chosen, as this is an accepted rough estimate for the in situ measurable Young's modulus of ice in the literature.

2.4.2 Poisson's ratio

Devoted little space in the literature, Poisson's ratio still is an important value for engineering applications, describing the relationship between directional strains and loading. Timco and Weeks (2010) claim that effective (measurable) Poisson's ratio is influenced by temperature, grain size, grain structure, loading direction, state of micro cracking and to a high extent by loading rate. For the latter, the work of Murat and Lainely (1982), based on Weeks and Assur (1967), propose that the effective Poisson's ratio for short term bearing capacity should be taken as 0.42.

Although Murat and Lainely (1982) should be given credit for their work, a Poisson's ratio of 0.33 was, and still is, what is regularly used. Considering that strain dependency will be neglected in order to the limited time available for this thesis, the regular choice of Poisson's ratio equal to 0.33 is found appropriate.

2.5 Density

Timco and Frederking (1996) concluded that a straightforward definition of the density of sea ice is difficult to obtain due to its composition of solid ice, solid salts, liquids and gas. They showed that the reported densities were scattered in the range of 720 to 940 kg/m³, with an average of 910 kg/m³.

Later, Timco and Weeks (2010) performed the same exercise and concluded that a sea ice density of 920 kg/m³ should serve as a general estimate for first-year ice unless precise values for specific samples are needed.

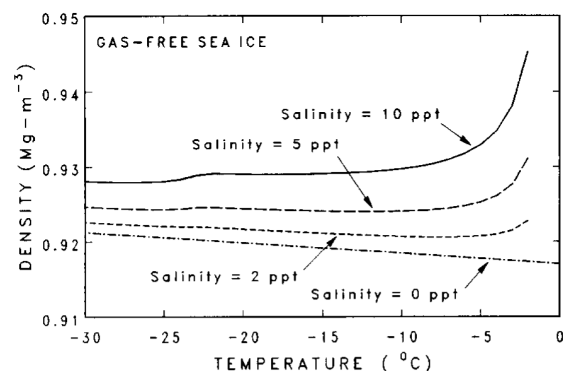


Figure 2-9 Plot of the density versus temperature for four different salinities for gas-free sea ice.

2.6 Friction coefficients for ice

Frederking and Barker (2002) provide friction coefficients for ice on painted steel, which would be a fair approximation for the ship-ice friction coefficient. They concluded that the appropriate static friction would be in the order of 0.25, while the kinetic friction at a sliding velocity (v_{sl}) of 0.1 m/s would be as low as 0.04. This is in good concurrence with ISO19906 (Table 2-1).

Table 2-1 Coefficients of steel-ice friction (ISO19906, Table A.8-5)

Material	$v_{sl} < 0.01$ m/s	$v_{sl} = 0.1$ m/s	$v_{sl} = 0.5$ m/s
Smooth steel	0.10	0.05	0.05
Smooth concrete	0.12	0.05	0.05
Corroded steel	0.15	0.10	0.10
Rough concrete	0.22	0.10	0.10

Experiments performed by Kennedy et al. (2000), prove that the kinetic ice-ice friction shows large variation with temperature and sliding velocity. Figure 2-10 provides scattered values in the range between $\mu_0=0.05$ to $\mu_0=0.8$ Schulson and Duval (2009, p.69) confirm these values. However, an averaged value would be appropriate for the approximate calculations performed later in this thesis. Hence, $\mu_0=0.5$ is chosen as default value for simple simulations, whereas the coefficients of Table 2-1 are used for the more complex simulations sin Abaqus.

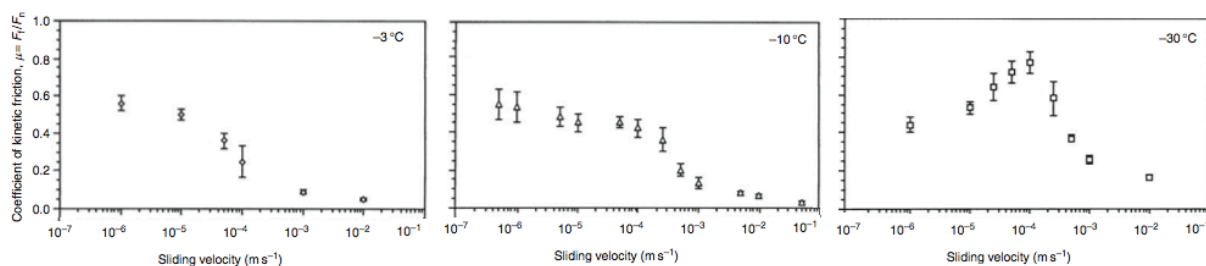


Figure 2-10 The kinetic friction coefficient of fresh-water granular ice sliding across itself across a smooth interface (Kennedy et al., 2000)

2.7 Indentation rate

For a laboratory tension test, it's common to define strain rate as the change in specimen length per time. Sanderson (1988, p.156) points out that in field deformation of ice clearly is not uniaxial. For full-scale experiments, specimen change in length per time is therefore neither a meaningful or possible measure. A different measure must therefore be adopted, as the rate dependency is of great importance to the behaviour of ice.

Indentation speed divided by a characteristic length could serve as an approximation to the strain rate. Although not based on physics, at least it provides the correct dimension of s^{-1} . For the characteristic length, both floe thickness and nominal contact area are possible metrics. Sanderson (1988) further states that scaled-to-fit uniaxial-results of the latter usually are adopted due to consistency for the structure being impacted. This is though only true for continuum behaviour, and would be subject to change as fracture occurs.

Different definitions of full-scale strain rate for ice might exist, but *indentation rate* of the floe – as relative indentation speed to the nominal contact width – is commonly used as measure for this quantity. Michel and Toussaint (1977) further complicate this relationship (Eq 2-3) by introducing a constant k in order to obtain a sensible indentation pressure-speed relationship. After Hill (1950), the pressure divided by 2.97, represents the ratio between indentation pressure and yield stress in plasticity analysis. The indentation speed (v_s), is rather arbitrarily divided by a factor k of 2 or 4 and the nominal contact width (W_L). Sanderson (1988, p.157) reasonably criticize the approach

in terms of the error introduced by treating ice as a plastic material, and the fact that k solely is based on empirical studies without any fundamental physical explanation.

$$\dot{\epsilon} = \frac{v_s}{kW_L} \quad \text{Eq 2-3}$$

One other possibility for calculating the strain rate is by utilizing the viscous strain, which in practical terms relates stress to strain rate. For instance will 1MPa correspond to $3 \cdot 10^{-7} \text{s}^{-1}$ for freshwater ice (Sanderson 1988, p.82). If the stress is known, the strain rate could be calculated directly from Eq 2-4. This implies that in order to reach a strain rate of 10^{-3}s^{-1} , one would according to Sanderson (1988, p.82) need to apply stresses of nearly 10 MPa. A discussion of whether this is a viable approach to calculate strain rate would be valuable, but is out of the scope of this report.

$$\dot{\epsilon}_{11} = A e^{\frac{Q}{RT}} \left[\frac{\sigma_{11}}{(1 - \sqrt{v_b / v_0})} \right]^3 \quad \text{Eq 2-4}$$

The conclusive remarks on rate of indentation is that this still is a field that would need further studies in order to give transferable relationships. One advantage by treating the ice floe (on the macro level) as a whole as a linear elastic-brittle material (Section 2.4) is that the stresses in the floe are decoupled from the strain rate, and the uncertainty of how to treat the strain and indentation rate are hence avoided.

2.8 Brittle versus ductile behaviour

Depending on strain rate and temperature, the material behaviour of ice is normally considered to either be elastic-brittle or viscoelastic-ductile (Michel and Toussaint, 1977). In general, the behaviour could be considered ductile when loaded slowly, and brittle when loaded rapidly (Schulson and Duval 2009, p.239). For ductile behaviour in ice, strain softening leads to a less violent failure mechanism, as strain energy is dissipated in a manner that prevents rapid fracture and the ice would tend to flow around the structure in an impact scenario. For brittle failure, all of the strain energy is suddenly released, leading to the possibility of fast propagation of a crack (Figure 2-11).

The ductile to brittle transition phase is an important characteristic of ice. At this point the ice compressive strength is at its highest level, and any upper bound criteria for the load exerted by ice-structure impact would have to consider the compressive strength of ice in this transition phase.

For fresh water ice, experiments indicate that the ductile to brittle transition happens somewhere near a strain rate of 10^{-3}s^{-1} . Considering the relationship between strain rate and stress, as noted in Section 2.7, one would notice the lack of transferability of this ductile-brittle transition criteria. Not all ice is capable of reaching a stress level of 10 MPa, at least not in terms of global ice-structure pressure. In large-scale tests, observations indicate that ice will fail in a brittle manner at stress levels of only 1-2 MPa, hence one could argue that the transition point between the ductile and brittle domain must be dependent on ice compressive strength. On the other hand, Figure 2-11 shows that the failure stress in the brittle domain decrease with increasing strain rate.

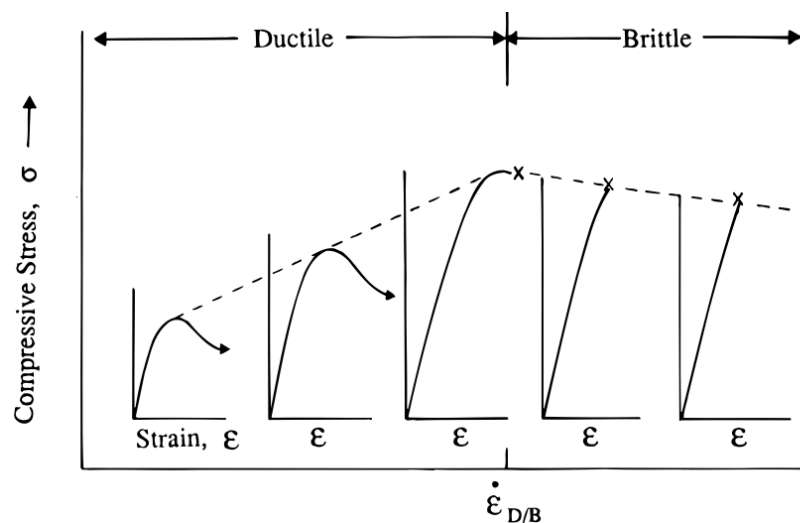


Figure 2-11 Transition from ductile to brittle behaviour for ice under compression (Schulson, 1990)

The transition between ductile and brittle behaviour is further dependent on the grain size. For the strain rate marking the transition phase for fresh water ice at 10^{-3} s^{-1} , Løset et al. (2006, p.70) show that a grain size of 1.5 mm would be another transition criteria. Only ice consisting of grains with size smaller than this would be governed by propagative, hence brittle, failure. The ductile-to-brittle strain rate dependency is shown in Figure 2-12. Temperature is another important factor to the change from ductile to brittle behaviour, since colder ice has a tendency to exhibit more brittle behaviour (Gold, 1977).

There's a strong link between the strain rate and grain size and the transition from ductile to brittle behaviour. For the proceeding chapters in this thesis, however, the ice will be treated as elastic-brittle. Slowly drifting ice floes would reasonably provide the lowest interaction velocities. With an expected drifting velocity in the order of 0.33 m/s (Hovland, 2012), the assumption of elastic brittle behaviour seems realistic for all encounterable ice-floater interactions.

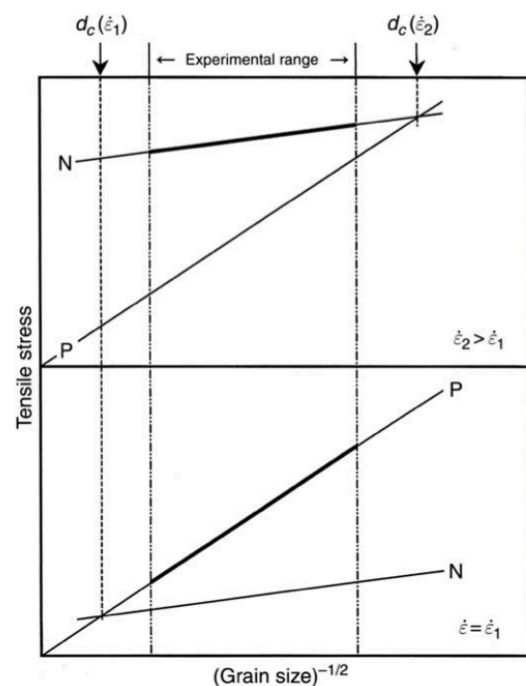


Figure 2-12 Grain size vs. strain rate for propagation (P) and nucleation (N) (Schulson and Duval 2009, p.223)

2.9 Compressive, tensile and flexural strength

Unlike many other materials, ice exhibits brittle behaviour at temperatures close to its melting point, and at strain rates significantly lower than those resulting in dynamic effects. According to Schulson and Duval (2009, p.212-235), the factors that affect this mode of failure are porosity, brine, temperature, strain rate, grain size, damage, growth texture and the size of the polycrystalline ice body. Strain rate influences the process

both directly and indirectly by altering the way the other factors affect the stress-strain relationship for the ice body.

For the compressive strength of ice, Timco and Frederking (1990) developed a model for calculating the compressive strength of ice through systemizing nearly 300 previously reported tests. The relationships for uniaxial strength of ice through the total porosity (η) for horizontally loaded columnar ice (σ_{cv}), vertically loaded columnar ice (σ_{ch}) and granular ice (σ_{cg}) as shown in Eq 2-5, accordingly. The measure for porosity (η) is ppm, and it's constituted by the sum of the inclusions of air and brine in the ice.

$$\sigma_{cv} = 37(\dot{\epsilon})^{0.22} \left[1 - \sqrt{\frac{\eta}{0.27}} \right], \sigma_{ch} = 160(\dot{\epsilon})^{0.22} \left[1 - \sqrt{\frac{\eta}{0.20}} \right], \sigma_{cg} = 49(\dot{\epsilon})^{0.22} \left[1 - \sqrt{\frac{\eta}{0.28}} \right] \quad \text{Eq 2-5}$$

Moslet (2007) did thorough experiments on the compressive strength of ice at Svalbard, and obtained some interesting conclusions. He stated that the strength and behaviour of ice not necessarily could be predicted by ice properties alone, but also are functions of the thermal history of each individual specimen. Timco and Weeks (2010) concludes that the compressive strength of ice should be taken to be somewhere between 0.5 and 5.0 MPa. As depicted in Figure 2-11 this range is related to the strain rate. Still, a reasonable value of $\sigma_c=1.0$ MPa, which is reasonably in concurrence with the choice of Lubbad and Løset (2011), is chosen.

Temperature is a parameter that affects the tensile strength in somewhat the same way as the strain rate. For freshwater ice, the temperature affects the tensile stress capacity in the same manner as it affects fracture toughness (Figure 4-7). In Figure 2-13 this relationship is made clear. For the effect of brine, Schulson and Duval (2009, p.225) show the relationship through Figure 2-14. The latter considers flexural strength, but the relationship is transferable to tensile strength, as they claim the flexural capacity usually to be 1.7 times the tensile. Hence, the equation evident in Figure 2-14 could also be used for tensile strength of ice, though without the premultiplied factor.

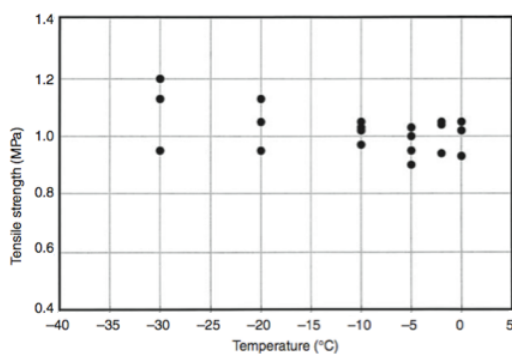


Figure 2-13 Tensile strength of sea ice by temperature (Schulson and Duval 2009, p.216)

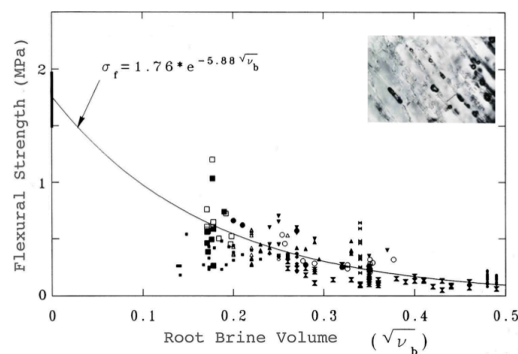


Figure 2-14 Flexural strength of sea ice by brine volume (Schulson and Duval 2009, p.224)

Intuitively, one might find it strange that the flexural strength of ice is higher than the tensile capacity. However, bending creates tension in the upper part of the floe and compression in the lower part. Due to the reduced rate of growth – caused by reduced thermal diffusion for the bottom side of the floe, as the floe gets thicker – Eq 2-1 predicts the upper part to be stronger than the lower (as evident from Figure 2-5). Further, it's obvious from the discussion above that $\sigma_c < \sigma_t$. Therefore, it's reasonable that the ice

flexural strength would provide higher capacity than for a case of pure tensile failure. Another implication of this would be that the flexural strength for upwards bending would be lower than the corresponding capacity for downwards breaking.

In order for ice to fracture under tensile loading, the applied stress must exceed the level required for crack nucleation. After nucleation has occurred, the stress still must be sufficient to propagate the cracks through the length of the floe. Grain size plays an important role in this process. The lower part of Figure 2-12 shows the required stress for propagation and nucleation for a strain rate in the ductile domain – once a crack is nucleated, there's still need to add more energy into the process to impose propagation.

On the other hand, we have the upper part of Figure 2-12, where the energy need for propagation already is exceeded when the criterion for nucleation is met. This is what leads to the rapid fracture in the brittle domain, and as seen from the figure, one could expect that larger grain size would lead to more violent fracture than for ice of smaller grains.

Crack nucleation is indisputably dependent of the specimen strain, but whether the dependency is connected to the level of total strain or the delayed elastic strain alone is still up for debate (Sanderson 1988, p.89). However, he states that for rather high strain rates of $>10^{-6} \text{ s}^{-1}$, the more valuable measure would be to apply the peak tensile strength. This tensile stress capacity is correlating with the grain size (d), as shown in Eq 2-6. However, comparing with the observations plotted in Figure 2-14 imply an appropriate approximation of $\sigma_t=300\text{kPa}$

$$\sigma_t(d) = \sigma_0 + \frac{k_1}{\sqrt{d}} = 0.6 \text{ MPa} + \frac{0.02 \text{ MPa}\sqrt{m}}{\sqrt{d}} \quad \text{Eq 2-6}$$

2.10 Chosen ice parameters

Based on the previous discussions, Table 2-2 depicts a summary of chosen parametric values. Unless otherwise specified, these are used in the following calculations.

Table 2-2 Suggested material parameters for ice

Input parameter	Symbol	Value	Unit
Young's modulus	E	3000	MPa
Poisson's ratio	ν	0.33	
Density	ρ_{ice}	920	kg/m ³
Compressive strength	σ_c	1000	kPa
Tensile strength	σ_t	300	kPa
Flexural strength	σ_f	500	kPa
Ice-ice friction (kinetic)	μ_0	0.5	
Ship-ice friction (kinetic)	μ	0.05	

3 Ship-ice interaction process

In order to fully understand load-releasing mechanisms for floaters in ice, proper understanding of the ice itself is not sufficient. The purpose of this chapter is therefore to provide some basic knowledge on typical floaters in ice-infested areas, and a general introduction to the failure process in ice when interacting with such structures.

3.1 Floaters in ice

Transport, costal guarding, research and – to some extent – tourism, are some of the reasons for why ships and floaters are present in ice-infested areas. However, it's mainly the Arctic offshore development, bound by the desire to exploit hydrocarbon resources that drives the development of floaters in ice, hence also being the focus for the following discussion. Figure 3-1 depicts the main categories of such floaters.



Figure 3-1 Arctic floating structures

3.1.1 Shape of hull

Evidently, the range of hull shapes vary significantly between the different floating structures present in the Arctic. The hull inclination angle (ψ) is of large importance to the development of the forces when initial (and possible following) crushing of an ice floe occurs (Figure 3-4).

The semisubmersible rig and the SPAR platform usually have vertical hull at the waterline ($\psi=90^\circ$). This is challenging in terms of failure modes of the ice, since there would be less natural ways for the ice to deflect and clear away from the structure. Within the category of ship shaped structures, there are also large variations in angle of the bow flare at the stem. One of the more extreme cases is the Oden Icebreaker, a vessel used by the Swedish Maritime Administration (Figure 3-2), with a bow flare of $\sim 180^\circ$.



Figure 3-2 Oden Icebreaker seen from above (Prof. Martin Jakobsson, <http://people.su.se/~mjako/>)

Even though the buttock angle is of importance to the ice-structure interaction scenario, the cross section shape of the structure is of less importance. As stated by Løset et al. (2006, p.112), the shape of the cross section form usually only affect 10-15% of the total ice actions. Still, the size of the cross section is of great importance to the total loads from ice.

3.1.2 Velocity of impact

The impact velocity is an important parameter to understand ship-ice interactions. For Shuttle Tankers and Ice Management Vessels (Figure 3-1 a)), the typical icebreaking velocity is approximately 3 knots (1.54 m/s).

For the geofixed structures (Figure 3-1 b-f)), the velocity of the drifting ice will be decisive for the impact velocity. This would, as understood from Section 2.7, be of importance for the behaviour of the ice. Too low velocities would violate the assumption of brittle ice. Low velocities would also be challenging for the assumption of full ventilation (Figure 3-6), as the floe would have time to be flooded when the process of rotation takes too long time, hence providing overly conservative loads (Valanto, 2001). The ice drift velocity is generally below 1 m/s, at least for the Barents Sea (Eik, 2011).

3.1.3 Icebreaking capabilities

Some tankers, like the depicted Mikhail Ulyanov (Figure 3-3), rated for 1.5m level ice, are of the type “Dual Direction Icebreaking”. This implies that it has icebreaking capabilities both by advancing forward and backward through the ice (Intecsea, 2012). One large advantage with this solution is that the hull could be optimized for regular waters at the stem and for icebreaking at the stern – hence able to obtain good performance for varying conditions.



Figure 3-3 Dual Direction Icebreaking Shuttle Tanker Mikhail Ulyanov (Aker Arctic)

3.2 Failure modes of ice

Observations made by Kärna and Jochmann (2003) in the Baltic Sea indicate that failure of ice usually takes form as splitting, bending, buckling or crushing. The occurrence of these modes proved dependent on quality, thickness and lateral confinement of the ice. This is in agreement with what is reported by Bhat et al. (1991), while Løset et al. (2006, p.110) point out that two more failure modes, creep and spalling, exist and are likely to occur at low and high interaction velocities, respectively. All these modes are depicted in Figure 3-4, while only the most relevant to the further discussions in this thesis will be treated in the following.

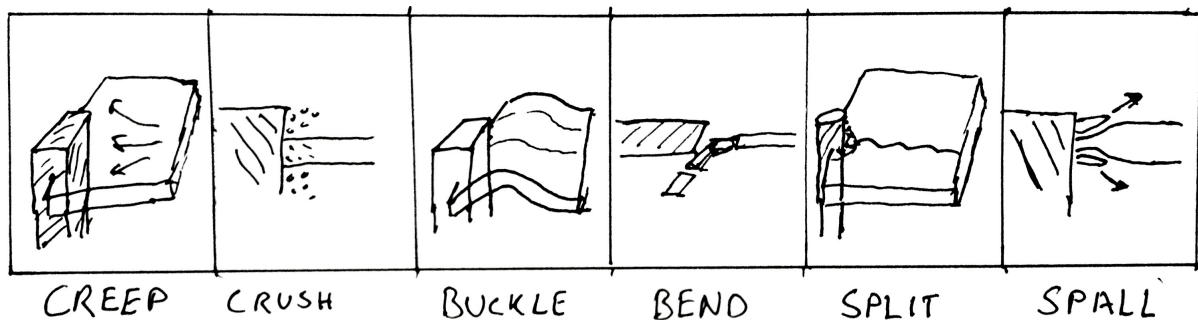


Figure 3-4 Failure modes for ice, after Sanderson (1988)

3.2.1 Crushing

Figure 3-5 depicts the development of the ice-ship contact area as the ship moves into the floe. The crushing height (v_h), will be central in the calculations of deflection and surge of the floe in Chapter 6 (given there as Figure 6-6).

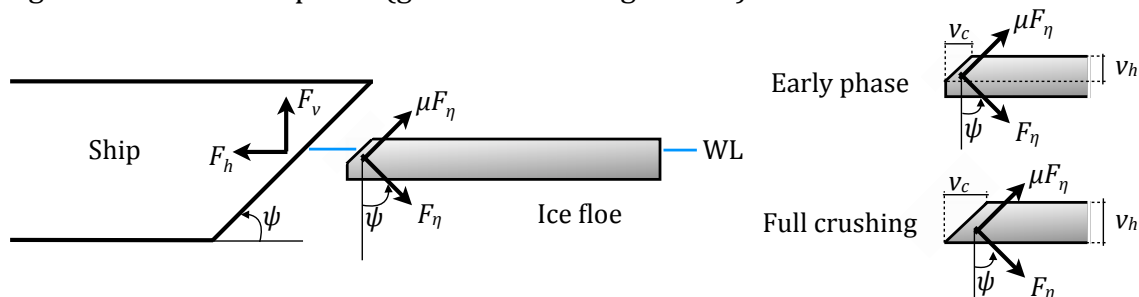


Figure 3-5 Forces acting on ice sheet and development of the crushing height (v_h) and length (v_c)

3.2.2 Bending

After the initial crushing depicted in Figure 6-6 has taken place, bending is often the following mode of failure. This given that the ship hull inclination angle is appropriate to produce sufficient bending stresses.

Based on the conclusions of Poznyak and Ionov (1981) and Kotras et al. (1983), the ship-ice interaction could be described through the following steps. A brief overview can be seen in Figure 3-6. Important to notice for further applications is the concept of ventilation, where the floe is rotating with dry top surface – even if partly submerged. Summarized, the process consists of breaking (if necessary), rotating, sliding and clearing of the floe (Lubbad, 2011).

The assumption of full ventilation would be conservative when considering the resistance a ship would encounter when advancing in ice. If the rotating ice floe is flooded, the extra weight of the water will accelerate the process of sliding, submerging and clearing of the floe.

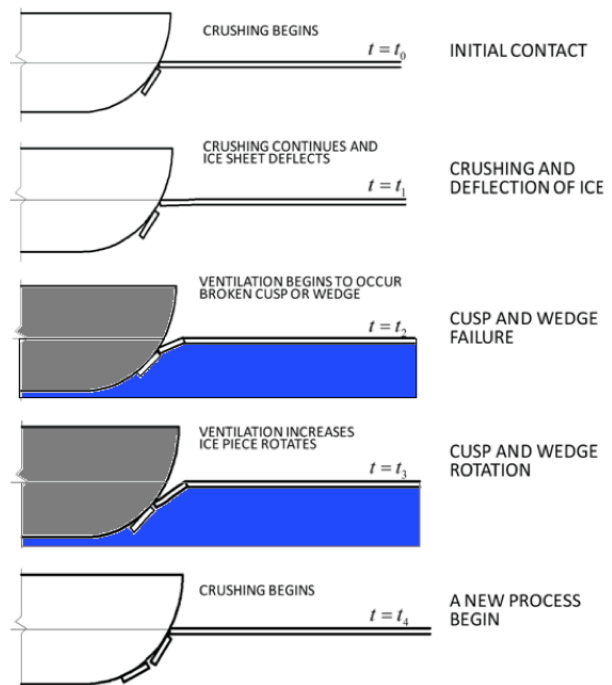


Figure 3-6 Level-ice interaction with a sloping surface (Lubbad, 2011 (after Kotras et al. 1983))

The interaction model shown in Figure 3-6 depicts failure for a floe that acts as a beam. This, however, is not always the case in nature. When an ice floe is loaded vertically on the upper surface, it might act as a plate. Then, tensile stresses will develop on the bottom (for radial) and top (for circumferential) surface. If these stresses exceed the critical stress of the floe (Section 2.9), cracks will develop as load releasing mechanisms. Behaving as a plate, the floe hence fails by initiation of *radial cracks* that eventually lead to *wedges* breaking off after latter formation of circumferential cracks (Kerr, 1996). Wedge failure is shown in Figure 3-7.

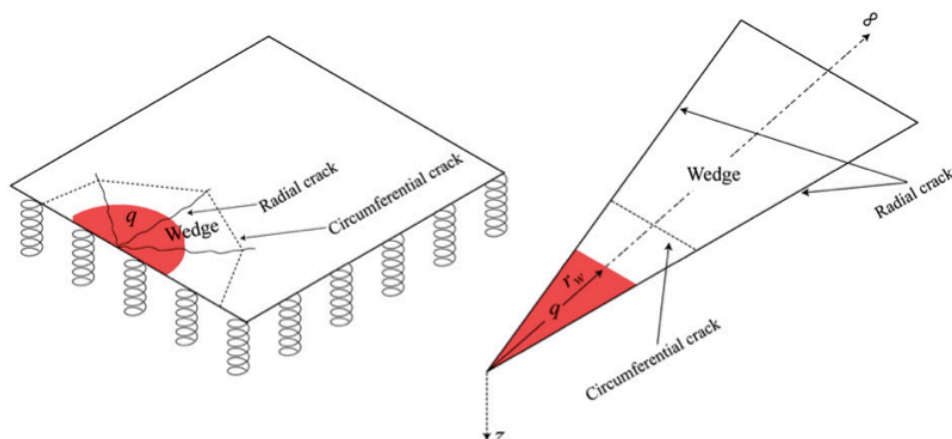


Figure 3-7 The replacement of the semi-infinite plate model with the model of adjacent wedge-shaped beams resting on an elastic foundation (Lubbad and Løset, 2011).

3.2.3 Splitting

Given that a radial crack initiates, as described in the previous subsection, and that the resulting forces after this crack initiation are larger than the limits for propagation, rapid splitting of the entire floe could be observed. This mode of failure is usually the one associated with the least ice actions exerted on the structure of consideration, for the modes of failure depicted in Figure 3-4 (Løset et al. 2006, p.112).

As stated by Bhat (1988), “ice is a very brittle material, and indeed one of the most conspicuous phenomena in the Arctic is the fracture of sea ice”. This especially holds for splitting, which due to its importance to this thesis is treated separately in Chapter 4.

3.3 Simplification of interaction

In order to do simplified calculations on ice floes, one need to define a few metrics that will be able to describe the geometry of an arbitrary ice floe. The floes considered in this thesis are treated as rectangles of length (L) and with (W) normal to the water surface. The thickness (h_{ice}) is assumed to be uniform.

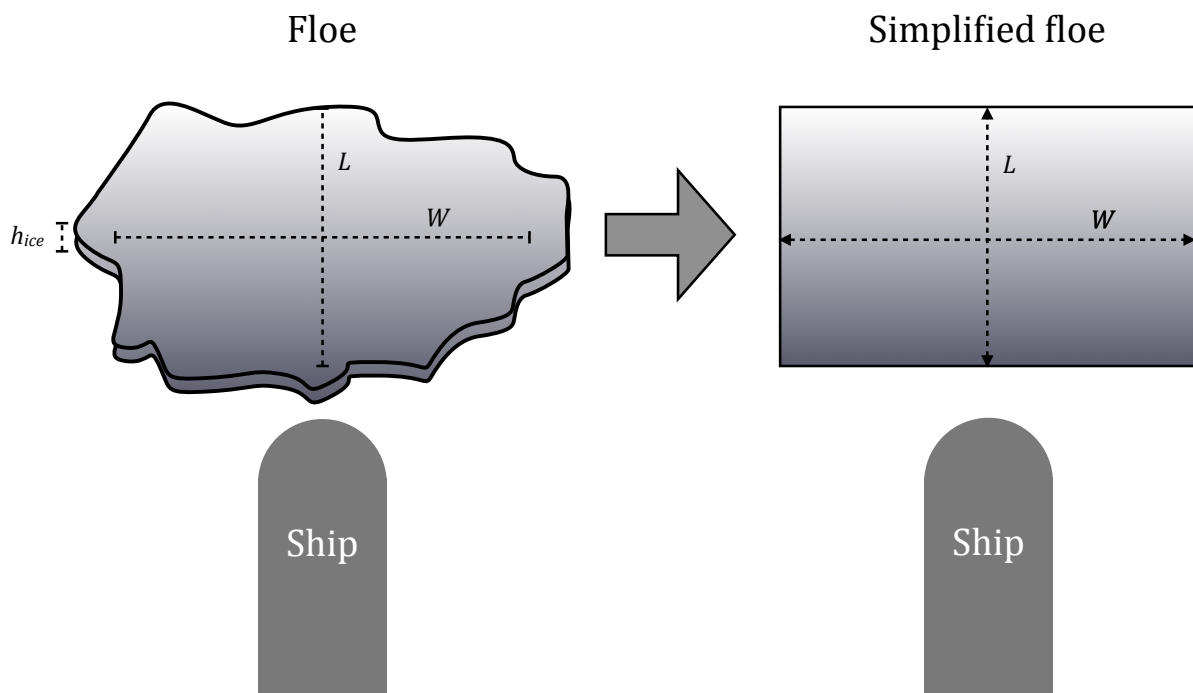


Figure 3-8 Simplification and measurement of ice floes

4 Splitting as a load releasing mechanism – a literature review

This chapter presents relevant theory on splitting as a load releasing mechanism with special focus on linear elastic fracture mechanics and the nonlinear cohesive zone method. Thereafter, the focus is turned to splitting of ice and discussion of important material parameters and modelling techniques for treatment of splitting.

4.1 Fracture mechanics as the basis for determination of splitting

Under influence of high levels of stress, large strain rates, or a critical level of strain, a specimen will fracture as it ceases its behaviour as a continuum (Sanderson 1988, p.88). Ordinary mechanics are then not sufficient to describe the material behaviour. Fracture mechanics, on the other hand, strictly deals with situations where a crack already exists. In essence its purpose is to predict the conditions required for crack growth, and whether the crack growth is stable (Løset et al. 1998, p.50). Understanding the processes of fracture is key to the understanding of splitting of any material.

The origin of fracture mechanics is usually linked to the work done by Griffith (1921) on brittle fracture of glass, where he developed a framework for treatment of propagation of cracks in solid materials. According to Sun and Jin (2012, p.5), he did this in order to prove that propagation of predominant micro cracks in glass would produce fracture at loads much lower than the theoretical strength. However, it was not until the massive fracture of the hull of more than one hundred *Liberty* cargo ships – of which 10 were split in half – built during World War II, that fracture mechanics was recognized as important to engineering applications (Rossmanith, 1997).

4.1.1 Splitting in fracture mechanics

Deformation modes resulting from crack propagation can be divided into three categories that by combination can describe any propagative deformation (Figure 4-1). The modes are termed as tensile (mode I), sliding (mode II) and tearing (mode III). While the two latter usually are more resistant to propagation, failure through mode I is the mechanism considered as splitting in this thesis.

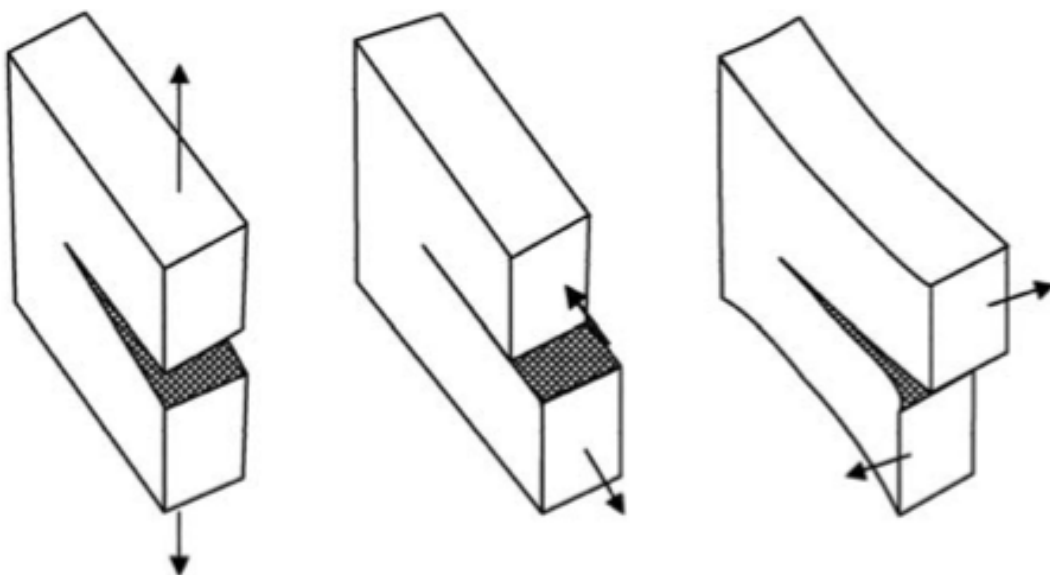


Figure 4-1 Crack propagation modes: Tensile, Sliding and Tearing mode (Schulson and Duval 2009, p.193)

4.1.2 Principle of Linear Elastic Fracture Mechanics (LEFM)

Griffith (1921) proposed that for mode I incremental extension of a crack (dc), the equilibrium of thermodynamics require the sum of the incremental change in energies (dU) to be balanced. Hence, the sum of change in external mechanical work, transportation of heat, internal energy, potential energy and the energy necessary for creating new crack surface, must be equal to zero.

$$\frac{dU}{dc} = 0 \quad \text{Eq 4-1}$$

Once formed, a crack will propagate if the stress intensity factor is equal to the material fracture toughness. The energy required for creation of new surface (γ_s) is, as shown in Eq 4-3, central to the discussion of crack propagation. Ashby (1989) proved that for ice, this surface energy is related to the oxygen-oxygen distance in the basal plane (a^*) through the following relationship:

$$\gamma_s \approx \frac{Ea^*}{20} \quad \text{Eq 4-2}$$

Further, the central assumption for LEFM is that the changes in heat transfer and internal work will be negligible compared to the change in mechanical energy, potential energy and the energy required to create new crack surface. By combining theory of elasticity and Griffith's concept of energy balance, we obtain Eq 4-3. This holds for a short crack, where σ_t is the applied tensional stress, c is half the crack length, γ_s represents the energy required to produce new surface, E' equals Young's modulus, and K_I is defined as the stress intensity factor for mode I failure.

$$\sigma_t = \sqrt{\frac{2\gamma_s E'}{\pi c}} \Rightarrow K_I = \sigma_t \sqrt{\pi c}, \quad \text{Eq 4-3}$$

Although developed for fracture in glass, Griffith's (1921) model for linear elastic fracture mechanics is transferrable to other materials. Based on the available literature, Sun and Jin (2012, p.6) recently confirmed that LEFM also provides good results for crack growth prediction in ceramics and other elastic-brittle materials.

4.1.3 Fracture toughness

One of the fundamental concepts of traditional fracture mechanics is to accept that the stresses at the tip of a crack is unbounded, but still not use this crack tip stress to directly determine how the crack extends (Sun and Jin 2012, p.3). Although stresses are unbound at the crack tip, introduction of a stress intensity factor – as a measure for the state of a material near the crack tip – would make prediction of crack growth possible.

Based on Eq 4-3, Irwin (1957) proposed that a viable criterion for crack growth would be to define a critical level of stress intensity as where crack extension would occur. The fracture toughness (K_{Ic}) is therefore nothing but the critical level of stress intensity that a given crack in a given material is able to resist. Hence, the stress intensity factor relates to the material fracture toughness in a comparable fashion to how one-dimensional stresses is linked to a material yield criteria.

The fracture toughness is a parameter that belongs to the material, rather than the individual specimen, and should therefore be independent of the size of any test specimen (Schulson and Duval 2009, p.195). There are, however, disputes both on whether the fracture toughness really is size independent and on feasible methods for determining appropriate value. In particular this is the case for inhomogeneous materials and materials where micro cracks, such as those Griffith (1921) predicted in glass, are present in the material (Dempsey, 1999). Looking at Eq 4-3, it's obvious that K_{IC} would be dependent of specimen size, if the critical crack length c_{cr} also depends on the size of the specimen it's embedded in.

4.1.4 Nucleation and propagation

There are different models considering how to treat fracture (Løset et al. 1988, p.60), mainly depending on whether the crack formation process is stable (ductile) or unstable (brittle). This classification will in turn decide whether the splitting process is governed by nucleation or propagation of cracks accordingly. While the first is based on the actions that are needed in order to produce a crack in a continuous material, the latter term is used for the process where an already existing crack extends and widens.

In other words, first, initiation of a crack in the previously continuous material needs to occur. Secondly, the crack needs to extend across a specimen in order to produce splitting. Within the latter sub process, distinction is made between two different scenarios: Slowly, *nucleation controlled crack growth*, where an incremental increase in crack length also requires increased loads, is termed ductile fracture; Rapid, *propagation controlled crack growth*, where the crack will run uncontrolled across the specimen without any increase in loads, is termed brittle fracture. Only the latter scenario is considered as splitting in this thesis. However, and read twice because this might be confusing, *nucleation of cracks* could also describe the phase of crack initiation. This definition is used in Section 4.4.

4.2 Upper bound theorem for plastic limit analysis of splitting

Ralston (1981) argues that theory of plasticity could be used to define the upper bound for the force required to propagate cracks to the extent of splitting of a continuous body. Taking advantage of the normality rule, he showed that for two materials with the same yield surface, the upper bound collapse limit for the first material also would be the upper bound for the other material. Following this assumption, a plastic failure criterion also would be the failure criterion for brittle splitting. However it should be noted that this upper bound might over estimate the critical load significantly.

The Drucker-Prager yield criterion for plastic material behaviour could also be used to establish an upper bound for splitting as a load releasing mechanism. Bhat et al. (1991) claimed that if a material acts elastic-brittle in the cases of splitting, a rigid-perfectly plastic material would represent the plastic (upper bound) limit case. The material parameters α and K , are defined by the relationship between compressive (σ_c) and tensile strength (σ_t).

$$f = \alpha J_1 + J_2^{1/2} = K, \quad f \leq K$$

Eq 4-4

$$\text{where } \alpha = \frac{1}{\sqrt{3}} \left(\frac{m-1}{m+1} \right), \quad K = \frac{2m}{\sqrt{3}(m+1)} \sigma_t, \quad m = \frac{\sigma_c}{\sigma_t}$$

Here, J_1 and J_2 represent the first and second stress invariants of the deviatoric stress tensor, based on the principal stresses σ_1 , σ_2 and σ_3 . For situations of plane stress, σ_3 , which often can be claimed for plates with width and length of larger order than the thickness, these coefficients will be as described in Eq 4-5.

$$J_1 = \sigma_1 + \sigma_2$$

$$J_2 = \frac{1}{6} \left[\sigma_1^2 + \sigma_2^2 + (\sigma_1 - \sigma_2)^2 \right]$$

Eq 4-5

4.3 Cohesive method for splitting purposes

Cohesive zone models (CZM) have evolved from LEFM. Griffith proposed already in his PhD-thesis, in 1921, that the cohesive forces of the molecules on either side of a crack in a body composed of molecules that attract each other would govern the crack growth. CZM is beneficial due to its ability to take into account the fracture process zone (FPZ) ahead of the crack tip, opposed to LEFM where the crack tip is singular. For fracture of quasi-brittle materials, such as concrete or ice, the FPZ might not be negligible.

Elaborating on Griffith's assumption, and considering a linearly elastic body to the point of failure, Barenblatt (1959, 1962) was the first to introduce the concept of cohesive modelling. Dugdale (1960) extended this application to perfectly plastic materials. Both of them had the Griffith crack of linear elastic fracture mechanics as basis for their derivations.

Barenblatt (1959) treats cracks in an elastic-brittle material, under the assumption that there exists a level of minimum stress applied to the contour of the crack that must be exceeded if the crack should open. As shown in Figure 4-2, he divided the crack into three main zones, namely traction region (a), transition region (b) and terminal region (d). Further, the width of the terminal region of the crack should be small in comparison with the size of the entire crack (Barenblatt, 1962).

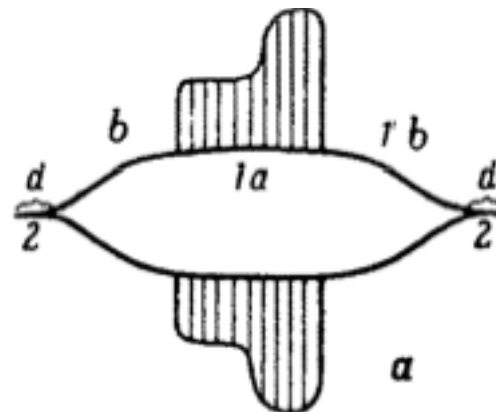


Figure 4-2 The three phases of a cohesive crack (Barenblatt, 1959)

Figure 4-3 compares the intra-crack distribution of stresses and displacements for an *ellipsoid* Griffith crack (absent of cohesive traction), with a *ductile* Dugdale-crack and a *brittle* Barenblatt-crack with cohesive forces. The latter is the relevant approach for the phenomena of splitting in ice considered in this thesis.

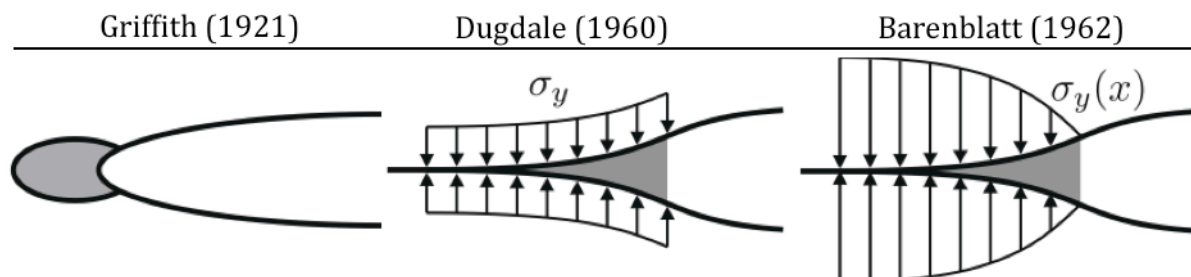


Figure 4-3 Crack tip models of Griffith, Dugdale and Barenblatt, after Geißler and Kaliske (2010)

Although the cohesive zone models of Dugdale and Barenblatt were introduced at the same time as the finite element method (FEM) had its breakthrough in civil and aeronautical engineering, it was not until Hillerborg et al. (1976) that cohesive modelling – under the name of the *fictitious crack model* – first was implemented in a finite element analysis. In their implementation, Hillerborg et al. (1976) argued that the Barenblatt-model could be simplified by assuming that the crack opening is what governs the cohesive tractions. In other words, they established the connection between the observed unloading behaviour in experimental tensile and flexural testing with the shape of the stress-separation curve (Mulmule and Dempsey, 1998). Hence, Hillerborg et al. (1976) introduced the traction-separation law for describing cohesive behaviour.

The CZM introduced by Barenblatt (1962) implies that there will be no infinite stresses at the crack tip due to distributed cohesive forces along the infinitesimal crack opening in the vicinity of the crack tip. Hillerborg et al. (1976) enhanced this method by introducing the concept of fracture energy as the energy required to split an interface at a predefined localization, and the crack tip stress that would produce propagation.

Geißler and Kaliske (2010) explain the connection between the mathematical crack opening, the physical crack opening and the traction-separation law of the Barenblatt-crack in Figure 4-3, as defined in Figure 4-4. This illustration clarifies that the cohesive forces in essence only affect the radius of the crack and the displacements within the main part of the crack.

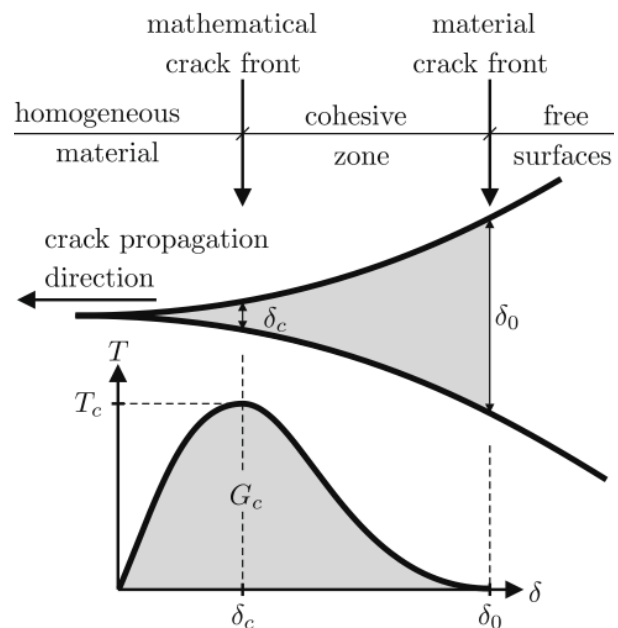


Figure 4-4 Assumptions and notations of the cohesive zone model (Geißler and Kaliske, 2010)

Elices et al. (2002) did an extensive review of the cohesive zone model. They concluded that the model, unlike most models of fracture mechanics, both is capable of properly predicting the response of bodies including cracks, and the behaviour of uncracked structures – including those with blunt notches. Even if CZM in finite element analyses is the heritage of the three-point bending of concrete beams (Hillerborg et al., 1976), Elices et al. (2002) prove that the approach in general is valid – not only for concrete but also for Polymethyl-methacrylate (a brittle polymer) and some non-ductile steels. Their conclusion is that CZM will be valid for several other brittle materials as well, provided thorough knowledge of the material parameters.

Despite being a valid approach, there are several drawbacks with the cohesive zone method. Among others, Foluk (2010) points out that the method, when applied in finite element analysis is severely mesh dependent, and that brittle materials require small mesh sizes to ensure stability.

Cuvilliez et al. (2012) conclude in their work that CZM in itself is not able to represent crack initiation in quasi-brittle structures, such as concrete, in a fulfilling manner. Therefore, they propose a new method, where a damage model is used in order to produce the first macro cracks, whereas CZM is utilized for crack propagation. This approach is comparable to the Drucker-Prager-LEFM method proposed by Bhat et al. (1991), described in Subsection 4.4.5.

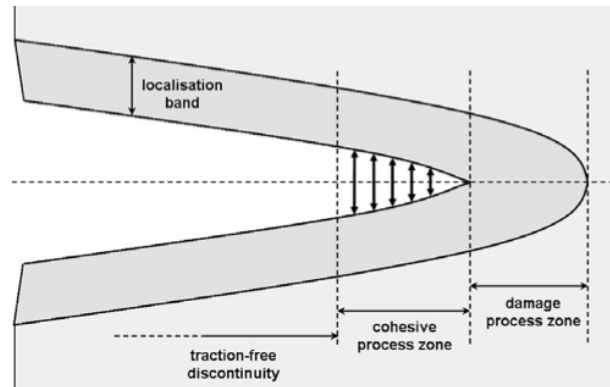


Figure 4-5 Coexisting descriptions of a damage model-cohesive zone crack (Cuvilliez et al., 2012))

4.4 Splitting as a load releasing mechanism for ice

Although understanding continuum behaviour of ice is quite complicated compared to other materials, Sanderson (1988, p.145) states that for ice, continuum is relatively easy to understand, while fracture is more difficult, but that the transition between them is far from understood. The recent review of available literature on ice by Timco and Weeks (2010) confirmed this statement. The transition is the most core and hence most important to the initial production of a crack, which might explain the lack of adequate theory for splitting as a load releasing mechanism in ice.

As will be shown, there's still established some common ground, in terms of that the phenomena of splitting consists of two main processes. Splitting is a result of nucleation of a micro crack, which for a given load will propagate through the floe and divide it into two or more parts. For sea ice, there's also mainly agreement that nucleation is the governing criteria.

Valanto (2001) states that the symmetry of stresses ahead the stem of a ship advancing in unbroken level ice would produce very high stresses, and that these stresses would be likely to split the ice cover in front of the ship. He also recognize this splitting phenomenon to be the same as what "can often be seen to appear straight ahead of the stem of a ship advancing in snow free level ice", as often takes place in nature.

Figure 4-6 shows the typical distribution of stresses in an ice sheet interacting with a straight walled cylinder. For interaction with an inclined hull or sloping structure, bending stresses might produce the initial crack. The illustration still provides valuable insight in how tensile stresses, that might cause splitting, originate.

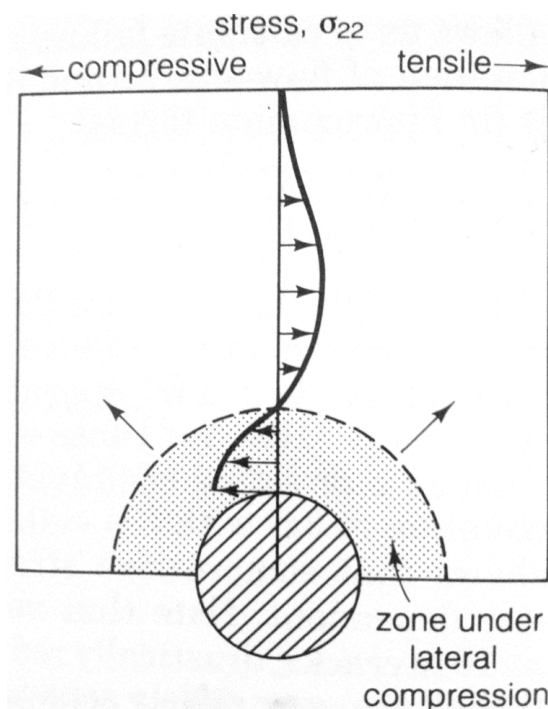


Figure 4-6 Tensile and compressive stress fields for radial crack analysis (Sanderson 1988, p.168)

Crack growth will depend on the loading situation, and *tensile* fracture of granular materials is usually associated with cracks following the grain boundaries. For fracture of ice by *compressive* loading, on the other hand, Hallam (1986) showed that as much as half of the cracks would be transgranular. For the tensile case, this implies that the size of cracks formed will be in the same order as the grain size. As shown in Section 2.8, the grain size is decisive for whether the crack growth, and hence fracture, will be governed by nucleation or propagation.

4.4.1 Nucleation and propagation of cracks in ice

Schulson and Duval (2009, p.229) concluded that the physical phenomenon controlling nucleation in ice, although several possibilities suggested in the literature, is connected to dislocation pile-ups and grain boundary sliding. Further, they claim that propagation more often is a limiting mechanism for ice tensile strength in laboratory than in nature, due to the fact that grain sizes here are much smaller than those present in the field. Increased grain size will cause larger cracks, which in turn will propagate more easily.

Ice found in the nature is affected by its thermal history and will contain several cracks and faults that will propagate at low loads. The question that arise is whether crack initiation would be necessary to consider in nature, since cracks and faults already exists. The simple answer is that a thermal crack not necessarily is enough for nucleation of a new crack to be redundant. Ice has the ability to “heal” itself by blunting of existing cracks (Renshaw and Schulson, 2001). In the event of an ice-structure impact, the existence of old thermally formed cracks might not exclude the need for crack nucleation in order to create the sharp point of singularity needed for propagation. Thereby, initiation of the crack process by nucleation must be considered as a possible governing criterion splitting type fracture of in-situ sea ice.

In the same way as larger grain size affects the tensile capacity of ice, the same holds for the specimen size. Observations indicate that a larger body will have lower tensile strength than a smaller one. This could be explained by the statistic probability of crack existence in the body increasing with its size (Schulson and Duval 2009, p.353).

According to Løset et al. (1998, p.56), LEFM produces good results as long as the size of the damaged zone is smaller than the size of the crack and the floe thickness. This becomes clearer if we remember that Griffith doesn't take creep and initiation of new cracks into account in his linear elastic fracture mechanics model. All dissipation of energy through inelastic work other than creation of new surface is neglected by LEFM.

Elaborating on the derivation of the previous equations in this chapter, it becomes clear that one of the most important assumptions of LEFM is that there exists a single (one) predominant crack prior to loading, and that it's only this crack that will grow during the interaction scenario. Although applicable under controllable conditions in the laboratory, it's obvious that this seldom will be the case in nature. The thermal history of the ice floe will most likely have produced several cracks, with no guarantee that only one of them will dominate during eventual splitting of the floe. LEFM could only predict the propagation of cracks once no longer in the nucleation-controlled domain. Hence, LEFM is not capable of predicting the creation of the crack itself.

Schulson and Duval (2009, p.190) state that linear elastic fracture mechanics is suitable for fast crack propagation through ice, due to the domination of energy dissipation from formation of new crack surface. For splitting of ice floes, Bhat (1988) indicates the crack velocity for sea ice to be in the order of 666 m/s. Observations by Lubbad et al. (2012) indicate that the uncontrolled crack propagation velocity could be as high as the dilatational speed of sound in ice. Dependent on Young's modulus this implies the velocity to be in the range 1-3 km/s. Eq 4-6 is shown as an example for the choice of Young's modulus in Section 2.10. LFM should therefore be appropriate for evaluation of splitting of ice floes.

$$c_d = \sqrt{\frac{E}{\rho_i}} = \sqrt{\frac{3 \cdot 10^9 \text{ N/m}^2}{920 \text{ kg/m}^3}} = 1806 \text{ m/s} \quad \text{Eq 4-6}$$

However, according to Løset et al. (2006, p.64) linear elastic fracture mechanics is a conservative approach, as no dissipation other than creation of new surface is incorporated in the model. In addition to this, they claim that LFM is the most commonly used method in fracture mechanics of ice this far. The question could then be whether non-linear fracture mechanics, like the cohesive zone method (Subsection 4.4.7), would prove significant improvements to the accuracy of ice load predictions.

4.4.2 Fracture toughness of ice

There are many different measurement methods available to identify the fracture toughness of ice, and they seldom give the same values (Schulson and Duval 2009, p.198). However, the ones obtained in the laboratory seem to be represented in the area close to values of 100 kPa√m, with only a weak dependency on temperature, as shown in Figure 4-7.

Despite claimed to be an independent material parameter, the concept of fracture toughness is strictly connected to the situation of LFM with no other dissipation of energy than new surface creation. In the laboratory tests, the effect of creep and nucleation of new cracks are excluded. For full-scale crack propagation of ice in nature, these dissipative processes could not be eliminated, and hence, they will affect the apparent fracture toughness. Chapter 2 illustrates that the mechanical properties of sea ice to a large extent are defined by other factors than the pure ice itself. Therefore, the comparison between lab-scale and in-situ tests is anything but straightforward.

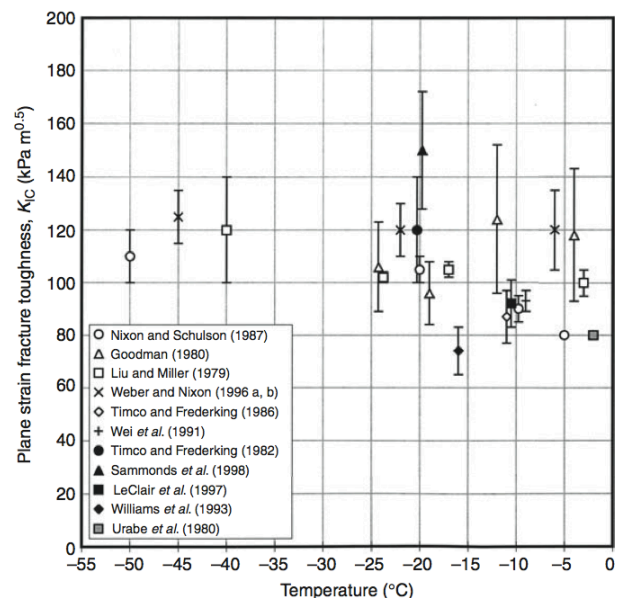


Figure 4-7 Fracture toughness of ice as function of temperature (Schulson and Duval 2009, p.199)

Regarding size dependency, the fracture toughness of ice seems to be dependent on the size of the body in the opposite way as tensile stress capacity. While tensile strength seems to decrease with increasing size, fracture toughness appears to increase. Scientists disagree about this effect, but it's reasonable to believe that it might be caused

by loading conditions other than those required for LEFM. With increasing specimen size, the rate of loading required to obtain brittle failure increases as well (Section 2.7). The size effect, apparent in Figure 4-8, could then be explained by the observations of Nixon and Weber (1983) of increased toughness by decreased loading rate (Figure 4-9).

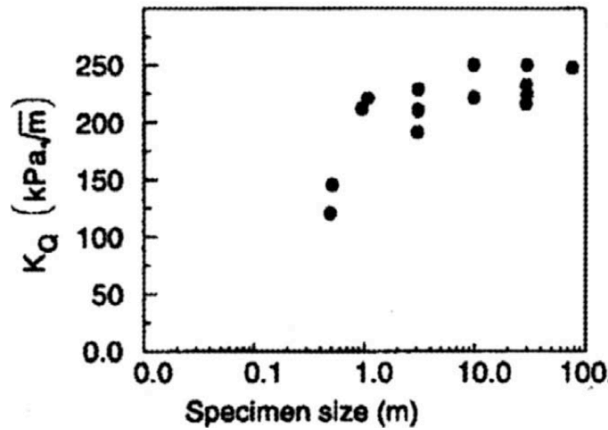


Figure 4-8 Apparent fracture toughness as function of specimen size (Schulson 2012, results of Dempsey)

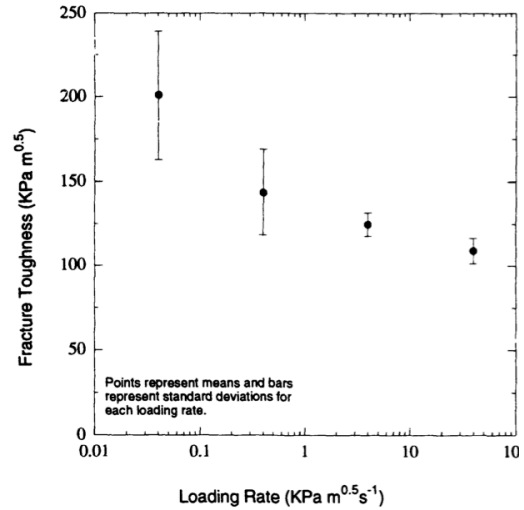


Figure 4-9 Variation of toughness with loading rate for columnar freshwater ice (Nixon and Weber, 1993)

Porosity is another factor that highly influences the fracture toughness of ice. Schulson and Duval (2009, p.202) show that increasing amounts of air and brine in ice reduce its corresponding fracture toughness proportionally. Despite presenting the relationship as a qualitative truth, they argue that the quantitative results might not be correct. Assuming that the suggestion of $K_{Ic} = 100 \text{ kPa}\sqrt{\text{m}}$ from Figure 4-7, obtained with non-porous, fresh water ice holds, Schulson (2012) claimed that the results in Figure 4-10 might be exaggerated by a factor of two. The fracture toughness at a given level of porosity (fraction of air and brine volume) can thus be expressed as in Eq 4-7.

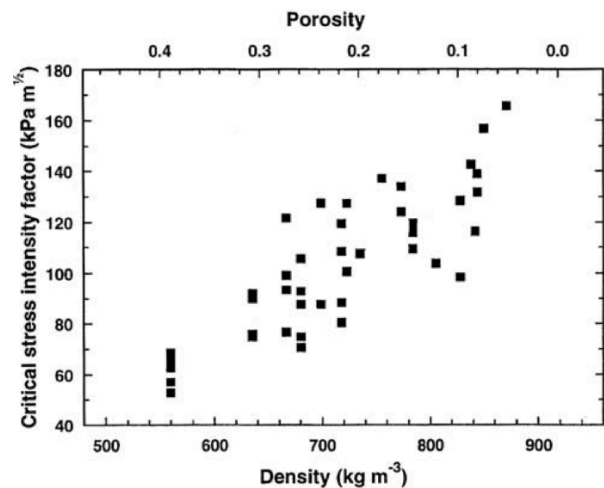


Figure 4-10 Plain strain fracture toughness as function of porosity (Schulson and Duval 2009, p.202)

$$K_{Ic}(\eta) = K_{Ic}(1 - \eta), \quad \text{Eq 4-7}$$

Generally there are two schools when it comes to material parameters of ice, and this is especially true for the fracture toughness. Although indisputably observed that larger ice floes seemingly have lower capacity than smaller specimens on the laboratory scale (Sanderson, 1988), the discussion regarding whether this observed size effect is an inherent property of ice, or if the effect is caused by dissimilar loading and boundary conditions. On the one side, Mulmule and Dempsey (1999) argue that there exists a size effect through that the “fracture toughness values measured at a lab scale may very well not be material properties”, but that observed behaviour from large-specimen tests should define the basis for analyses. On the other side, Timco and Weeks (2001) claims

that the observed size effect is due to inconsistent loading conditions rather than being an inherent property of the ice.

Timco and Weeks (2010) gave the values for the fracture toughness in terms of those who do believe (250 kPa√m) and those who don't believe (115 kPa√m) in the size effect. They also explain the larger fracture toughness results of Dempsey et al. (1999) by work contribution from creep deformation, due to the low rate of loading at which the experiments were performed. There are several scientists that support the concept of size effect in other materials (Bažant, 2000), but to this day there are still controversies regarding the size effect in the ice community. On the same basis as Timco and Weeks (2010), Schulson and Duval (2009) concluded their comprehensive book on Creep and Fracture of Sea Ice with the following quote:

“Our sense at this juncture, therefore, is that the evidence for scale independence is stronger than the argument against.”

4.4.3 Compressive splitting of ice

Ralston (1981) was among the first to examine splitting of ice floes, with the aim to present results and calculation procedures for splitting of ice in general. His experiments were based on fresh water ice, but although the properties of sea ice are quite different, the principles are still transferable.

By considering orthotropic S2 ice, Ralston (1981) obtained an upper bound, plane stress failure criteria (Eq 4-8) for his splitting analysis. Taking into account the material symmetry, only four independent material constants (a_i) need to be determined in order to express the plastic yield criterion.

$$f(\sigma) = a_1(\sigma_x^2 + \sigma_y^2) + a_3(\sigma_x - \sigma_y)^2 + a_6\tau_{xy}^2 + a_7(\sigma_x + \sigma_y) - 1 \quad \text{Eq 4-8}$$

The Brazilian test could be applied for determining the material parameters for ice in Ralston's model. The logic behind this test is to create tensile stresses in a cylinder test specimen by loading it compressively along a diameter. This is in accordance with Løset et al. (2006, p.136), claiming that it's the lateral stresses, set up by the structure penetrating into the ice, that induce tensile stresses around the interaction point (see also Figure 4-6). Due to the principle of principal stresses, these tensile stresses will act perpendicular to the loaded diameter.

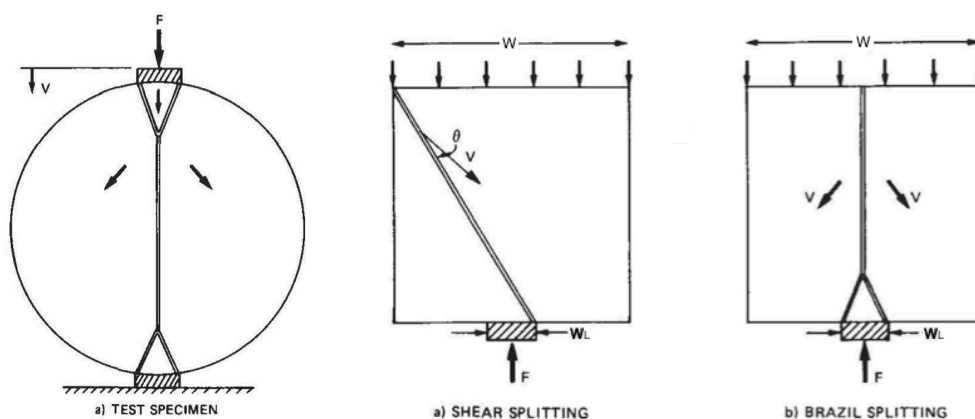


Figure 4-11 Brazilian test failure geometry and velocity fields, for circular and quadratic floes (Ralston, 1981)

Through the Brazilian test, Ralston (1981) discovered that the failure mode of an ice floe was highly dependent on the relationship between the width of a quadratic floe (W) and the width of the indenter (W_L , Figure 4-11). For ratios of *floe width* six to eight times the *width of the indenter*, the floe would fail in crushing instead of Brazil splitting, as seen in Table 4-1. Ralston (1981) puts emphasis on that the terms “warm ice” and “cold ice” are more a feeling he had than exactly measured temperatures.

Table 4-1 Transition between failure modes for thin ice sheets after Ralston (1981)

W/W_L	Warm ice (>-10°C)	Cold ice (<-10°C)
>6	Crushing	Crushing
3-6	Brazil splitting	Crushing
0-3	Shear splitting	Brazil splitting

Ralston (1981) explains the transition with the size dependent confinement exerted by the quadratic ice floe. He claimed that for wide floes, the forces from the indenter would not be affected by the floe boundaries. Hence, localized crushing will be the only available dissipative mechanism. One interpretation of this statement is that the stress field the indenter causes in the floe must be able to reach the floe perimeters in order to cause splitting failure. In Figure 4-11 this stress field is illustrated as constant stress distributed on the far side of the floe, but as Ralston (1981) emphasizes, the shape of this stress distribution is arbitrary - it does not affect his results.

Splitting through compressive shear failure can occur, as evident from Table 4-1. However, Ralston (1981) also discovered that larger floes would have a tendency to require higher loads for this mode than for tensile splitting. Further, colder (more brittle) ice will increase the probability for tensional instead of shearing failure.

Worth mentioning is that Schulson and Duval (2009, p.213) claim that the spatially varying stress state imposed by the Brazil test lead to underestimation of the tensile strength, if compared with uniaxial loading experiments. This could be taken as an argument for not considering uniaxial tensional strength in the case of Brazil splitting.

4.4.4 Tensile splitting of rectangular ice floes

Bhat (1988) states that it is the initiation and propagation of radial cracks that causes splitting of ice floes. He further emphasizes that these radial cracks, originating in the structure-ice contact area, need to run through the whole thickness of the floe in order to split it. The splitting load required to initiate unstable failure in his experiments, proved to be reached at a level where the crack only represented a small fraction of the total length of the floe.

The results derived from Bhat (1988) are based on impact between a bottom fixed structure of radius (r), interacting with a rectangular level ice floe of length (L), width (W) and uniform thickness (h_{ice}). On the contrary to Ralston (1981), this choice of parameters provides a criterion for splitting as function of the floe aspect ratio, rather than the ratio between the indenter and floe width. Further, he assumes that the length of penetration and the size of the zone damaged by instantaneous crushing are small compared to length of the crack a (commonly noted c in this thesis) and the length of the floe (L), as described in Figure 4-12.

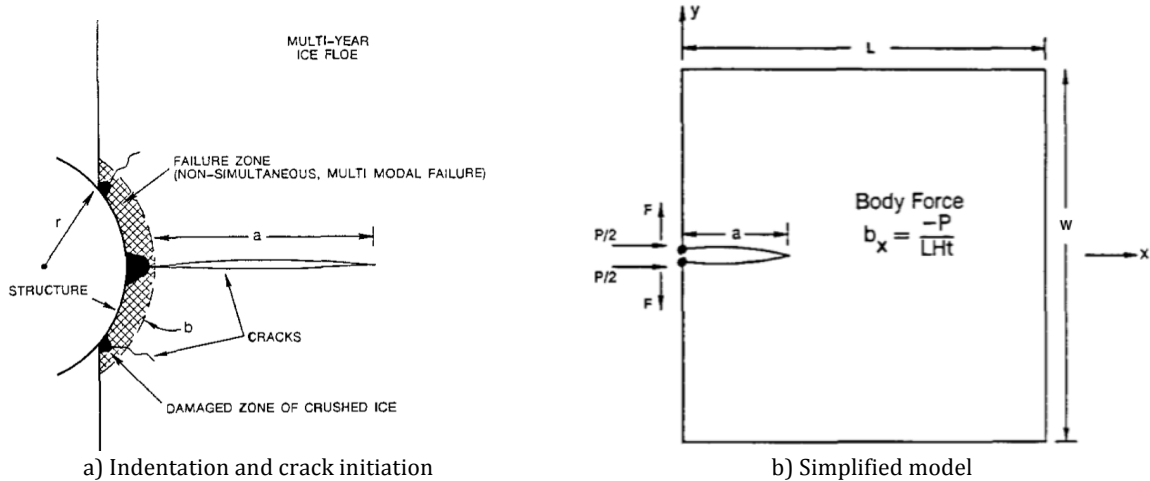


Figure 4-12 Radial cracks propagation model as described by Bhat (1988)

Based on experimental data from Hans Island, Bhat (1988) states that the acceleration of the floe can be modelled as a rigid body, $\ddot{u}(x,y,z)=\ddot{u}_G$. Hence, the impact force (P) is reasonably assumed to be a function of the floe mass and the acceleration of its centre of gravity, according to Newton's 2nd law. The splitting force used to set up the necessary tensile stresses is set to half of the impact force ($\beta=0.5$, ref Eq 4-9), although it is acknowledged that this might be a rather rough assumption considering the diversity of possible ice-structure impact situations.

$$F = \beta P \quad \text{Eq 4-9}$$

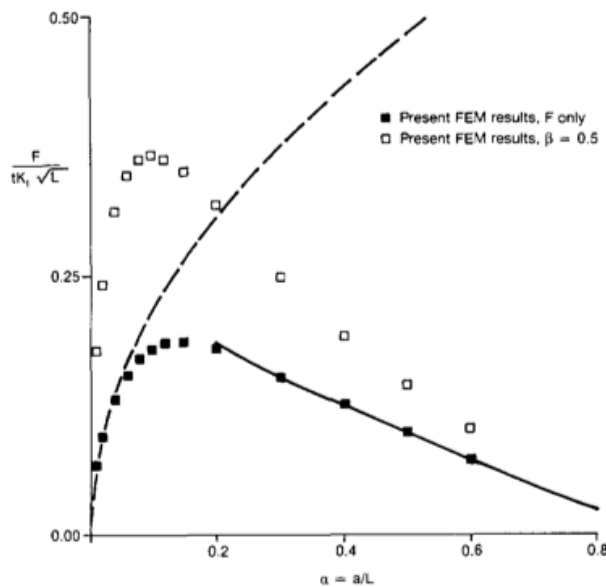


Figure 4-13 Results from Finite Element Analysis for crack tip stress intensity factors. Solid squares are based on tensile loading (F) only. Open squares also include the body force of Figure 4-12 b) (Bhat, 1988)

Bhat (1988) suggests that for $\beta=0.5$, a crack length of more than 10 % of floe length would result in unstable propagation (Figure 4-13), given that the ice behaves as an ideal Griffith elastic-brittle material. This relationship was derived from numerical FEM simulations, and it turned out that the critical impact load for splitting of the floe would be dependent on the floe size according to the following expression (for square floes), as given in Eq 4-11. Worth noticing is that splitting has been observed at loads of only 10-50% of what the model predicts to be the force required to initiate macro cracks that propagates and splits the floe (Bhat et al., 1991). For the case of only tensile loading, the load required for splitting is given in Eq 4-10.

$$P^* (\beta = 0.5) = 0.38 h_{ice} K_{Ic} \sqrt{L} \quad \text{Eq 4-10}$$

$$P (\beta = 0.5) = 0.74 h_{ice} K_{Ic} \sqrt{L} \quad \text{Eq 4-11}$$

The ratio between P and F (Eq 4-9) would in many cases be different from $\beta=0.5$, since it also depends on the ratio between the crack length and floe length ($\alpha=a/L$). Therefore, Bhat (1988) also did a parametric study to determine what would be the upper bound to produce splitting (Eq 4-12). Sodhi and Chin (1995) did the same kind of analysis on their results, and obtained essentially the same expression (where p_{\max} is contact pressure and d is contact width), as shown in Eq 4-13. Both of these include the body force discussed above.

$$P_{\max} = P(\beta = \beta_{\min}) = 3.3h_{ice}K_{Ic}\sqrt{L} \quad \text{Eq 4-12}$$

$$p_{\max} = 3.77\frac{1}{d}K_{Ic}\sqrt{L} \quad \text{Eq 4-13}$$

Sodhi and Chin (1995) assumed $\beta=0.3$ in their analysis setup (Figure 4-14). However, Bhat (1988) based their estimates for the maximum load by an expected value for $\beta_{\min}=1/\pi$ during an impact scenario, hence the limit for splitting obtained by Sodhi and Chin (1995) is expected to be larger, as seen in Eq 4-12 and Eq 4-13.

As seen from Eq 4-11, Eq 4-12 and Eq 4-13, the theoretical critical splitting load is dependent on floe size, through the floe length (L). However, these equations treat isolated, square ice floes, and do not say anything about the dependency between splitting forces and confinement caused by floe length-to-width ratio or surrounding ice. It is rather obvious that the load required to split a floe, would be affected by this ratio. In order to adjust for the lack of confinement dependency in splitting criterion, Bhat (1988) derived the rather useful relationship expressed in Figure 4-15. In this figure, L and W represent floe length and width, as in Figure 4-12.

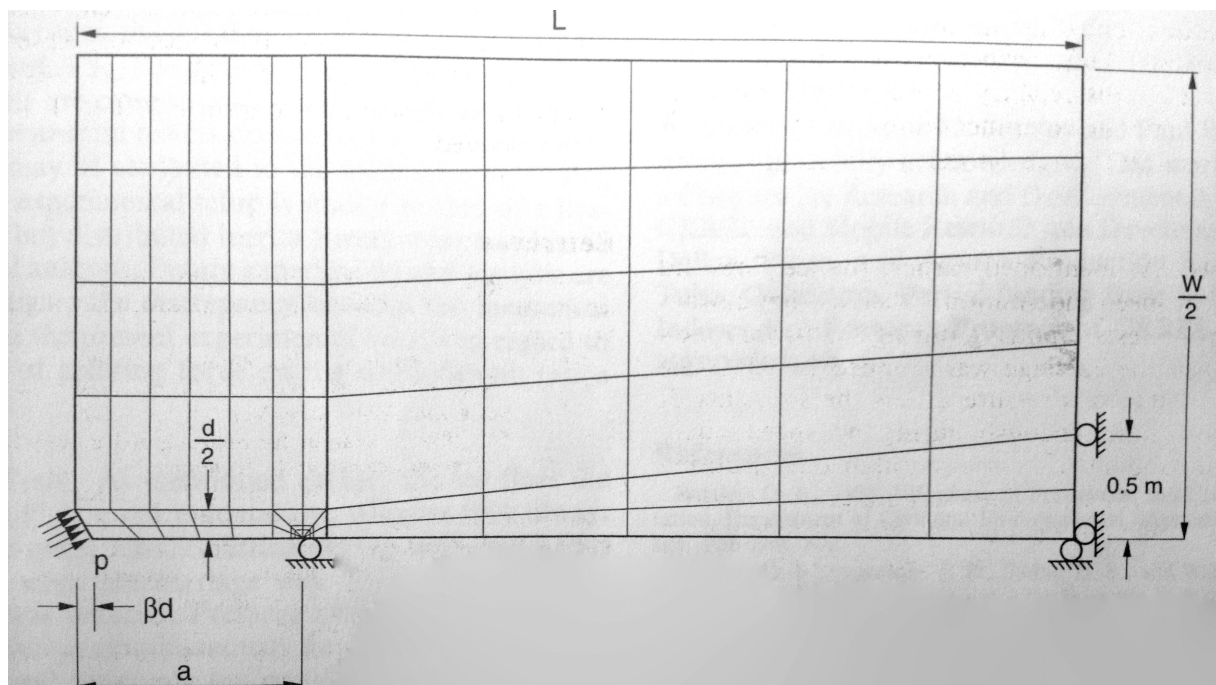


Figure 4-14 Finite element analysis mesh, load and boundary conditions used by Sodhi and Chin (1995)

Based on superposition of the cases of splitting with and without body forces, Bhat (1988) also derived the dependency on aspect ratio. As the width becomes more than twice the length of the floe, the load scale factor approaches infinity. At high aspect ratios splitting will therefore no longer be the mode of failure associated with the lowest required energy, and the floe would tend to fail in crushing or horizontal bending instead (opposed to vertical bending as of Section 3.2). Worth mentioning is that the load scaling factor (\tilde{P}^*) in Figure 4-15 corresponds to that shown in Eq 4-12 ($\tilde{P}^*(\beta_{\min})=3.3$ for a square floe).

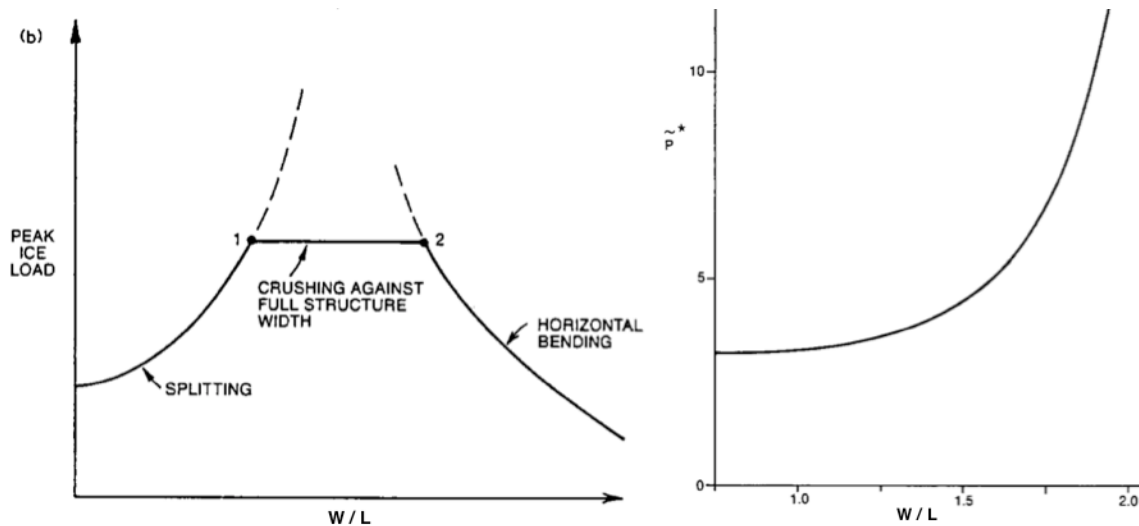


Figure 4-15 Expected changes in failure modes as a function of aspect ratio changes (Bhat, 1988)

4.4.5 Tensile splitting of circular ice floes

Based on Ralston (1981) and Bhat (1988), Bhat et al. (1991) analysed splitting failure of ice floes impacting with fixed Arctic offshore structures. Modelling the floes as edge-loaded, inertia-driven, thin circular disks, they obtained critical splitting loads different from those cited in Section 4.4.4. By treating “failure” as a common term for both plastic yielding and brittle fracture, they suggested that the ice floe should obey the Drucker-Prager failure criterion (Section 4.2) as an upper bound for splitting fracture.

The critical splitting load for the circular discs is similar to what required for rectangular floes. The critical crack-length-to-floe-diameter ratio is somewhat below 10 %, and as the crack length reaches this ratio, uncontrolled rapid fracture of the rest of the floe would occur. Figure 4-16 shows the dependence between the load distribution factor β (Eq 4-9) and the limit for unstable fracture. It should be noted that as β approaches its minimum value of $1/\pi$, the critical crack length to diameter ratio is only 1 % (Bhat et al., 1991).

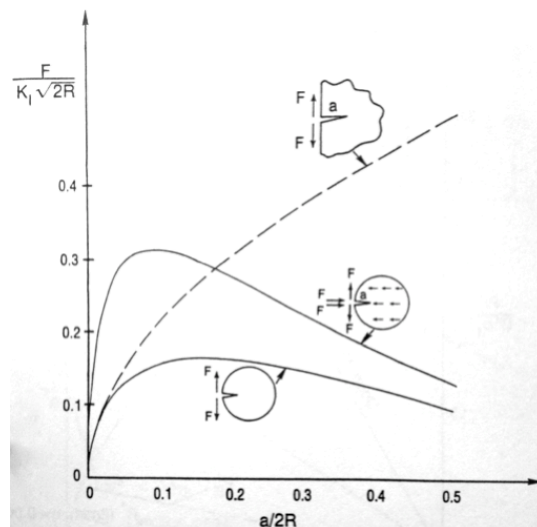


Figure 4-16 Stress intensity factors for an edge crack in a circular floe (Bhat et al. 1991)

In accordance with Ralston (1981), Bath et al. (1991) claim that a brittle material would be within the upper limit case for a plastic, strain softening material. This was obtained by utilizing that plastic instantaneous failure along the full crack path naturally would require a larger load than a propagating crack. The Drucker-Prager yield criterion is thereby established as a viable failure criterion for ice floes. Utilizing their assumption of elastic-brittle constitutive relation, Bhat et al. (1991) state that the ice will behave elastic until crack initiation is indicated by the Drucker-Prager failure criterion. Although admitting lack of consistency, they let the process zone ahead of the crack be governed by regular (mode I) rate-independent LFM and the fracture toughness (K_{IC}), instead of the Drucker-Prager failure criterion. Hence, the latter is only used for determining when and where the initial crack will occur.

Ralston (1981) emphasizes that the contact area or size of indenter is important for the load required for splitting the floe. Considering the contact area, Bhat et al. (1991) confirm this, both in terms of load required for initiation (nucleation) of cracks and propagation to complete failure. They claim that the necessary load for nucleation to dramatically decline as full envelopment of the impacting structure (Figure 4-6) is developed. More precisely, Bhat et al. (1991) specify that the propagative load, where the indenter has obtained full penetration (P_{fp}^*), corresponds to Eq 4-14, while Eq 4-15 would act as an upper bound for the more complicated non-penetrated case (P_{np}^*). Hence, the likeliness for splitting the floe would increase with increased penetration.

$$P_{fp}^*(\beta = 0.5) = 0.62 t K_{IC} \sqrt{2R} \quad \text{Eq 4-14}$$

$$P_{np}^*(\beta = \beta_{min}) = 3.0 t K_{IC} \sqrt{2R} \quad \text{Eq 4-15}$$

It's also important to consider that the results obtained by Bhat et al. (1991) indicate that it's nucleation, not propagation, is the governing criteria most difficult to fulfil for splitting in the Arctic. This could imply that nucleation is the governing criteria for splitting loads on structures. Utilizing Drucker-Prager (Section 4.2) with $m=2.5$ and $m=5$, in the full penetration case, it could be shown that the force required to nucleate a tensile crack is given in Eq 4-16 and Eq 4-17, respectively.

$$P = 2.1 \cdot h_{ice} r_s \sigma_t \quad \text{Eq 4-16}$$

$$P = 2.6 \cdot h_{ice} r_s \sigma_t \quad \text{Eq 4-17}$$

Equating the force required for propagation in Eq 4-14 compared to the nucleation requirement in either Eq 4-16 or Eq 4-17, with parameters of $K_{IC}=115\text{kPa}\sqrt{\text{m}}$, $h_{ice}=1\text{m}$, $R=1000\text{m}$, $r_s=15\text{m}$ and tensile strength of 300 kPa, it's clear that the process is nucleation controlled. These likely values correspond well to the values suggested by Bhat et al. (1991). Hence, they discuss splitting for indenter-to-floe width ratios that by far exceed the limits suggested by Ralston (1981). However, Bhat et al. (1991) don't necessarily disprove Ralston (1981). Where Bhat et al. consider the case where the ice floe already is penetrated by the structure, Ralston only considers the non-penetrated case of the Brazil test.

4.4.6 Indentation speed dependence for splitting of ice

Performing indoor basin tests on unconfined freshwater ice, Sodhi and Chin (1995) claimed that splitting ice floes at drift speeds higher than 100 mm/s is prevented, “*the main difference between the results of low-speed and high-speed tests is the occurrence and the non-occurrence of floe splitting*”. The reason for this, they postulate, is that high indentation speeds lead to brittle crushing and spalling of the ice, in a manner that dissipate energy to an extent that prevents the necessary splitting load to be reached.

The results seem to concur with those obtained by Ralston (1981) and Hallam (1986). According to observations by Hallam (1986), higher strain rates would produce brittle behaviour. Utilizing that colder ice also imply more brittle ice, Ralston (1981) could be interpreted to claim that more brittle ice is more likely to crush rather than split (see Table 4-1). However, Sanderson (1988, p.209) states that for ice floes in the Arctic, cracks could nucleate at stresses below 1 MPa for slow loading rates, or in other words when cracks are allowed to develop as a function of accumulated delayed elastic strain.

Higher drift speeds should, due to increased momenta, also provide higher impact forces. In that case, the observations by Sodhi and Chin (1995) seem to oppose what stated by Bhat et al. (1991), where higher impact loads are what drive the crack propagation behind the “damaged area”. What could cause this discrepancy is the fact that for their tests, Sodhi and Chin used different aspect ratios for their floes while testing impact between structure and ice floe with fast and slow indentation speeds. The dimensions for the tests were as follows:

Slow (0.2-8 mm/s): $H = 8$ m, $W = 4.5$ m, Fast (>100 mm/s): $H = 6$ m, $W = 30$ m

Given that Eq 4-12 is satisfactory for calculating the required splitting load, and that cracks would nucleate, the force required to produce failure by propagation would be lower in the slow case compared to the fast one. This implies that it might as well be the difference in specimen size, and not the difference in indentation speeds that resulted in different failure modes for the experiments done by Sodhi and Chin (1995).

It’s tempting to explain the divergence of Sodhi and Chin’s (1995) observations of splitting at lower and non-splitting at higher indentation rates with the difference in test setup for these two cases. Further, another important aspect of these results is that they only performed two tests in the case of high indentation speeds, and that the reliability of these data therefore could be questionable.

Still, it’s interesting to observe that the description of the splitting at lower speeds happened at 11.5 m of the 30 m long floe with 75 % of the initial 100 mm/s indentation speed. This could imply that the rate of indentation in the fast case actually was too high to achieve splitting, and that there under some circumstances exist an indentation rate upper bound for splitting. On the other hand, another interpretation would be that crack length to floe length ratio only proved to be high enough for splitting to occur when the floe length had decreased to less than 20 meters. In that case, the fact that they slowed the speed down in this domain could have produced a false evidence of splitting dependent on velocity.

Sodhi and Chin (1995) conclude that their results are transferable to in-field conditions, and that one should expect brittle flaking for indentation speeds of more than 100 mm/s, due to the fact that this failure mode will prevent the necessary splitting force to build up. Although no more than speculations, the introduction of a given indentation speed as an upper limit for nucleation could also have important implications for understanding of splitting. Lubbad et al. (2012) have observed splitting for an icebreaker advancing in ice at considerably higher indentation speeds than the limit described by Sodhi and Chin (1995). If the indentation speed limit is to be trusted, this could be taken as an argument for that in-field splitting, at typical impact velocities for a ship, would not occur unless pre-nucleated cracks are present in the ice. Still, there's an important difference in the fact that Sodhi and Chin (1995) considered splitting as of Figure 4-6, while the splitting in the case of Lubbad et al. (2012) was a result of propagation of one of the radial cracks resulting from bending (Figure 3-7).

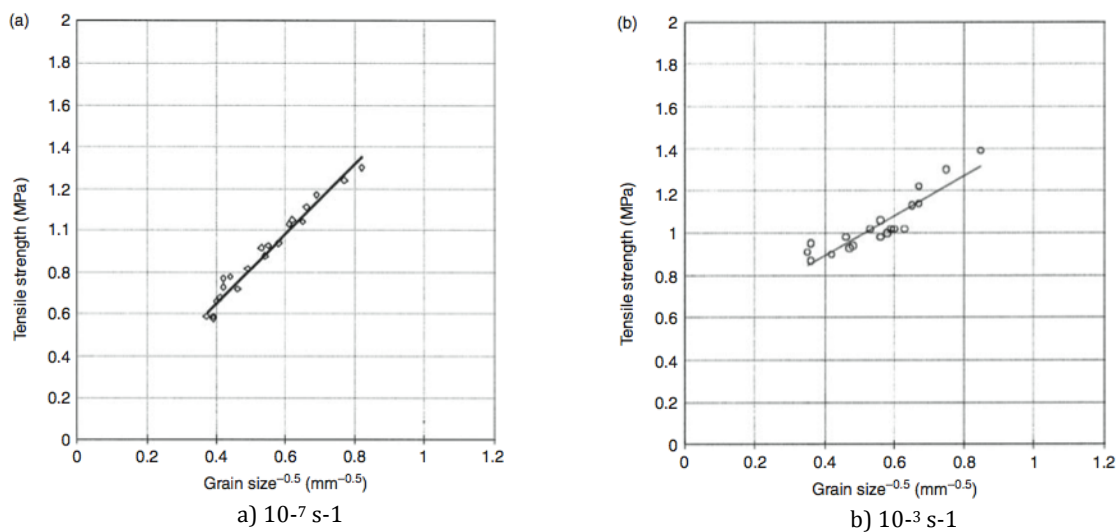


Figure 4-17 Tensile strength of freshwater granular ice at strain rate and (Schulson and Duval 2009, p.220)

The graphs from Figure 4-17 correspond to Eq 4-18 (Figure 4-17 a)) and Eq 4-19 (Figure 4-17 b)) accordingly. Worth mentioning is that the constants in the latter expression increase with increasing strain rate. The values are obtained for bubble free freshwater ice, and need to be adjusted for sea ice. Note that the values here differ somewhat from the corresponding values for the same expression in Eq 2-6, and illustrate the uncertainties when dealing with material properties of ice.

$$\sigma_i = \frac{K}{\sqrt{d}} = \frac{0.052 \text{ MPa } \sqrt{m}}{\sqrt{d}} \quad \text{Eq 4-18}$$

$$\sigma_i = \sigma_0 + \frac{k_i}{\sqrt{d}} = 0.52 \text{ MPa} + \frac{0.030 \text{ MPa } \sqrt{m}}{\sqrt{d}} \quad \text{Eq 4-19}$$

Given the above discussion, it's interesting to notice that the crack propagation, reported from the fast indentation test by Sodhi and Chin (1995), not only did occur after the speed slowed down, but also in the vicinity of a crack existing prior to the test. This could further strengthen the argument that crack propagation observed when ships advance in ice at high (>100 mm/s) speeds is due to the occurrence of pre-existing cracks, opposed to nucleation during the ice-ship impact scenario.

4.4.7 Cohesive zone method for splitting of ice floes

While the cohesive zone method (CZM) has been widely used in the consideration of splitting in other materials, it's not until recently this approach has been used to determine actions from ice. Mulmule and Dempsey (1998) derived a traction-separation relationship for ice, based on the fictitious crack model of Hillerborg et al. (1976). Instead of using linear elasticity, they found it necessary to utilize viscoelastic behaviour, due to the observed inadequacy of LEFM for large-scale in situ fracture tests. The most important LEFM-invalidation factor was the creep micro cracking ahead of the crack, associated with the slow strain rate applied. Although Mulmule and Dempsey considered viscoelastic material, it's important to notice that this is no prerequisite for the use of CZM. One could, as Barenblatt (1962), assume that the body as linearly elastic until the point of failure.

The viscoelastic fictitious crack model (VFCM) exhibits a highly nonlinear material behaviour. Still, the material parameters required for the VFCM are difficult to obtain, resulting in that Mulmule and Dempsey (1998) needed to base their material constants derivation on LEFM after all. Hence, their resulting stress-separation curve was assumed to be rate independent, although they acknowledge it should be rate of loading. Figure 4-18 depicts this relationship through the *cohesive stress* (σ_{coh}) and the *crack opening distance* (COD).

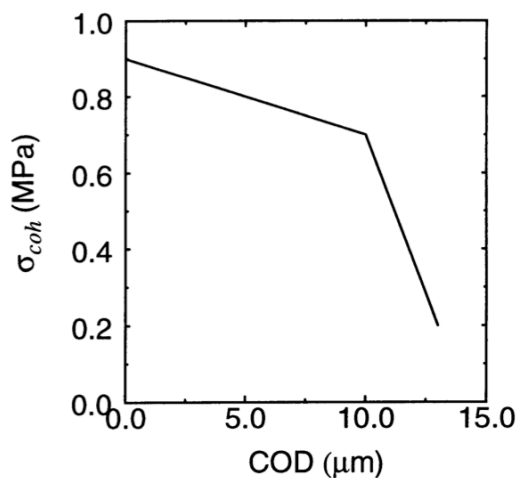


Figure 4-18 Deducted stress-separation curve (Mulmule and Dempsey, 1998)

Mulmule and Dempsey (1999) claim that the stress-separation curve should be considered as a material property. Still, they present the different curves for different specimen sizes (Figure 4-19), providing insight to the size-effect debate, previously discussed in this chapter. Cornec et al. (2003) state that the shape of the traction-separation line is of minor importance compared to the fracture energy, G_c (see Figure 4-4). Hence, they claim G_c to govern the process zone.

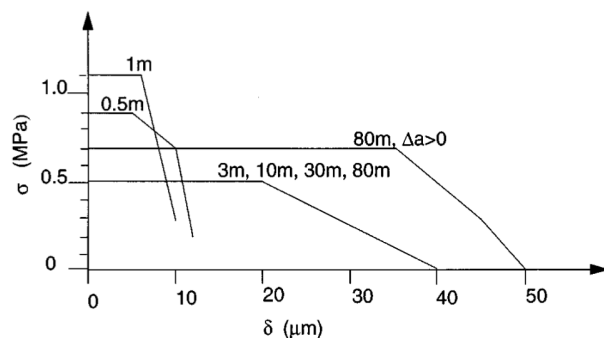


Figure 4-19 Constructed stress-separation curves for various specimen sizes (Mulmule and Dempsey, 1999)

Based on the SIMI'94 field experiments, Dempsey et al. (1999) suggested the fracture energy to be 15 J/m^2 for pre-fabricated cracks in Arctic first year ice, while multi-year ice was reported to $23 < G_c < 47 \text{ J/m}^2$ (Dempsey et al., 2012). Later research performed by Kuutti et al. (2013), disprove Cornec et al. (2003) by performing a 2D mesh sensitivity study for linear, exponential and plastic softening. From this study it became clear that different starting point (e.g. different material softening curve) would produce different results. Lu et al. (2012b) put emphasis on the fact that there are disagreements regarding fracture energy for ice, where Schulson and Duval (2009) questions the values

of Dempsey on the basis of laboratory scale tests, where $G_c=1 \text{ J/m}^2$ is a more common result. Further will calculation of the equivalent γ_c of Ashby's relationship (Eq 4-2) give $G_c=0.13 \text{ J/m}^2$, when the O-O distance of Figure 2-3 and the true elastic modulus of Subsection 2.4.1 are used as input variables.

Regarding the applicability of the fracture energy release rate obtained by Dempsey et al. (1999), there are several concerns. Not only is there a large spread in likely values, but it was also obtained from a single experiment, and it doesn't seem like any similar attempts to obtain the fracture energy release rate have been pursued to this day. Considering what claimed by Elices et al. (2002) on the need for extensive knowledge of the material properties in order to obtain sensible results by use of *Cohesive Zone Methods*, results obtained using CEM on ice should be treated with care.

According to Timco and Weeks (2010), the fracture toughness is directly related to the strain energy release rate (Eq 4-19). Therefore the discussion on the different approaches on how to obtain the fracture toughness is of relevance the consistency of the energy release rate that would be utilized for an eventual analysis.

$$G_c E = K_{IC}^2 (1 - \mu^2) \quad \text{Eq 4-20}$$

The modulus of elasticity for cohesive elements (K_{nn}) is a different concept than for regular bulk material elements (E). Where the elastic curve for a regular material often is given in terms of a stress-strain relationship (σ - ε), the traction-separation curve (σ - δ) of cohesive behaviour implies a different meaning of the stiffness. The latter would be comparable to the stiffness of a linear spring until the failure stress is reached (Eq 4-21).

$$F = \sigma A = E \varepsilon A = EA \frac{L - L_0}{L_0} = \frac{EA}{L_0} \delta \Rightarrow \sigma = K_{nn} \delta, \quad K_{nn} = \frac{E}{L_0} \quad \text{Eq 4-21}$$

Lu et al. (2012a) performed a comparative study of Element erosion, the Cohesive Element Method (CEM), the Discrete Element Method (DEM) and the Extended finite element method (XFEM) for the case of modelling bending failure by the means of CZM. In their study, performed with linear softening for $G_c=15 \text{ J/m}^2$, they concluded that XFEM still is in its development; DEM is very computational expensive; Element erosion is largely dependent on the applied constitutive model and suffers from mass imbalance; while CEM, as for element erosion and DEM, is mesh dependent due to the requirement of on-element boundary cracks. This serves as an argument for using CEM for further investigations on splitting of ice floes.

Konuk et al. (2009a) utilized CEM for a study on dynamic ice-structure interactions. They claimed that for an ice floe impacting a cylinder, "*the effect of the parent boundary conditions for the coupled model's ability to actually simulate continuous crushing is noteworthy*". As seen from Figure 4-20, splitting-like behaviour is present in the model considering a finite floe, while only crushing is present in the infinite floe simulation. Conclusions could be taken to indicate that they as well could have observed through thickness splitting of their floe, if appropriate boundary conditions, floe aspect ratio, loading rate and constitutive model had been applied.

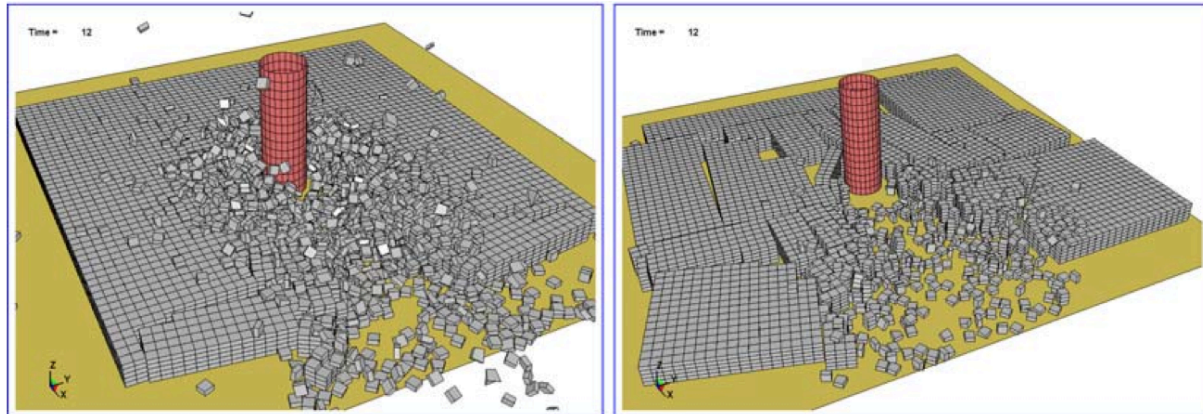


Figure 4-20 Illustration of cohesive element results for infinite (left frames) and finite (right frames) ice floe simulations at the same instance of simulation time (Konuk et al., 2009a)

Lu et al. (2012b) presented another viable discretization method, where triangular bulk elements are separated by thin cohesive elements (Figure 4-21). The main advantage with this method compared with the one developed by Konuk et al. (2009a) is that cracks also will be able to propagate in a 45 degree manner, without the need to travel $\sqrt{2}$ times the real length “around” the brick elements, leading to extra surface energy consumption. Hence, this improvement is of significance for splitting purposes.

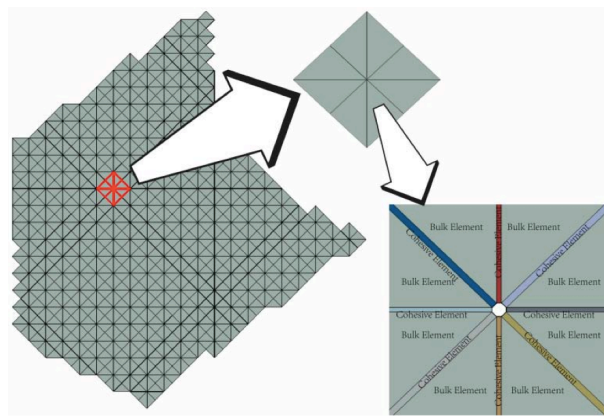


Figure 4-21 Cross triangle structured mesh pattern (Lu et al., 2012b)

Regarding energy convergence, which often is the problem associated with the mesh dependency continuously reported for the cohesive element method, Lu et al. (2012b) examined three different contra measures. The first was to refine the mesh of the 3D-model using homogenous material property. However, they concluded with this practically being out of reach by means of ordinary computer power of today. Secondly, they performed simulations with a randomized fracture energy field in order to facilitate fracture localization. This approach was found to give convergence much faster than the homogenous alternative. Lastly they indicated, that using the bulk energy dissipation described by Bažant and Planas (1998) to obtain a *mean fracture energy* for the cohesive zone could be obtain mesh objectivity for their mesh pattern (Figure 4-21).

Although both the model of Konuk et al. (2009a) and Lu et al. (2012b) probably could have been used for investigation of splitting as a load releasing mechanism for floaters in ice, there is, to the author’s knowledge, still not presented any sound approach for using CEM to model splitting of level ice floes in the literature. This could be due to that the advantage over LFM in representing both crack initiation and propagation would be counterbalanced by the uncertainties related to the cohesive constitutive model through the fracture energy release rate.

5 Breakdown structure for problem approach

The motivation for choosing “splitting as a load releasing mechanism for a floater in ice” as the topic for the thesis was, as stated in the introduction, to contribute to the further development of the numerical model for real-time simulation of ship-ice interactions by Lubbad and Løset (2011). As seen in Figure 5-1, splitting is one of several modes of failure not yet implemented in their *Mathematical Ice Model*.

What also is evident is that the model treats interaction between a ship and a floe differently regarding if the floe is treated as breakable or unbreakable. As will be shown in Chapter 6, this criterion haven't been given too much attention earlier. The unbreakable-criterion is of importance in order to reduce the computational expense spent on obtaining internal stresses of floes that never will be subject to other modes of failure than rigid body motion (and edge crushing). In order to implement treatment of splitting and other modes of failure for the ice, a well-defined selection mechanism for unbreakable floes should therefore be in place. Since the purpose of the criterion is to save computational expense, it's obvious that the selection mechanism itself must be computationally inexpensive.

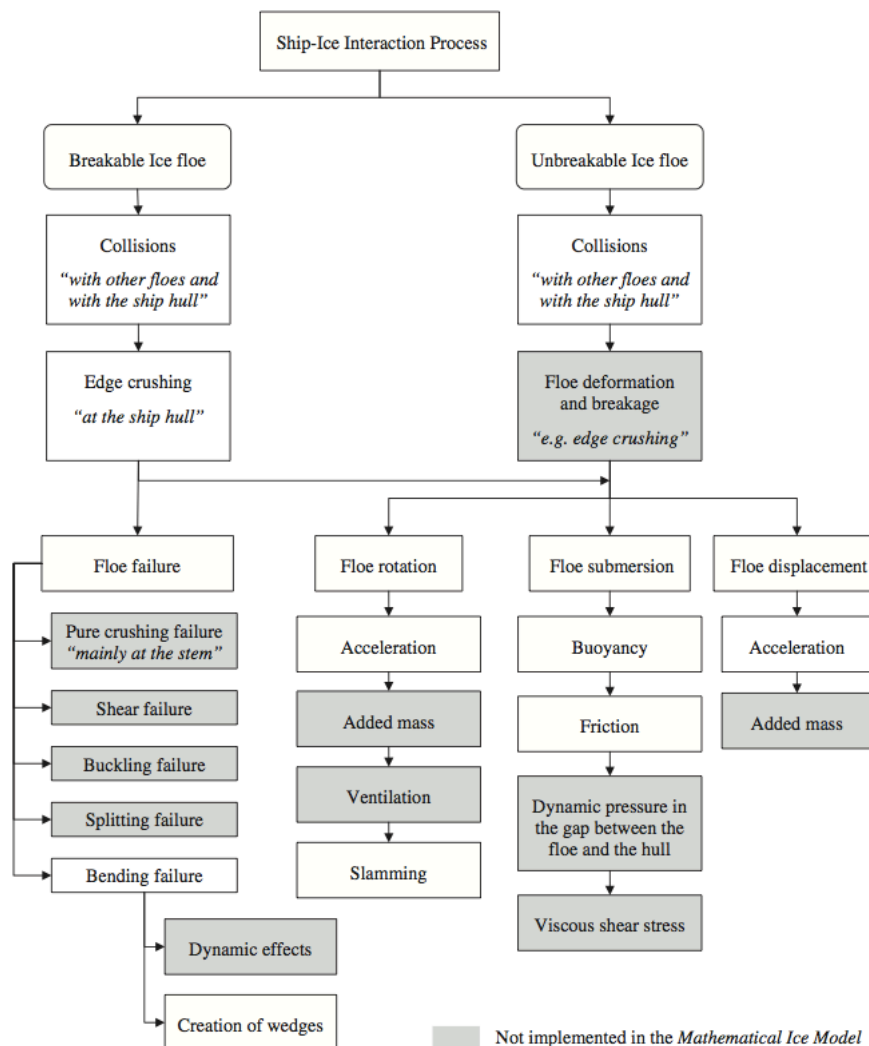


Figure 5-1 The processes that take place during the interaction between ship and ice. The major processes are modelled in the simulator. The minor processes are shown in grey colour. (Lubbad and Løset, 2011)

In order to approach the complex phenomenon of splitting as a load releasing mechanism for a floater in ice, the problem was structured as depicted in Figure 5-2, which also serves as a relevant algorithm for implementation of splitting in the numerical model for real-time simulation of ship-ice interaction developed by Lubbad and Løset (2011).

The initial intention for the work flow of this thesis was to define if a floe is breakable; determine when closed form analytical solutions for stress calculations in plates and beams are applicable for determining the stresses in the floe; and determination of whether a produced radial crack will propagate and split the floe or if cusp/wedge failure would occur instead.

The reason for including the criterion for beam or plate in the scope is the need for efficient calculations of bending failure of the ice floe. By also verifying the applicability of existing closed form analytical expressions for obtaining the critical internal stresses of an arbitrary beam or plate, one would provide valuable insight to real-time simulations of bending failure and crack initiation. However, this scope proved to be too large for the limited time available for this thesis. Therefore, the question of whether a given floe would behave as a beam or plate is left to later research.

The breakdown structure depicted in Figure 5-2 clearly shows the criteria that need to be developed for sound implementation of splitting failure. Several of these will not only be important in order to provide insight to the conspicuous phenomenon of splitting, but also prove to clarify important aspects in relation to the numerical model for real-time simulation of ship-ice interaction developed by Lubbad and Løset (2011). The full criterion for splitting is not derived, but the phenomenon is examined, and recommendations for future research are made.

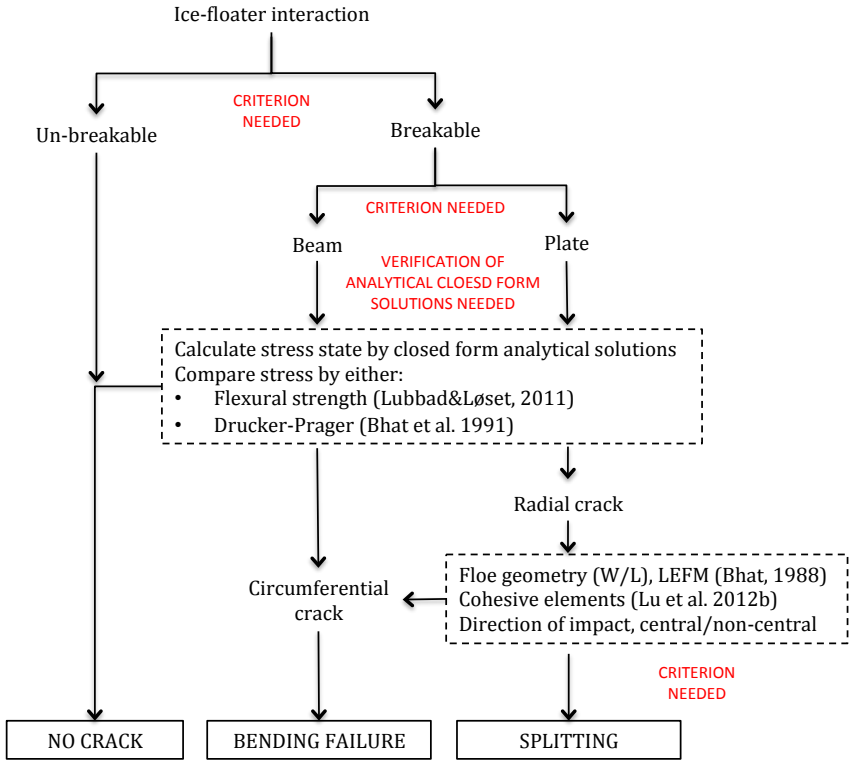


Figure 5-2 Breakdown structure for ice-structure interaction that show how splitting may be determined

6 A criterion to determine if an ice floe is breakable or unbreakable

This chapter will present two new approaches to estimate the criterion for an unbreakable floe. One method rooted in analytical solutions, based on decoupling of the modes of motion; and another, more comprehensive approach, through use of the commercial finite element software *Abaqus 6.12-1*. Thereafter, the methods are compared and finally a criterion for unbreakable ice floes is presented.

The idea of determining if an ice floe is breakable or unbreakable originates from the desire of developing a real-time simulator for ice-structure interaction (Lubbad and Løset, 2011). During an impact scenario the structure will likely be in contact with several floes of varying size, and the vast amount of calculations necessary for each time step represents a major challenge. Being able to instantly determine whether each of these floes will be subject only to rigid body motion, and hence the avoiding calculations of irrelevant internal floe stresses, would reduce the computational expense significantly. A simple and robust criterion to determine whether a floe is breakable or unbreakable is therefore vital to the performance of real-time ship-ice interaction simulations.

Increasing computational efficiency in order to enable complex ice structure analysis is the motivation for development of the criterion, which implies that the criterion itself should be easy to evaluate. While treating an unbreakable floe as breakable would be computationally expensive, treatment of a breakable floe as unbreakable would produce erroneous results invalidating the simulation. The main challenge in defining a viable criterion is therefore to make sure that no floes that are *breakable* is treated as *unbreakable*, while as few unbreakable floes as possible is treated as breakable, as shown in Figure 6-1. A more conservative solution would therefore imply additional computational expense.

	Treated as breakable	Treated as unbreakable
Breakable ice floe	As intended	Not acceptable
Unbreakable ice floe	Computationally expensive	As intended

Figure 6-1 Challenges considering development of a criterion for unbreakable floes

6.1 Previous approaches

The literature is not rich in terms of suggested approaches or variation in criteria for breakable or unbreakable ice floes. An important factor to explain the lack of relevant theory is that it's only with the later years development of computational power that real-time simulations of ship-ice interaction have become feasible (Lubbad and Løset, 2011) – and so far it's only for this purpose the criterion has been desirable. There are, to the author's knowledge, only two previously proposed criteria for determination of unbreakable ice floes.

Lubbad and Løset (2011) developed a real-time simulator for ship-ice interaction. In their model they took advantage of considering ice floes as breakable or unbreakable. However, they did not investigate the criterion any further than claiming that a floe with

lateral area less than the thickness squared should be treated as breakable. In addition, they assumed that floes broken off from a continuous ice cover also would be unbreakable. The main disadvantage with such a criterion is that that this obviously will require calculation of stresses in unnecessarily many floes, for other conditions than interaction with a continuous cover of level ice.

Hovland (2012) developed the criterion further. She estimated a breakable-unbreakable criterion by analysing the behaviour of edge-loaded beams on elastic foundation. Her conclusions were that the critical length for a breakable floe with thickness of 1m would be approx. 20 m. For 1m thick beams, supported on Winkler foundation and vertically loaded at one end, Figure 6-2 imply that the critical length would decrease with increasing effects of inertia. For information on inclusion of the inertia effects, see Evans and Parmeter (1985).

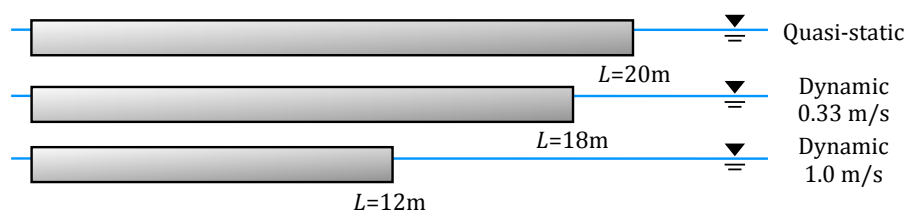


Figure 6-2 Solutions for when a floe, of $h_{ice}=1\text{m}$, can be considered unbreakable (after Hovland, 2012)

Although the observed effect of inertia is of interest, a major drawback with the approach of Hovland is that she only considers deflection, hence neglecting the other modes of motion of the floe. The simplification by assuming Winkler-foundation, which prevents rotation of the floe, could also be problematic. Further, her criterion is based on analytical expressions for bending of beams (Hetenyi, 1946), claiming that the floes would be unbreakable as the deflections exceeds half of the ice thickness, possibly violating the underlying assumption of small deflections. Hence, the rather arbitrary criterion for a floe to be unbreakable is defined by the deflection of the far end of the floe (y_b) to be more than or equal to half the ice thickness. Invalidity of beam theory doesn't necessarily imply that the floe would be prevented from breaking.

6.2 Decoupled approach by analytical expressions

Instead of singlehandedly base the criterion on the stresses in a floe, as done by Hovland (2012), a different approach is proposed. By considering the forces exerted on the floe during ship-ice interaction, and comparing the forces needed for the floe to displace through rotation, surge or bending, one could determine a dependence on length and thickness that together will constitute the criteria for an unbreakable ice floe. These three modes of motion will always be coupled for ice-structure interactions in nature, but as a simplification they are here treated as decoupled events (Figure 6-3). The governing domain for the force required to obtain terminal condition of each mode (angle of rotation, velocity or flexural stress) is what will constitute the criterion.

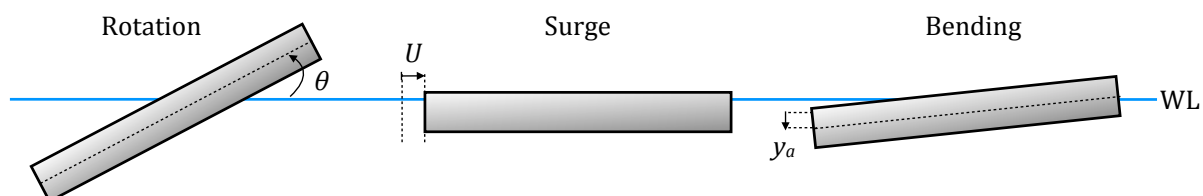


Figure 6-3 Decoupled motions of movement for an ice floe interacting with a floating structure

The results of the three uncoupled modes are defined by the relationships between the ship-ice contact force and *rotation*, *surge* and *bending* of the floe, accordingly. In order to obtain a criterion for unbreakable ice floes, these relationships must be compared and examined, as will be shown in Subsection 6.2.4. Important to notice are the restrictions imposed on the floe in each case in order to obtain sufficient boundary conditions for each decoupled mode. For *Rotation*, no movement in surge or deflection due to bending is allowed; for *Surge*, no rotation or bending is allowed; for *Bending*, no surge or rotation other than what naturally follows from reactions in the Winkler foundation is allowed.

In order to obtain equations for parametric studies, analytical solutions are preferred to evaluate the reactions of each mode. Through his seminal work, Valanto (2001) presented analytical solutions for the rotation of a floe; Hetenyi (1946) developed analytical solutions for beams on elastic foundations that could be relevant for ice floes; and the simple case of displacement by surge can be solved by Newton's equations of motion. Hence, sound theoretical foundation for the considered modes already exists.

The assumptions necessary for each mode of motion are stated separately in the following sections. Common for all of them is that effects of added mass and other dynamic effects are left out. For consistency, the "lost mass" of the floe due to crushing of the floe edges is not taken into account either. Valanto (2001) criticize this approach by stating that the "ice failure processes are often treated as static problems in the literature, although velocity effects clearly are of great importance to the result". Still, the errors introduced by static simplification in the development of the unbreakable- criterion, would not be critical. Firstly, the main purpose is not to describe the loads, but to define in what range each mode would be dominant. Secondly, decoupling of the modes would make it problematic to include the dynamic effects in a consistent manner. Hence, static solutions are chosen.

The boundary conditions assumed in this section imply isolated floes, not being in contact with a continuous ice cover or adjacent floes. Further, all the floes are given as squares, in order to make them more representative for circular floes as well. Square floes could imply considering the floes as plates instead of beams. However, the loading conditions, given as loading of the full floe width; partly floe loading; and loading by cone (Figure 6-4), to a large degree decide whether the floe is a plate or a beam. This makes beam theory appropriate for describing actions and reactions of the three uncoupled modes of motion. At least if the representative width (W_L) is not small compared to the floe width (W). For the latter mode of loading, this will not be a problem for floes in the range of the unbreakable criterion (Baratta, 1981).

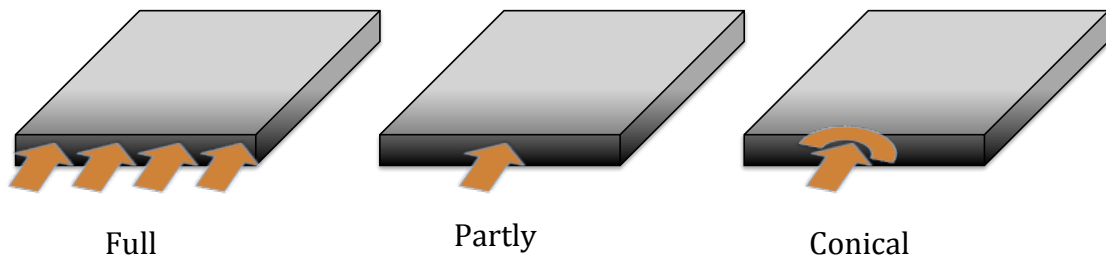


Figure 6-4 Description of different modes of loading

The representative width of loading (W_L) is of importance for further applications in this section, and would to a large degree be decisive for the maximum load the ice floe would be capable to resist.

An assumed loading condition with full or partly (constant) loading width of the ice floe would not be adequate in most cases, as the contact width naturally would increase with penetration. Hence, the loading width varies with the crushing length. Based on the geometric relationship of a circle intersecting a square (Figure 6-5), W_L is derived (Eq 6-1) for the conical interaction described in Figure 6-4.

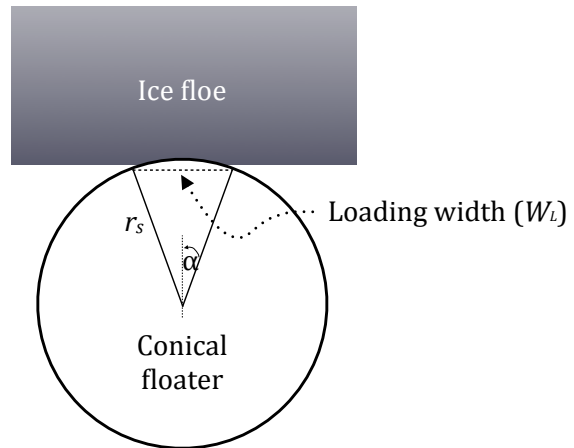


Figure 6-5 Geometric relationship for conical loading

$$W_L = 2\sqrt{r_s^2 - (r_s - v_c)^2} \leq W \quad \text{Eq 6-1}$$

The decoupled analysis described in Subsections 6.2.1, 6.2.2 and 6.2.3 is to a large extent dependent on the potential resistance of the floe at a given time step. The compressive strength of the ice defines what pressure the floe is able to sustain without crushing. Utilizing the compressive strength to define the maximum horizontal force capacity (F_h) for a given crushing length (v_c), the hull inclination angle (ψ) and the geometric relationships derived in Figure 6-6 would automatically give the corresponding vertical (F_v) and normal-to-hull contact force (F_η). This assumption is fair as long as the angle of rotation of the floe (θ) is small.

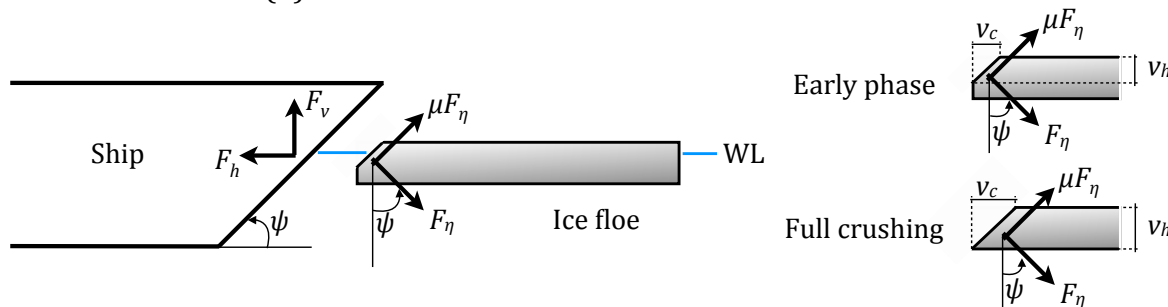


Figure 6-6 Forces acting on ice sheet and development of the crushing height (v_h) and length (v_c)

Another assumption common for all modes of motion is that the ice floe is treated as a homogenous solid. The effects of formation, thermal history and predominant cracks could be of significant. However, these effects are omitted by the same argument as for neglecting dynamic effects – comparison of the modes is the main interest for the chosen approach, and unnecessary complications might disprove the ability to make sound conclusions.

There are several parameters that must be defined in order to perform the calculations following in this section. Unless otherwise stated, the values given in Table 6-1 are used. For material parameters, reference is given to Table 2-2.

Table 6-1 Coefficients used in numerical implementation of the analytical expressions in Matlab

Input parameter	Symbol	Value	Unit
Acceleration of gravity	g	9.81	m/s ²
Density of sea water	ρ_w	1025	kg/m ³
Inclination of hull	ψ	45°	
Radius of conical structure	r_s	10.0	m
Velocity of ship	v_s	1.5	m/s

6.2.1 Displacement by surge

Surge could easily be expressed by simple equations of motion and Newtonian mechanics. The main principle that will be taken advantage of is Newton's second law, stating that the sum of forces on a body must equal the acceleration of the body multiplied by its mass. Due to the decoupling of modes of motion, only the horizontal forces in surge direction would be of interest.

6.2.1.1 Analytical solution for displacement by surge

The first simplification made, in order to produce a viable discretization of the problem, is the assumption of that the body of the ice floe will act as a rigid body. Hence, the acceleration (\ddot{u}) and velocity (\dot{u}) of all points within the continuous body will be assigned the acceleration and velocity of the centre of gravity (Eq 6-2).

$$\ddot{u}(x, y, z) \approx \ddot{u}_G, \quad \dot{u}(x, y, z) \approx \dot{u}_G \quad \text{Eq 6-2}$$

The horizontal component of the ship-ice contact force (F_h) would be limited by the compressive strength of the ice (σ_c), the representative width of loading (W_L), the hull inclination angle (ψ) and the height of crushing ($v_h = v_c \tan \psi \leq h_{ice}$). Assumed is also that the nominal ship-ice contact area will be fully utilized, neglecting that the reality always would be an effective contact area less than the nominal contact area (Sanderson 1988, p.156). The geometric basis of Eq 6-3 is presented in Figure 6-6.

$$F_h(v_c) = \begin{cases} \sigma_c W \tan \psi \cdot v_c, & \text{for } v_c < \frac{h_{ice}}{\tan \psi} \\ \sigma_c W h_{ice} & , \text{ for } v_c \geq \frac{h_{ice}}{\tan \psi} \end{cases} \quad \text{Eq 6-3}$$

Drag force (F_d) and skin friction (F_s) could be expressed as functions of the drag coefficient (C_d) and floe velocity (\dot{u}) as shown in Eq 6-4, while the force due floe-water friction (F_s) during surge is expressed by the skin friction coefficient (C_s) as shown in Eq 6-5.

$$F_d = C_d \rho_w W \left(\frac{\rho_{ice}}{\rho_w} h_{ice} \right) (\dot{u})^2 \quad \text{Eq 6-4}$$

$$F_s = C_s \rho_w L W (\dot{u}) \quad \text{Eq 6-5}$$

However, the contribution from F_d and F_s compared to the inertia will in most cases be negligible. Even for a $L=H=15\text{m}$ floe hit by ship with a velocity of 3 m/s, the error of \ddot{u} by omitting F_d and F_s will be less than 1% (Figure 6-7), if typical values of $C_d=1.00$ and $C_s=10^{-3}$ are chosen (Løset, 2012d).

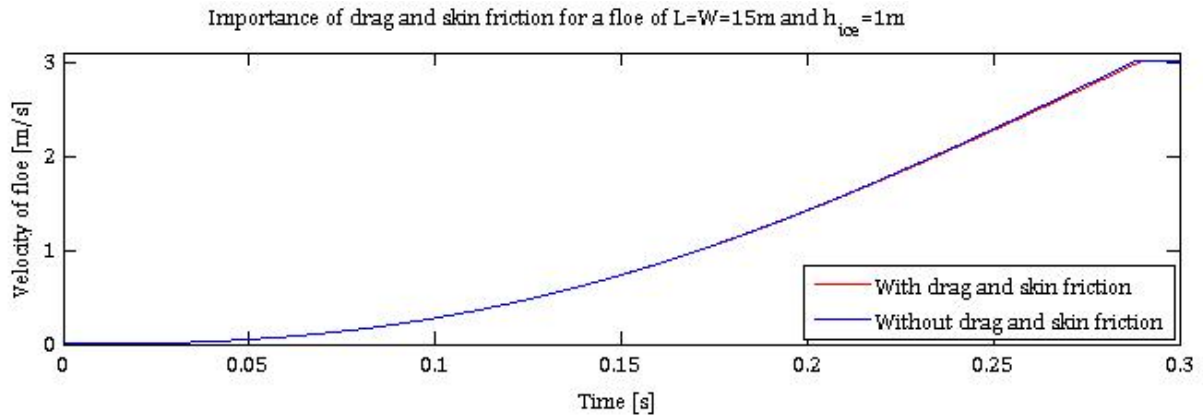


Figure 6-7 Negligible importance of drag and skin friction forces for development of floe velocity

Provided only contact forces and inertia, Newton's second law (Eq 6-6) gives the relationship between the sum of forces in the horizontal direction, the horizontal acceleration (\ddot{u}) and the mass of the floe.

$$\sum F = m\ddot{u} \Rightarrow \ddot{u} = \frac{F_h}{LWh_{ice}\rho_{ice}} \quad \text{Eq 6-6}$$

6.2.1.2 Implementation in Matlab

In order to obtain the ship-ice contact force during impact, the crushing distance (v_c) must be determined. This distance is dependent on the position of the ship and the ice floe, of which the latter in turn is dependent on v_c . Lubbad and Løset (2011) solve this by defining the ship-ice intersection as the difference between the position of the ship (u_s) at the current time step (n) and the position of the floe (u) at the previous time step ($n-1$), as shown in Eq 6-7. For sufficiently small time increments, the error introduced by letting the floe lag one time step behind the position of the ship would be negligible. Due to computationally inexpensive equations, running the analysis with small ($<10^{-4}\text{s}$) time steps is unproblematic.

$$v_c^n = u_s^n - u^{n-1} \quad \text{Eq 6-7}$$

After determination of v_c , the horizontal force (F_h) could be obtained from Eq 6-3 and Figure 6-6. With no other significant forces present, Eq 6-6 will give the acceleration of the floe, which in turn will provide basis for calculation of the position and velocity of the floe for the next time step, as shown in Eq 6-8.

$$\begin{aligned} u^{n+1} &= u^n + (\Delta t)\dot{u}^n \\ \dot{u}^{n+1} &= \dot{u}^n + (\Delta t)\ddot{u}^n \end{aligned} \quad \text{Eq 6-8}$$

Figure 6-8 depicts the development of the surge acceleration dependent on choice of loading conditions (ref. Figure 6-4). Larger contact area implies larger forces. Hence, the time spent for the floe to obtain terminal velocity (the velocity of the ship) varies inversely with the representative loading width.

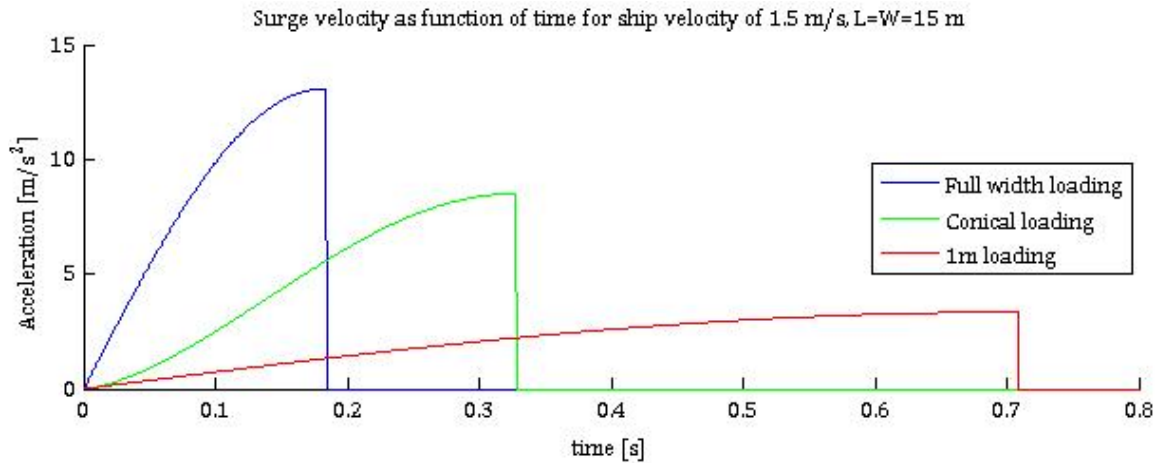


Figure 6-8 Development of surge reactions of ice floe during ship-ice interaction for $h_{ice}=1\text{m}$

Important to notice with the approach outlined above, is that the formulation of v_c , and hence $F_h(v_c)$, indirectly implies that the contact condition behaves elastic. The acceleration of the floe at the increment after the floe has reached the same velocity as the ship implies $u > u_s$, and hence provides negative F_h . This error is avoided by correcting $v_c=0$ if $v_c^n < v_c^{n-1}$, making the contact force constant as this limit is reached. A control mechanism to make sure that $v_h = v_c \tan \psi \leq h_{ice}$ is also implemented (APPENDIX A).

6.2.1.3 Discussion

The velocity of the ship is assumed to be constant during the interaction process. For small floes, the assumption is fair, but the validity is disputable when the mass of the floe (m_{ice}) becomes significant relative to the mass of the ship (m_{ship}). If treated as inelastic impact, where only momenta is conserved, the post interaction velocity of the ship ($v_{s,1}$) would relate to the pre interaction velocity ($v_{s,0}$) as follows from Eq 6-9. This should be taken into account for increased accuracy if utilizing the results in further studies, but is of less relevance to the criterion developed in this chapter.

$$v_{s,1} = \frac{m_{ice} + m_{ship}}{m_{ship}} v_{s,0} \tag{Eq 6-9}$$

6.2.2 Displacement by bending

Seawater could be considered as an incompressible fluid. Hence, the force required to submerge a given area of an ice floe would be equal to the weight of the displaced fluid. When a ship interacts with an ice floe, the response could therefore be simplified as a beam on elastic foundation. The foundation could be treated as linear-elastic (Winkler foundation), with foundation modulus (k) as function of the seawater density (ρ_w). The pressure exerted by the foundation on the beam at a given point, $p(x)$, is the product of the foundation modulus and the deflection of the beam ($y(x)$), as seen in Eq 6-10. This formulation of the foundation modulus is analogous to the stiffness of a linear spring.

Figure 6-9 shows a simple sketch of how the vertical force will affect the bending of the floe. One necessary simplification is that the Winkler foundation is capable of both compression and tension. This implies that the solution would cease its validity as end b lifts out of the water with increasing loads. Another simplification is that full ventilation (as described in Figure 3-6) will be assumed for the top surface of the floe near point a when this is submerged below the initial water line. Due to the short timespan for which the deflection process occurs, this is a valid assumption (Valanto, 2001).

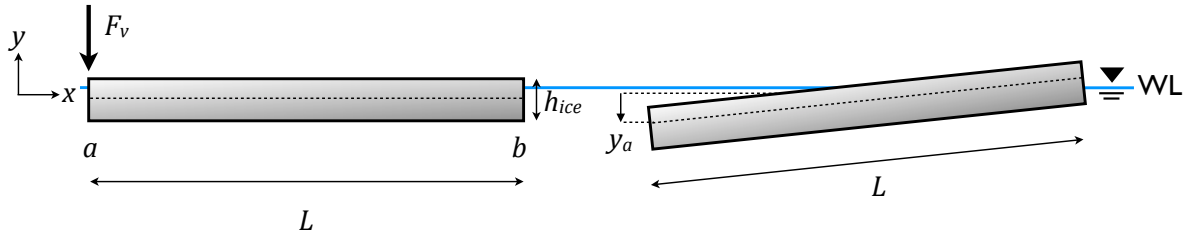


Figure 6-9 Simplified model of the ice floe bending process

6.2.2.1 Analytical solution for bending of a beam on elastic foundation

Hetenyi (1946) provided analytical solutions for beams on elastic foundations. By applying the fourth order differential equation for bending of a finite Navier-Bernoulli beam on Winkler foundation, subject to point load at one edge, the problem is defined by the expression in Eq 6-10.

$$\underbrace{EI \frac{d^4 y}{dx^4}}_{\text{Navier-Bernoulli}} + \underbrace{\tilde{k}y}_{\text{Winkler-foundation}} = \underbrace{\tilde{p}}_{\text{Load}} \quad \text{Eq 6-10}$$

The static solution to this problem is given as follows by Eq 6-11, where x represents the distance from point a , and $x'=L-x$ is defined by the distance from b to the point of consideration.

$$y(x) = F_v \frac{2\lambda}{k} \frac{\sinh(\lambda L) \cos(\lambda x) \cosh(\lambda x') - \sin(\lambda L) \cosh(\lambda x) \cos(\lambda x')}{\sinh^2(\lambda L) - \sin^2(\lambda L)} \quad \text{Eq 6-11}$$

Solving for y at $x=0$ and $x=L$, gives the deflection for deflection at each end of the beam as expressed in the solutions of Hetenyi (1946), presented in Eq 6-12.

$$y_A = F_v \frac{2\lambda}{k} \frac{\sinh(\lambda L) \cosh(\lambda L) - \sin(\lambda L) \cos(\lambda L)}{\sinh^2(\lambda L) - \sin^2(\lambda L)} \quad \text{Eq 6-12}$$

$$y_B = F_v \frac{2\lambda}{k} \frac{\sinh(\lambda L) \cos(\lambda L) - \sin(\lambda L) \cosh(\lambda L)}{\sinh^2(\lambda L) - \sin^2(\lambda L)}$$

These equations are based on the following definitions with E is Young's modulus for ice and I as the second moment of area. Hence, EI represents the flexural rigidity of the floe. λ defines the inverse of the characteristic length of the beam.

$$\lambda = \sqrt[4]{\frac{k}{4EI}}, \quad k = W\rho_w g, \quad I = \frac{Wh_{ice}^3}{12} \Rightarrow \lambda = \sqrt[4]{\frac{W\rho_w g}{4E \frac{Wh_{ice}^3}{12}}} = \sqrt[4]{3 \frac{\rho_w g}{Eh_{ice}^3}} \quad \text{Eq 6-13}$$

The magnitude of the vertical force component of the ship-ice contact force F_v , is limited by the horizontal compressive strength of the floe (Eq 6-3), and the geometric relationships depicted in Figure 6-6. Hence, for a given floe, the crushing length will decide the vertical force as described in Eq 6-14. Again, note the representative width of loading (W_L), as discussed in Section 6.2.

$$F_v = F_n [\cos(\psi) - \mu \sin(\psi)] = F_h(v_c) \left[\frac{\overbrace{\cos(\psi) - \mu \sin(\psi)}^{C_\psi}}{\sin \psi + \mu \cos \psi} \right]$$

$$F_v(v_c) = \begin{cases} C_\psi \sigma_c W \tan \psi \cdot v_c, & \text{for } v_c < \frac{h_{ice}}{\tan \psi} \\ C_\psi \sigma_c W h_{ice} & , \text{ for } v_c \geq \frac{h_{ice}}{\tan \psi} \end{cases} \quad \text{Eq 6-14}$$

As the floe would be incapable of resisting larger loads than what would be limited by the flexural stress capacity (σ_f), the moment must be determined in order to predict when the floe would fail. The equation of moment is used to calculate the stresses along the beam (σ_{max}) after the formulas given in Eq 6-15 and Eq 6-16 (Hetenyi, 1946).

$$M(x) = \frac{F_v}{\lambda} \frac{\sinh(\lambda L) \sin(\lambda x) \sinh(\lambda x') - \sin(\lambda L) \sinh(\lambda x) \sin(\lambda x')}{\sinh^2(\lambda L) - \sin^2(\lambda L)} \quad \text{Eq 6-15}$$

$$\sigma_{max} = \frac{M_{max}}{I} \frac{h_{ice}}{2} = \frac{6M_{max}}{Wh_{ice}^2} \quad \text{Eq 6-16}$$

Dynamic effects are neglected. However, if implementation would be desirable for later approaches to this problem, Evans and Parmeter (1985) could be used together with the formulas of Hetenyi (1946).

6.2.2.2 Numerical implementation in Matlab

The implementation of the mode of deflection in Matlab is straightforward. For each combination of floe length (W), ice thickness (h_{ice}) and time step (n), discrete stresses are calculated along the beam. The maximum stress is thereafter found for each of these combinations. This maximum stress is then controlled against the flexural stress (σ_f).

The calculations are stopped when maximum load is reached ($v_c = \tan \psi h_{ice}$) or if the maximum flexural stress is reached. However, as stated above, the Winkler foundation would not be a valid assumption as the far end of the floe lifts out of the water (initiating the process of rotation). Hence, one could – in accordance with Hovland (2012) – alter the code to not accept further increase in load as the deflection of point b exceeds the submerged part of the floe while at rest. Limiting to the submerged height of the floe ($y_b \leq y_{b,lim}$) would produce conservative results, as initiation of rotation wouldn't guarantee floe failure. However, to be on the safe side – and due to lack of analytical solutions for decoupled Winkler foundation – Eq 6-17 is used as limiting mechanism for the decoupled approach.

$$y_{b,lim} = \frac{\rho_i}{\rho_w} h_{ice} \quad \text{Eq 6-17}$$

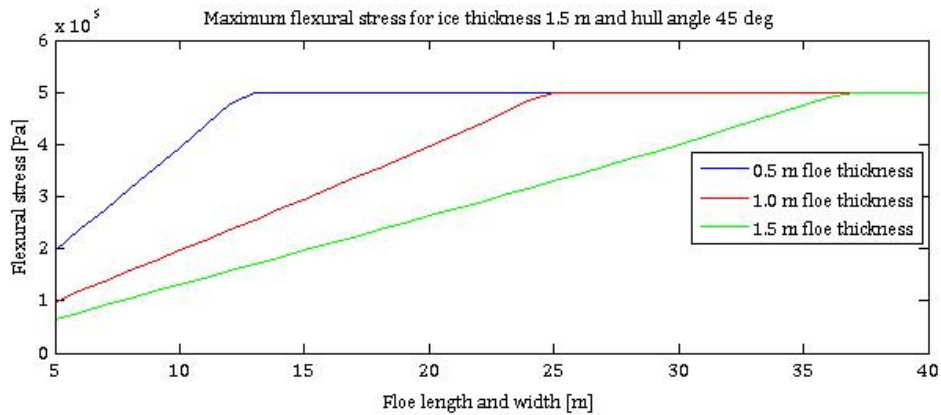


Figure 6-10 Maximum stress for different floe sizes limited by end *b* of the floe lifting out of the water

Figure 6-10 shows the development of the maximum allowable flexural stress, if end *b* of the floes is denied to lift out of the water. If the criterion in Eq 6-17 is used, only floes of length larger than 12m, 25 m and 36 m will reach maximum stress for floe thicknesses of 0.5m, 1.0m and 1.5m respectively.

6.2.2.3 Discussion

The suggested criterion for maximum deflection stated above only considers the far end of the floe. What could also be of interest is to take into account that the loaded edge of the floe would submerge long before the far end lifts. By submerging end *a* of the floe, one would expect that the Hetenyi theory would cease its validity due to non-constant foundation modulus. The reason for not encountering this with a similar criterion for y_a as for y_b , however, is that ventilation – or at least partly ventilation – would prevent backfilling of water to invalidate the assumptions of Hetenyi at the loaded edge.

Another possible problem with the validity of the formulas of Hetenyi (1946) is the assumption that the floe could be treated as a beam. The loading conditions are clearly of importance here, but as long as the representative width of loading exceeds 10% of the width of the floe (Hovland, 2012), and the width of the floe is less than 20 times the thickness, beam theory will not introduce too large errors for brittle non-metallic materials (Baratta, 1984).

The main error introduced with this approach, is that the floe is restrained from movement in surge. For time domain calculations, this would imply that the forces are allowed to build up over a significantly shorter period than what would be the case for in situ ship-ice interaction, where the floe is able to partly “escape” as it’s being pushed forward. The force corresponding to failure of the floe would, however not be affected. The main implication is therefore that the absolute values of the force required to reach the terminal condition for each floe should be compared – not the time it takes to reach this force.

6.2.3 Displacement by rotation

Valanto (2001) developed a 3D-model for determination of ice actions exerted on a ship advancing in level ice. His intention was not to produce a criterion for an unbreakable floe, but the analytical solutions he derived for the force that develops when a broken ice floe rotate as an advancing ship runs over it, could be used to in the development of the breakable/unbreakable criterion.

6.2.3.1 Analytical solution for displacement by rotation

The hull-ice contact force that will be present as a ship advance in ice is depicted in Figure 6-6, and will be normal to the ship hull. This force is the basis of the equations that describes the relation between the contact force (F_η) and the angle of rotation (θ) of the ice floe, as described by Valanto (2001). Figure 6-11 shows a conceptual sketch of the process of rotation.

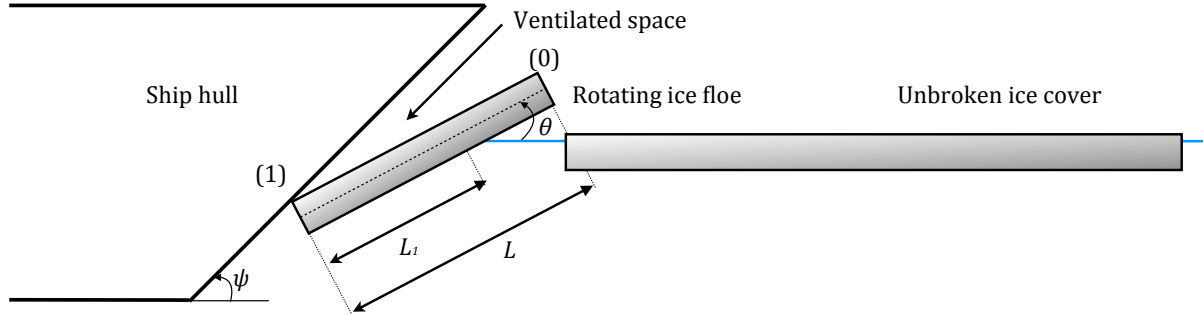


Figure 6-11 Sketch of the turning floe in the normal section of the ship during the main phase of rotation. Length of floe (L) and ventilated length of floe (L_1) is shown (after Valanto, 2001)

In order to model the rotation correctly, Valanto (2001) split the process in two – *the initial floe rotation* about the edge of the unbroken ice cover, and *the main rotation phase* in which the centre of rotation is varying along the length of the floe (L). The contact force-angle of rotation relationship for the *initial* phase can be described as in Eq 6-18. Note the definitions of the C -constants, which will be used in Eq 6-25.

$$F_\eta = \left\{ \frac{1}{3L} (L - L_0)^3 (\rho_w - \rho_{ice}) g \sin(\theta) + \frac{L_0^2}{2L} \left(L - \frac{L_0}{3} \right) \rho_w g \sin(\theta) \right. \\ \left. + \frac{L_0}{L} \left(L - \frac{L_0}{2} \right) (\rho_w - \rho_{ice}) g h_{ice} \cos(\theta) + F_{\Delta\rho} \sin(\psi - \theta) \right\} \frac{C_\mu}{[1 - \mu \tan(\psi - \theta)]} \quad \text{Eq 6-18}$$

Here, ρ_{ice} and ρ_w represent the ice and seawater density respectively, μ is the ice-ship coefficient of friction, h_{ice} is the thickness of the ice, g is the acceleration of gravity, ψ describes the inclination of the ship hull, and L_0 represent the length of the ventilated upper side of the floe (Eq 6-19) – similar to L_1 in Figure 6-11.

$$L_0 = L - \left(1 - \frac{\rho_{ice}}{\rho_w} \right) \frac{h_{ice}}{\tan \theta}, \quad L_0 \geq 0 \quad \text{Eq 6-19}$$

The force from the previously broken and submerged floes that will act parallel to the ship hull is represented by $F_{\Delta\rho}$ as in Eq 6-20.

$$F_{\Delta\rho} = 1.5 (\rho_w - \rho_{ice}) g h_{ice} L (\sin \psi - \mu \cos \psi) \quad \text{Eq 6-20}$$

The force-rotation relationship becomes somewhat more complicated for the *main phase* of rotation. However, by recognizing that the contribution from forces of inertia could be neglected due to only minor changes in floe acceleration during this phase,

Valanto (2001) could consider the problem as static with sum of the moments about each tip of the rotating floe (point 0 and point 1 in Figure 6-11) equal to zero.

The moment equilibrium equations (Eq 6-21 and Eq 6-23) consist of the previously declared variables in addition to L_1 as the length of the submerged part of the floe, and the contact force between the floe and the unbroken ice cover. For the moment at point 0, the lever arm is sufficiently small to neglect the floe-unbroken ice cover contact force.

$$\begin{aligned} \sum M_0 = & -L_1 \frac{1}{2} \rho_w g L_1 \sin(\theta) \left(L - \frac{L_1}{3} \right) + (L - L_1) \rho_{ice} g h_{ice} \cos(\theta) \frac{(L - L_1)}{2} \\ & - L_1 \left(L - \frac{L_1}{2} \right) (\rho_w - \rho_{ice}) g h_{ice} \cos(\theta) + F_\eta L [1 - \mu \tan(\psi - \theta)] - F_{\Delta\rho} \sin(\psi - \theta) L = 0 \end{aligned} \quad \text{Eq 6-21}$$

For the moment at point 1, the ice-ice contact force at point 0 is of relevance. Valanto (2001) showed that the horizontal and vertical components of this force would be dependent of the induced axial force (F_ξ). With large angles of rotation, this force will become negative (Eq 6-22). Negative ice-ice contact force is not likely to occur. This does not imply that the equations are wrong, but rather that the contact force must be set to zero as full separation at point 0 leads to diminishing contact force. This is taken care of by altering $C_\mu=0$. The ice-ice friction coefficient is represented by μ_0 . F_v could hence be considered as a regular resistance by friction, where F_h acts as the normal force.

$$\begin{aligned} F_h = F_\xi \cos\theta, \quad F_v = \mu_0 F_h \\ F_\xi = \begin{pmatrix} F_\eta [\mu + \tan(\psi - \theta)] - (L - L_1) \rho_{ice} g h_{ice} \sin\theta \\ + L_1 (\rho_w - \rho_{ice}) g h_{ice} \sin\theta + F_{\Delta\rho} \cos(\psi - \theta) \end{pmatrix} \end{aligned} \quad \text{Eq 6-22}$$

Full ventilation (Figure 6-11) is an important assumption for all the equations in this subsection. This implies that the upper side of the part of the floe characterized by L_0 and L_1 is treated as “dry”. Hence, no water pressure will act on this surface. Valanto (2001) confirms that this assumption holds for all but very slow (in the order of creeping) ship-ice interaction velocities. This is reasonably in concurrence with what stated in Section 2.8 on ductile and brittle behaviour of ice.

With the ice-ice contact forces clearly defined, the equation of moment equilibrium at point 1 (Figure 6-11) could be written as follows from Eq 6-23.

$$\begin{aligned} \sum M_1 = & \frac{1}{6} L_1^3 \rho_w g \sin\theta - \frac{1}{2} (L^2 - L_1^2) \rho_{ice} g h_{ice} \cos\theta \\ & + \frac{L_1^2}{2} (\rho_w - \rho_{ice}) g h_{ice} \cos\theta + L \overbrace{(\sin\theta - \mu_0 \cos\theta)}^{C_\mu} F_h = 0 \end{aligned} \quad \text{Eq 6-23}$$

By combining Eq 6-21 and Eq 6-23, and rewriting

$$C_{\psi\theta} = \cos(\theta) [\mu + \tan(\psi - \theta)], \quad \text{Eq 6-24}$$

Valanto (2001) derived the expression for the length of the submerged part of the floe (L_1) as a third degree analytical expression as follows,

$$\begin{aligned}
 & L_1^3 (1 - C_\mu C_{\psi\theta} C_{\mu t}) \tan \theta \\
 & + 3L_1^2 \left[h_{ice} (1 - C_\mu C_{\psi\theta} C_{\mu t}) + LC_\mu C_{\psi\theta} C_{\mu t} \tan \theta \right] \\
 & + 6L_1 LC_\mu h_{ice} (C_{\psi\theta} C_{\mu t} + \sin \theta) \\
 & - 3L^2 \left(\frac{\rho_{ice}}{\rho_w} \right) h_{ice} \left[(1 + C_\mu C_{\psi\theta} C_{\mu t}) + 2C_\mu \sin \theta \right] + 6LC_\mu \frac{F_{\Delta\rho}}{\rho_w g} \left[\frac{C_{\psi\theta} C_{\mu t} \frac{\sin(\psi - \theta)}{\cos(\theta)}}{+ \cos(\psi - \theta)} \right] = 0
 \end{aligned} \tag{Eq 6-25}$$

Solving for the real solution of L_1 of Eq 6-25 provides the last necessary input in order to calculate the ship hull-ice floe contact force for the main phase of the floe rotation, as shown in Eq 6-26.

$$\begin{aligned}
 F_\eta = & \left\{ -\frac{1}{6L} L_1^3 \rho_w g \sin \theta + \frac{L_1^2}{2} \rho_w g \sin \theta - \frac{(L - L_1)^2}{2L} \rho_{ice} g h_{ice} \cos \theta \right. \\
 & \left. + \frac{L_1}{L} \left(L - \frac{L_1}{2} \right) (\rho_w - \rho_{ice}) g h_{ice} \cos \theta + F_{\Delta\rho} \sin(\psi - \theta) \right\} C_\mu
 \end{aligned} \tag{Eq 6-26}$$

Now, the basis for calculation of the ship-ice contact force (F_η) – both for rotation about point 0 and varying centre of rotation – have been established. Still, in order to obtain the correct contact force, one needs a criterion for when to choose between the two scenarios. Valanto (2001) states that the change between them will occur when the vertical force at the joint exceeds the friction force that is able to hold point 0 of the floe at its original position. However, for an isolated ice floe, which would be relevant for the criterion to be developed in this chapter, only the latter method would be applicable due to no adjacent floes to develop contact forces with. Utilizing isolated floes, Eq 6-25 and Eq 6-26 could be simplified by assuming $C_\mu=0$ and $F_{\Delta\rho}=0$. Hence, Eq 6-27 would be the relevant equation to solve.

$$\begin{aligned}
 & L_1^3 \tan \theta + 3L_1^2 h_{ice} - 3L^2 \left(\frac{\rho_{ice}}{\rho_w} \right) h_{ice} = 0 \\
 F_\eta = & \left\{ -\frac{1}{6L} L_1^3 \rho_w g \sin \theta + \frac{L_1^2}{2} \rho_w g \sin \theta \right. \\
 & \left. - \frac{(L - L_1)^2}{2L} \rho_{ice} g h_{ice} \cos \theta + \frac{L_1}{L} \left(L - \frac{L_1}{2} \right) (\rho_w - \rho_{ice}) g h_{ice} \cos \theta \right\} C_\mu
 \end{aligned} \tag{Eq 6-27}$$

Subsection 6.2.1.1 gives the maximum horizontal force applicable for the ice floe. As previously described, $F_{h,max}$ impose a limit on the normal-to-hull contact force ($F_{\eta,max}$). In other words, if the force required to rotate the floe would exceed the available force, rotation would not be possible and another mode of motion or failure must occur instead. Due to the rotation, the ship-ice contact area is of less relevance since it's the

dimensions of the floe that would define the resistance towards rotation. Hence, only the case of full crushing is considered as limiting mechanism in Eq 6-28.

$$\left. \begin{aligned} F_h &= F_\eta [\sin(\psi) + \mu \cos(\psi)] \\ F_\eta &= \frac{F_h}{\sin(\psi) + \mu \cos(\psi)} \end{aligned} \right\} \Rightarrow F_{\eta, \max}(v_c) = \frac{\sigma_c W_L}{\sin(\psi) + \mu \cos(\psi)} h_{ice} \quad \text{Eq 6-28}$$

Although a viable relationship between floe rotation and the ship-ice contact force has been established, there still lacks one important definition. In order to compare the force-displacement results with the two other cases of displacement by surge and deflection, a measure for the dependency of the contact force on the ship movement in the straight forward horizontal direction is needed. Conveniently, Valanto (2001) derived this relationship (Eq 6-29) for the case of no surge movement of the floe. Here, u_s is the horizontal forward (surge) movement of the ship, \dot{u}_s is the constant velocity of the ship in the surge direction, and t represents time.

$$u_s = \dot{u}_s t = \left(\frac{\sin \theta}{\tan \psi} + 1 - \cos \theta \right) L_1, \quad \text{Eq 6-29}$$

As stated, there are numerous assumptions required for this model. Still, Valanto (2001) states that the numerical and experimental verification performed indicates good correlation with available sources of comparison.

6.2.3.2 Numerical implementation in Matlab

The initial rotation of the floe is supposed to be $\theta=0$ rad. However, this would produce numerical error as $h_{ice}/\tan\theta$ in Eq 6-19 would imply division by zero. Therefore, an initial value of the floe rotation was chosen as a sufficiently small value not to introduce other errors, $\theta(t=0)=10^{-6}$ rad.

The seemingly looping dependencies, as $L_1 = f(C_\mu)$, $C_\mu = f(F_\xi)$, $F_\xi = f(F_\eta)$, $F_\eta = f(L_1)$, and hence $L_1 = f(L_1)$, must be overcome. In order to solve this system, an algorithm as shown in Figure 6-12 was implemented in the Matlab code.

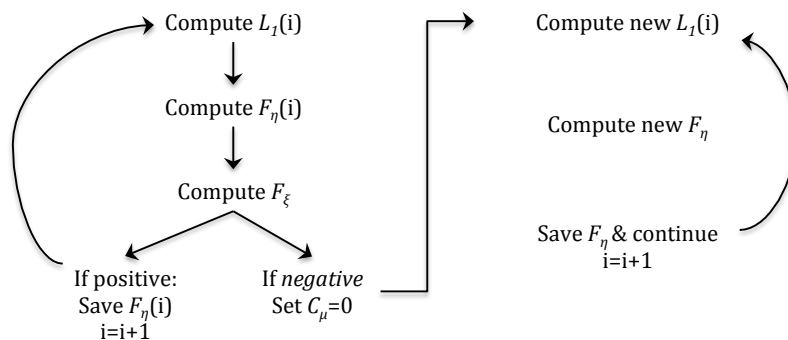


Figure 6-12 Flowchart for calculation of the ship-ice contact force according to Eq 6-20 to Eq 6-26

Although Eq 6-27 is preferred over Eq 6-25 and Eq 6-26 for the comparison between the modes, calculation was performed in order to provide a holistic view of the process of rotation. Further development of the criterion to include non-isolated floes, would

benefit from the observations made. Figure 6-13 shows the development of ventilated floe length and contact force for both the initial and the main phase of rotation.

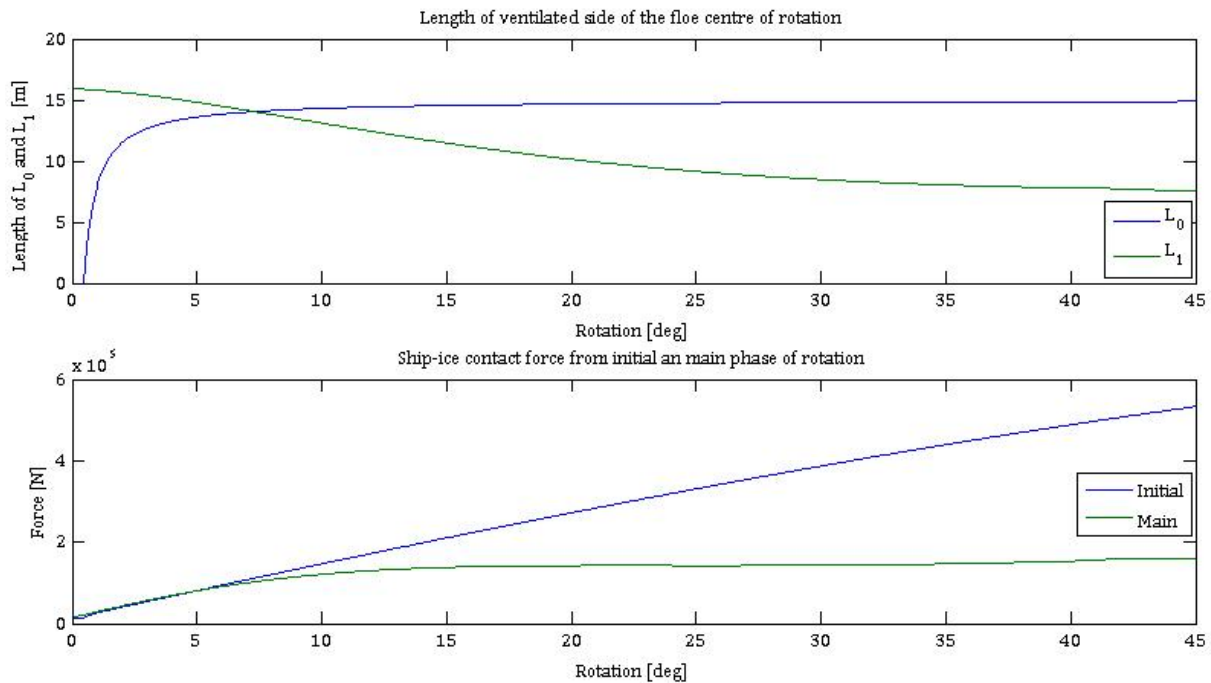


Figure 6-13 Development of ship-ice contact force during rotation of an ice floe with Valanto's (2001) method. Force given per meter of floe width for a floe of $L=W=15\text{m}$, $h_{ice}=1\text{m}$, $\psi=45^\circ$.

Independent of the simplified method of an isolated floe, or the width adjacent floes, the third degree polynomials in Eq 6-25 and Eq 6-27 must be solved. However, Matlab is easily capable of finding the real roots of such third degree polynomials.

For the isolated floe, where only the main phase of rotation is considered, a trace-type of iteration is utilized in order to determine the θ that corresponds to the available load. Since F_η is dependent on L_1 , iteration on L_1 must be done as well. The iteration is performed as a while-sentence where the rotation of a given floe is done gradually and terminated as the calculated force at rotation exceeds the predefined maximum force. If the maximum force is not exceeded, the terminal angle of rotation equals ψ .

6.2.3.3 Discussion

The relevance of utilizing the equations of Valanto (2001), that originally was intended for calculating the resistance of a ship advancing in level ice, for determination of the force required to rotate an isolated floe is disputable. The ship movement-floe rotation relationship given in Eq 6-29 is based on the assumption of forces from adjacent floes preventing the floe from rotating. Such forces are not present in the isolated floe model considered for the decoupled approach. However, as the angle of rotation increase and the ice-ice contact cease, the equations should be comparable. Hence, comparison with the main phase of rotation would be of more interest than the initial phase of rotation.

Unlike the modes of surge and deflection, the loading condition is of less importance for the rotation of the floe. Since the equations for determining the angle of rotation (θ) and contact force (F_η) are given independently of how the floe is loaded, the only dependency linked to the effective loading width, is through the maximum allowable horizontal component of the contact force. The implication of this is that the time

domain is not comparable with the calculations of bending and surge. The force required to rotate a given floe could still serve as a metric for comparison with modes of response.

6.2.4 Comparison of results from the decoupled approach

In order to reduce the variables to a controllable level, only one mode of loading is considered when comparing the results from the decoupled modes of motion. Although icebreakers like Oden (Figure 3-2) easily could be claimed to produce a loading condition equal to that of full loading, and more conventional ships reasonable could be simplified to represent partly loading of the floe (Figure 6-4), the conical loading condition (Figure 6-5) is chosen for further calculations. The main reason for this choice is the simple, yet realistic, relationship for increasing contact width (W_L) as function of increased penetration (v_c).

For simplicity, only ship hulls of $\psi=45^\circ$ are considered for the development of the criteria itself. However, playing with this parameter shows that the critical length for an unbreakable floe is slightly lower for smaller angles and correspondingly larger for larger angles. This is expected, as smaller angles would imply a larger vertical component of the ship-ice contact force, even though some of this contribution is cancelled out by the lesser need for rotation. Keeping the inclination constant at $\psi=45^\circ$ seems therefore like an appropriate choice.

The decoupled motions of surge, deflection and rotation all behave differently during loading. By comparing the time to reach terminal velocity ($v=v_s$), full rotation ($\theta=\psi$) or flexural failure ($\sigma_x=\sigma_f$), the domain of domination of each mode could be determined. In order to predict when each mode will dominate, the development of an equivalent horizontal force – resulting from all three modes of motion – could be utilized for comparison. This equivalent force from deflection and rotation is obtained by the relationships given in Figure 6-14 and Eq 6-28, accordingly.

Figure 6-14 depict the development of the forces associated with the modes of surge, deflection and rotation, for the time domain relevant for each mode. The idea of the graphs is not to depict which mode of motion would be governing at a given time step during the interaction process. As stated above, the underlying assumptions of the decoupling would not give realistic estimates of the required force at a given time. However, the following graphs give an overview of the maximum required force to obtain terminal condition in any of the decoupled modes. Hence would the criterion for unbreakable floes be where rotation requires less force than surge or bending.

In principle this implies that the limiting case is where the maximum equivalent horizontal force required to fully rotate the floe equals that of lifting the floe out of the water. This limit would be conservative, as the governing flexural capacity is limited to the force required to lift the force out of the water, disregarding the potential additional flexural strength in the floe, as discussed with Figure 6-10.

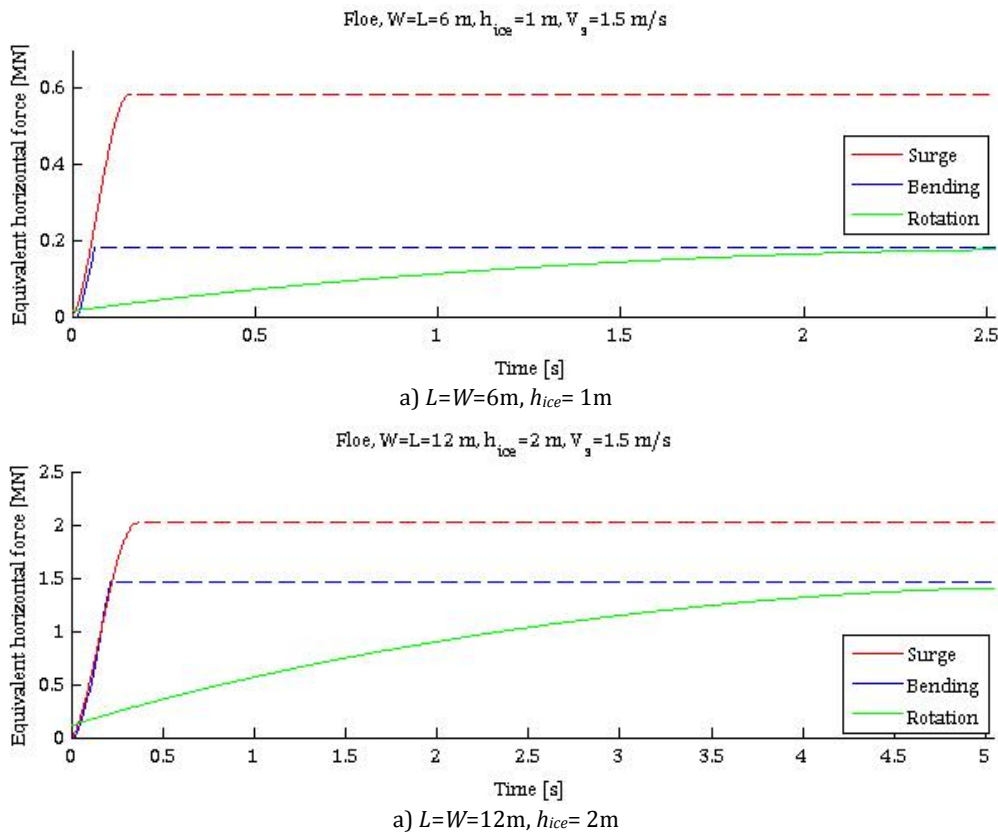


Figure 6-14 Limit case where equivalent maximum horizontal force for rotation equals that of bending

Important to notice is that the forces given in the two previous figures, due to the simplifications previously stated in this chapter, not necessarily represent the real forces during ship-ice interaction. However, for the purpose of comparison of modes, the real values of the forces are not of importance as long as they are derived in the same manner.

Although consistent derivation of equations from the basis of the approach has been performed, emphasis is put on the fact that the proposed criterion would not be exact. The largest error made is probably the one of the decoupled motions itself. As evident from Figure 6-14, the equivalent horizontal momentum ($I = \int F_{h,eq} dt$) during rotation will be much larger than what required to obtain terminal velocity for the floe. However, recoupling of the modes to understand how they affect each other is not desirable. Firstly, recoupling would violate the boundary conditions that serve as basis for the derived equations. Secondly, the considered approach only treat the maximum force required for each mode, hence the time domain would not be directly comparable. Lastly, considering the results decoupled will be on the conservative side, since recoupling would imply that terminal velocity could be reached at a lower load during rotation or bending.

The nature of the unbreakable-criterion is to be conservative. The curve for surge should in some cases be expected to be lower than depicted in the following figures, but the errors introduced by the decoupling would not disprove the developed criterion. It would only be somewhat less effective in limiting the computational expense of the real-time ship-ice interaction simulator than an optimal criterion.

As evident from the described model, the floe is not likely to achieve terminal velocity before it fails by bending failure. Still, pushing of floes is often observed in the field (Lubbad, 2013). The reason for this, in addition to that of momenta, as discussed in the previous paragraph, is partly due to the unrealistic assumption of central ship-ice impact. With a hit slightly off centre, it would be possible to push the ice floe aside without it necessarily reaching the velocity of the ship first. However, a robust criterion should also be valid for the extreme case of central hit, and the assumption of decoupling require the forces to be treated independently. Hence, this observation is of less importance for the consistency of the approach, but would serve as proof of that the decoupled approach is on the conservative side.

With the modes of motion presented in a comparable fashion, one still needs to define a limit to identify unbreakable ice. A viable approach could therefore be to define the floe as breakable as long as the forces required to rotate the floe completely exceeds those of either surge or deflection. As previously stated, this would probably be somewhat conservative. However, the nature of the criterion advocates the use of a conservative limit (Figure 6-1).

Figure 6-14 indicate that the limit would be for beams of relatively short length (L) compared to thickness (h_{ice}). This geometric relationship challenges the hypothesis of Navier ($h \ll L$), which is required for the relationships derived by of Hetenyi (1946). Therefore, a simple 3D Abaqus model was built with 10-node modified quadratic tetrahedron elements (C3D10M), for increased accuracy (Cook, 2001). Table 2-2 gives the material parameters. In order to avoid singularities, the load was applied as a uniformly distributed pressure over a 0.1m wide strip, instead of as a point load as described in Subsection 6.2.2.

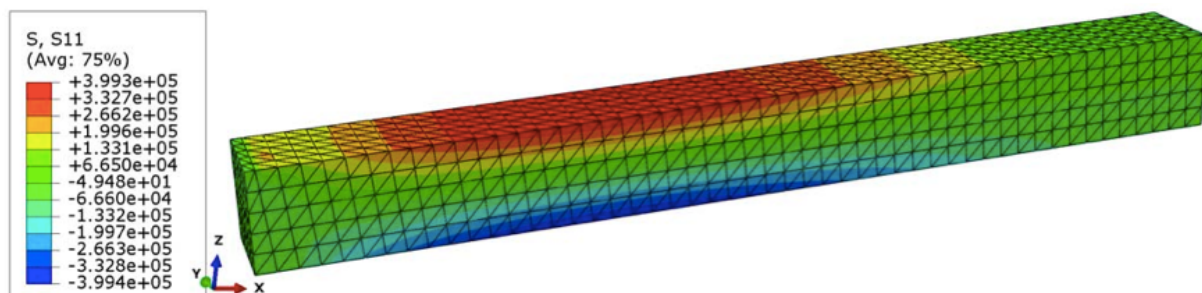


Figure 6-15 Abaqus verification stress plot for case limited by $y_{b,lim}=0.897m$, $F_v=45.85kN/m$, $L=10m$, $W=h_{ice}=1m$.

The verification proved good compliance for both the case limited by maximum deflection and maximum stress (with large deflections in the elastic foundation) down to $L = 6m$ for $W=h_{ice}=1m$. Figure 6-15 serves as example. The deviation is within what could be explained by the slight difference in loading conditions. Violation of the assumptions of beam theory should therefore not be a problem for the considered approach.

Table 6-2 Comparison of analytical results and implicit numerical analysis on elastic foundation for beams of $L=W=10m$, $h_{ice}=1m$, limited by the far end of the floe lifting out of the water and maximum flexural stress.

$y_{b,lim}=0.897m$	Hetenyi	44.22kN	$\sigma_f=500kPa$	Hetenyi	56.29kN
	Abaqus	45.85kN		Abaqus	57.42kN

6.2.5 Criterion based on decoupled events

Corresponding length and width of the square floes required to fulfil the criterion of equal maximum horizontal component of the deflection and rotation of ice floe, is presented in Table 6-3. The results are obtained by altering the parameters in the matlab script in order to obtain overlapping curves as in Figure 6-14. Further, no dependency on ship velocity was observed other than that the mode of deflection would be likely to dominate over the mode of surge.

Table 6-3 Length/width to thickness relationship for square floes at point of transition to unbreakable

Length ($L=W$)	3.0m	6.0m	9.0m	12.0m	15.0m
Thickness (h_{ice})	0.5m	1.0m	1.5m	2.0m	2.5m

Based on Table 6-3 and the observations in the previous sections, the suggested criterion for unbreakable ice floes as function of floe height and thickness is proposed as in Eq 6-30, for square floes. Note that the presented criterion here is the result of the knowledge available by the decoupled analysis. For the final criterion, see Eq 6-35.

$$\text{Unbreakable if: } L < 6h_{ice} \quad \text{Eq 6-30}$$

Summarizing, the assumptions underlying for the decoupled criterion are:

- Isolated, square floes of homogenous ice with parameters as of Table 2-2
- Decoupled modes of motion (surge, deflection, rotation) treated separately
- Quasi-static development of effective loading width as for a conical structure
- Central ship-ice floe impact and hull inclination angle of $\psi=45^\circ$
- Equivalent horizontal force for each mode limited by ice compressive strength
- Dynamic effects and lost mass of floe due to crushing neglected
- Possible invalid range of beam theory is neglected
- The floe would be unbreakable if the maximum force required to rotate the floe is less than the force corresponding to the flexural strength during bending

Thorough verification of the decoupled criterion was not performed, but an interesting observation is that the proposed criterion is within the limits of what usually is considered as the limit for the breaking length during ice-structure interaction. ISO19906 (A.8.2.6.2), states that the breaking length in terms of bending failure is in the order of 3-10 times the thickness of the ice. Hence, the criterion developed by approach of decoupling the modes of motion is within a plausible range.

6.3 Coupled approach in Abaqus

The response of the floe after it lifts out of the water is not obvious, hence demanding severely conservative assumptions for the criterion developed by analytical solutions. Better understanding of the process would provide the possibility for a more efficient criterion, thereby serving as motivation for examining the problem further by numerical finite element verification.

Two different *Abaqus 6.12-1 Explicit* models were made in order to describe the coupled approach. One model, where coupling of the modes was simulated by applying multiple loads; The other model, where the coupling was ensured through an impact simulation. Common for both models was that added mass and dynamic effects were also left out due to assumed slow interaction velocities. Also, the development of flexural stresses is measured for the node that will ultimately reach maximum stress. Decoupling of the Winkler foundation for the parts of the floe elevated above the water level was ensured by a Fortran user subroutine, as given in APPENDIX B. This subroutine also takes care of the gravity load introduced for elevated parts of the floe. Validation of the explicit-analysis with subroutine against a similar floe on elastic foundation in an implicit analysis with *Abaqus 6.12-1 Standard* proved good results.

6.3.1 Semi-coupled approach through multiple loads

The semi-coupled model was based on multiple loading through linearly increasing-with-time surface pressure applied along the loaded edge of the floe. The forces were in other words applied as in the decoupled model, but applied simultaneously in order to understand how they affect each other.

The horizontal (F_h) and vertical (F_v) loads (ref. Section 6.2) were applied over strips of width 0.9 m along the impacting edge of the floe. The magnitude was decided as follows: The compressive strength of ice, $\sigma_c=1000$ kPa, defines the pressure in the horizontal direction. In order to apply the loads consistently with the crushing pattern depicted in Figure 6-6, C_ψ as of Eq 6-14 define the vertical pressure load to be 905 kPa. The loads were applied linearly increasing over a time period of 2.0 seconds, in order to simulate the gradually increasing pressure resulting from the crushing process at an ice-structure impact scenario.

The reason for not choosing point loads was to avoid singularities. However, by applying loads as surface pressure, these will follow the nodal rotation of the floe, hence not being representative for true loads when deflections become large. For the purpose of comparison with the analytical results, however, this error is necessary.

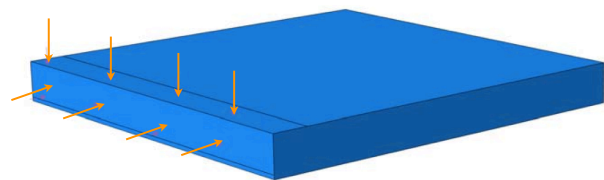


Figure 6-16 Loading conditions for floe with semi-coupled loading in Abaqus

In order to save computational expense for the explicit calculations, 8-node linear brick elements with reduced integration and hourglass control (C3D8R), was used. The floe was meshed with an approximate element size of 0.1m. The time increment for an explicit analysis is important to control in order to obtain convergence of the results. Generally, the solution will become unstable as the time step is larger than the time it

takes for a wave to propagate through an element of the given material at its dilatational speed of sound. Abaqus takes care of this by default.

Regarding the results from this model, the rotation is calculated based on the difference in vertical displacement of the loaded end and the far end of the floe, as shown in Eq 6-33. For the considered range of $\sigma_x < \sigma_f$, the deflections are of several orders larger than the elastic deformations of the floe, hence being within the required limit for this choice.

$$\theta(t) = \sin^{-1} \left(\frac{y(t, x=L) - y(t, x=0)}{L} \right) \quad \text{Eq 6-31}$$

The flexural stresses, on the other hand were taken from a single point in the *Abaqus* model, which ultimately would be the point where maximum flexural stress would occur. Figure 6-17 depicts the distribution of flexural stresses in a floe of $L=W=6\text{m}$, $h_{ice}=1\text{m}$, as the far end of the floe gets lifted out of the water.

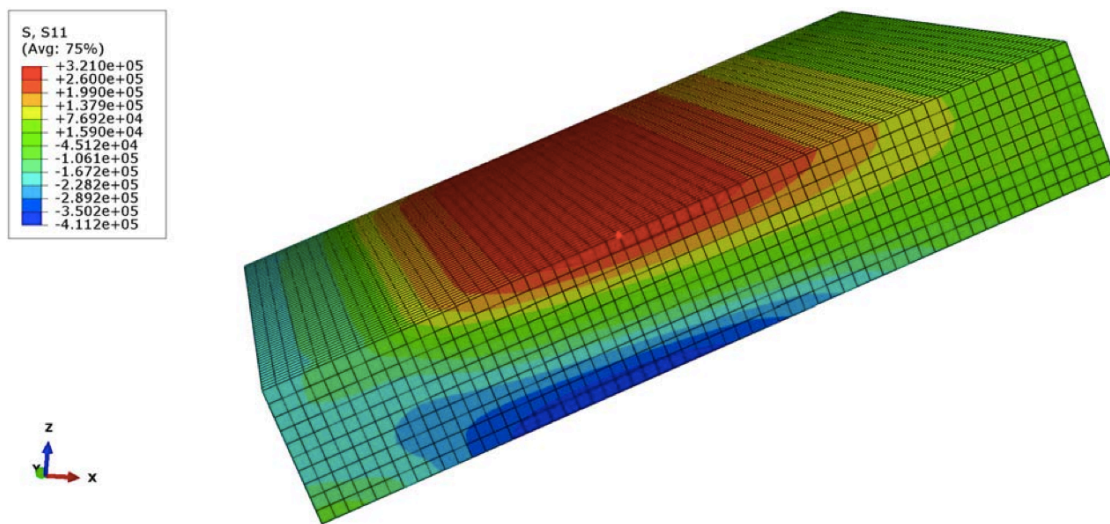


Figure 6-17 Flexural stresses for $L=W=6\text{m}$, $h_{ice}=1\text{m}$, at $y_b=y_{b,lim}$. Point of $\sigma_{f,max}$ indicated. Deflections are exaggerated.

The most important observation made from the semi-coupled Abaqus model, was that the stresses – both with and without ventilation – would cease to increase as the floe lifts out of the water. This is shown conceptually in Figure 6-18, disregarding violation of flexural strength criterion. By analysing the boundary conditions, one would see that this reduction in stresses would be expected as the load on the far end of the floe reduces to its self-weight. This self-load will further diminish during rotation, as the component contributing to bending decrease with increased angle of rotation.

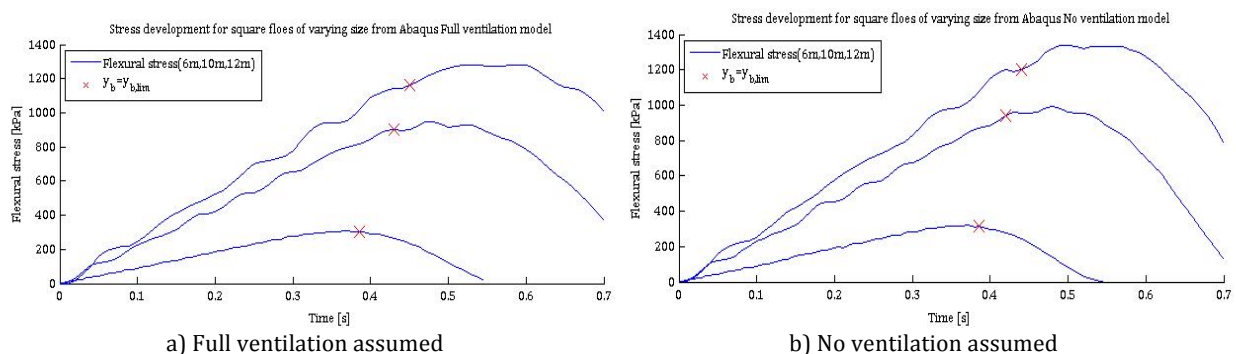
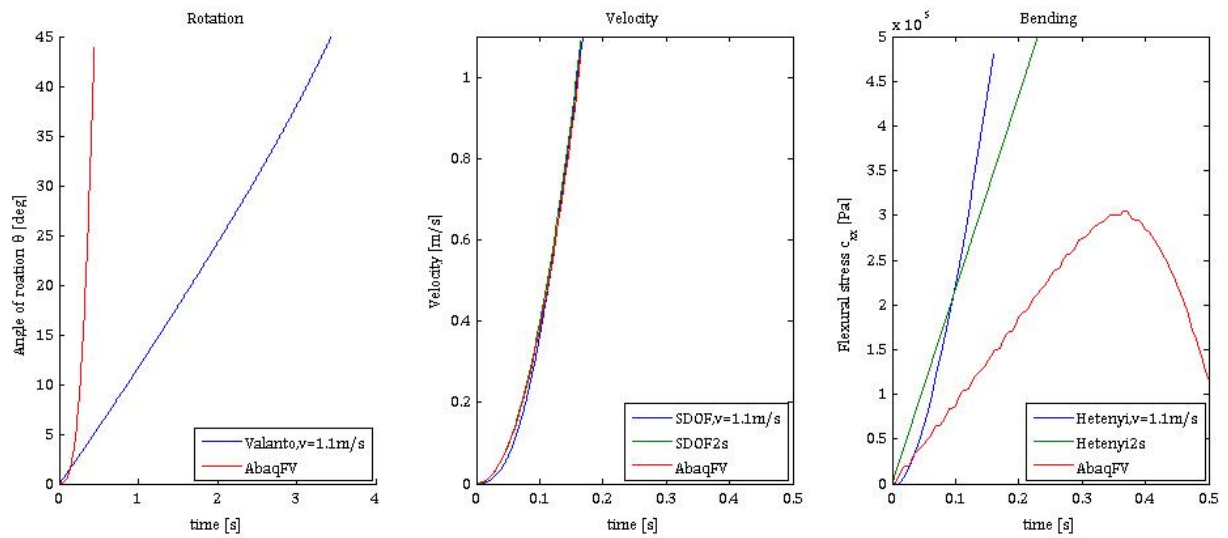


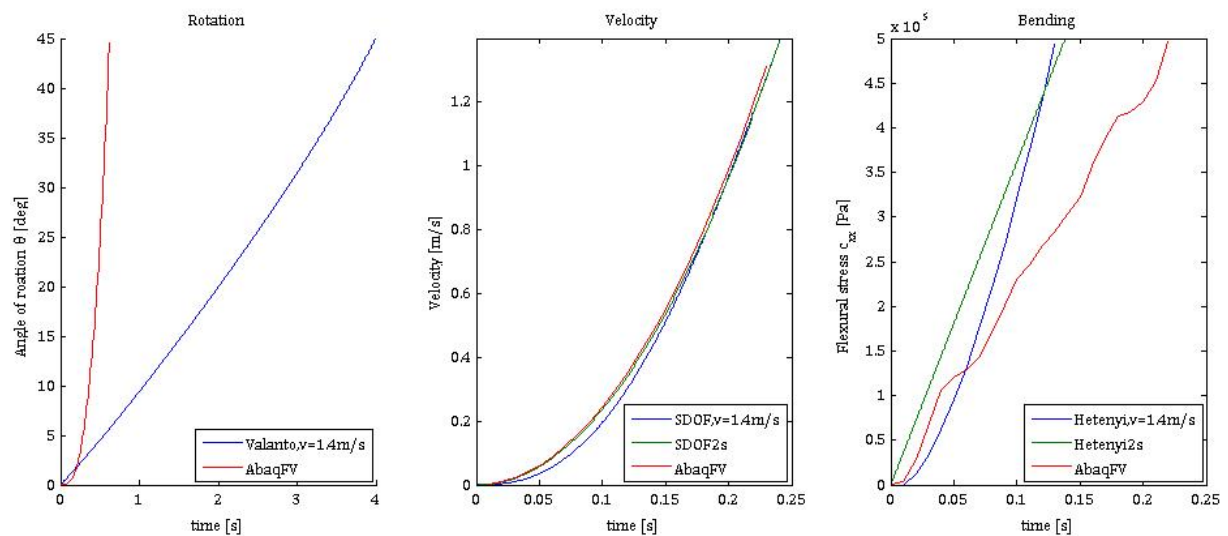
Figure 6-18 Theoretical stresses in floe, for $h_{ice}=1\text{m}$. Point where the far end is lifted out of the water is indicated.

As expected from the discussions in Section 6.2, the value of the decoupled solutions in the time domain is of limited value. Figure 6-19 compares the development of forces related to rotation, surge and bending with time. The curves associated with $v=1.1$ m/s (for $L=6$ m) and $v=1.4$ m/s (for $L=10$ m) are the same as those in Section 6.2. The ones denoted “2s”, are obtained by applying the given force linearly over a period of 2 seconds in the analytical expressions.

The curves in Figure 6-19 labelled AbaqFV are derived from semi-coupled simulations in Abaqus with full ventilation assumed. The given load corresponds to the pressure loads defined for Figure 6-16. Also here the load was applied linearly over a period of 2 seconds. The conclusion that could be made is that the decoupled approach is on the conservative side, especially for smaller floes, but that the mode of surge seems to compare well for decoupling. Similar results were obtained for floes of length 8m and 12m.



a) With $t_{rotation}=0.5$ s, $t_{surge}=0.17$ s and $t_{bending}=0.23$ s, surge is considered the governing mode. $L=W=6$ m, $h_{ice}=1$ m.



b) With $t_{rotation}=0.5$ s, $t_{surge}=0.24$ s and $t_{bending}=0.14$ s, bending is considered the governing mode. $L=W=10$ m, $h_{ice}=1$ m.

Figure 6-19 Limited value of decoupled solutions in time domain

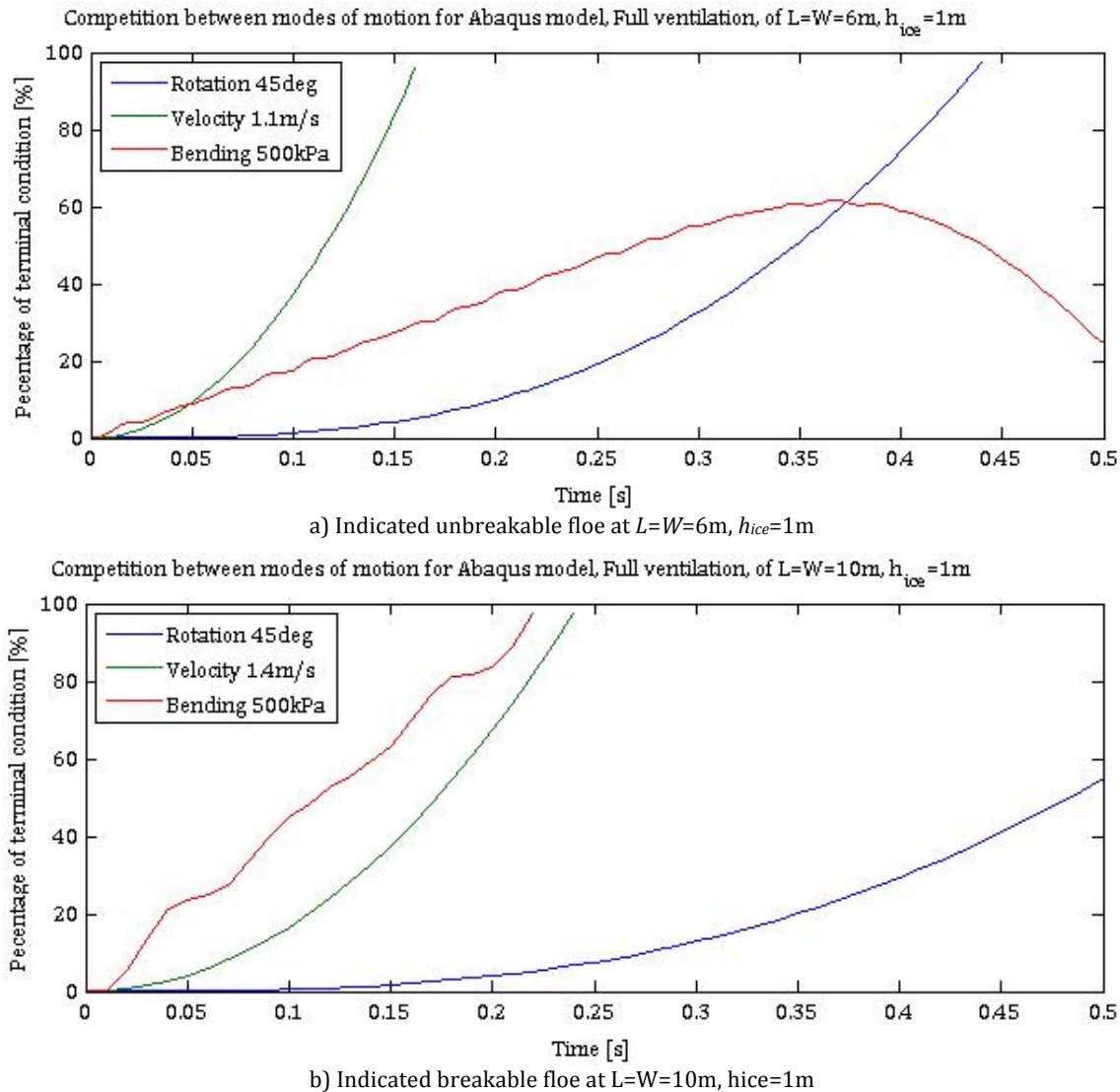


Figure 6-20 Time domain plots extracted from Abaqus model showing competition between modes of motion

The fundamental goal of decoupling of the modes was to obtain time domain plots showing the competition between the different modes of motion. As discussed in Section 6.2, this proved to be difficult due to the assumption of decoupling itself. Still, by extracting the same parameters from the semi-coupled Abaqus analysis, one is able to gain further insight to the breakable-unbreakable criterion, through the relationships depicted in Figure 6-20, where surge and bending seems to be the more relevant modes for development of the unbreakable-criterion.

One possible erroneous assumption is that the expected terminal velocity for the given loading condition (Figure 6-16) is iterated to comply with the expected curve fit for velocity as seen in Figure 6-19, as it's not given what this would be appropriate for a linearly increased load. The graphs support that the critical length for a floe of $h_{ice}=1m$ should be approximately 10 meters. However, due to the imperfect coupling, this number should however not be given too much attention other than serving as an indicator for the final result. Another finding is that the rotation doesn't seem to be governing in any case for isolated floes. This is reasonable, as the process of rotation would be difficult to facilitate without restrictions towards movement in surge, imposed by adjacent floes.

6.3.2 Coupled approach through ice-structure impact simulation

The coupled model simulates the ice-structure impact in a more consistent manner than the previously mentioned approaches through a 3D impact simulation between the ship hull and the ice floe. This simulation was performed in *Abaqus 6.12-1 Explicit*.

For simplicity, and to reduce the complexity of the simulation cases, only a floe of $L=W=10\text{m}$ and $h_{ice}=1\text{m}$ was considered for the purpose of validation. The ship hull was modelled as a $20\text{m}\times 20\text{m}\times 1\text{m}$ steel plate, as shown in Figure 6-21. The large difference in elastic parameters for steel and ice makes this approach feasible, and one avoids the necessity of modelling the ship hull as a rigid instance. As for the previous subsection, the floe was modelled as a homogenous solid with material parameters given in Table 2-2, but static and dynamic friction coefficients are taken from Table 2-1 (ISO19906).

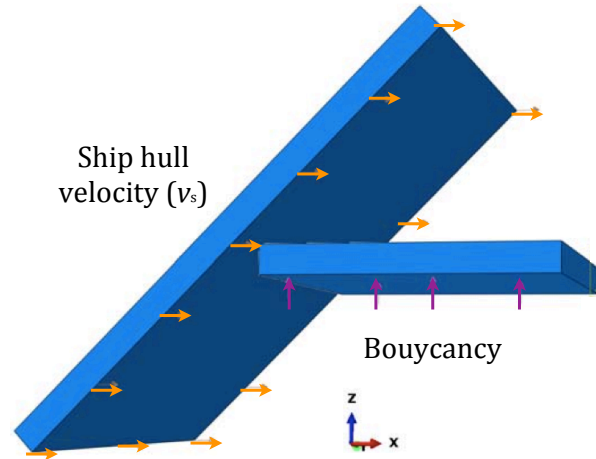


Figure 6-21 Coupled ship-ice interaction model. The ship is modelled as a single degree of freedom instance with constant velocity (v_s) in surge (x -direction), while the floe is initially at rest.

For interaction between non-rigid solids, soft contact could be applied. For normal-to-surface behaviour, this contact formulation provides the possibility of indirectly modelling the crushing of the ice. The contact stiffness (k_c) could be determined on basis of the crushing length (v_c) and the geometric relationships defined in Figure 6-6, as utilized in Eq 6-32. Tangential contact was modelled with friction coefficients as of Table 2-2. The option to include all surface pairs was chosen, with global automatically assigned surface smoothing.

$$F_c = k_c v_c = \sigma_c \frac{A(v_c) W}{\cos \theta} v_c \Rightarrow k_c = \frac{\sigma_c W}{\cos \theta} = \frac{1000\text{kPa} \cdot 10\text{m}}{\cos(45^\circ)} = 14.1 \text{ kN/m}, \quad v_c < \frac{h_{ice}}{\tan \psi} \quad \text{Eq 6-32}$$

Regarding the applied loads and boundary conditions, the constant velocity of the ship hull was varied up to 2.0 m/s in different model setups. The ship hull and the floe were modelled explicitly, but in order to avoid CFD-calculations, the effect of buoyancy was modelled as a surface pressure on the bottom side on the floe. Since inclusion of gravity in the model would cause need for damping in order to avoid severe oscillations, the gravity effect is for reasons of simplicity included as negative surface load on the bottom side of the floe when elevated above the water line. The buoyancy, ventilation and gravity of the elevated part of floe were accounted for through the Fortran user subroutine given in APPENDIX B.

The approximate element size for the mesh chosen for the analysis was 0.15m 8-node linear brick elements with reduced integration and hourglass control (C3D8R) – for which energy convergence was obtained – are used. The ship hull instance is meshed quite coarse, as shown in the following stress plots, with C3D8R of approximate size 1m.

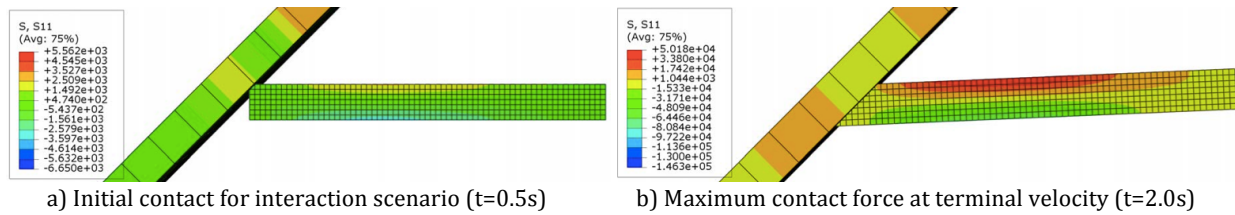


Figure 6-22 Flexural stresses plotted for interaction scenario with $v_s=1.5\text{m/s}$, $L=W=10\text{m}$, $h_{ice}=1\text{m}$

For an interaction scenario where the ship speed is 1.5m/s , the bending process can be illustrated as follows from Figure 6-22. It takes approximately 1.5s for the floe to reach terminal velocity in the coupled analysis, for a ship of velocity 1.5 m/s impacting a floe of $L=W=10\text{m}$, $h_{ice}=1\text{m}$. Looking back to Figure 6-19, where loading over a time period of 2.0s compared to a terminal velocity of 1.4 m/s for floes of the same size, this compares well, hence serving as an argument for decoupling the mode of surge. As seen, the terminal velocity is reached before $\sigma_x=\sigma_f$.

Another important observation made in the perfectly coupled model was that rotation would not be expected to occur for isolated floes. Even for the case with ship impact velocity of 2.0 m/s (Figure 6-23 b)), the maximum lift of the far end of the floe was only one third of the deflection required to violate the criterion of the Winkler foundation. Without some sort of confining pressure from adjacent floes or an unbroken ice cover, the floe would either obtain its terminal velocity, or it would fail without rotating.

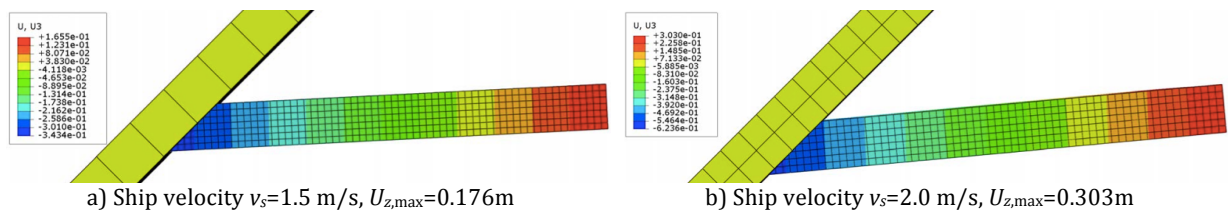


Figure 6-23 Maximum deflection of ice floe during 3D model interaction scenario for $L=W=10\text{m}$, $h_{ice}=1\text{m}$

In order to obtain rotation of the floe in the 3D model, a restriction in the form of restricting the far end of the floe from movement in the x -direction (while not imposing constraints on the other degrees of freedom) must be introduced. This added boundary condition corresponds to the longitudinal confinement a floe would be subjected to from adjacent floes as often is present in nature.

Figure 6-24 shows the development of rotation and bending stress for the case of no ventilation (Figure 6-25). There are two important aspects that one should take notice of when considering the stresses in the floe. Firstly, the conclusion made in Subsection 6.3.1 of reduced stresses after the far end of the floe is lifted out of the water is supported. Secondly, the absolute value of the tensile flexural stresses are lower in this case, due to the compression introduced by the boundary condition, hence preventing the floe from failing by bending

With conditions of no ventilation assumed, Figure 6-24 – where the angle of rotation is obtained as of Eq 6-31 – provides results that compare well with the theory of Valanto (2001) in terms of time spent to fully rotate the floe. These observations indicate that the decoupling of the motion of rotation, as suggested in Figure 6-19 would produce erroneous results.

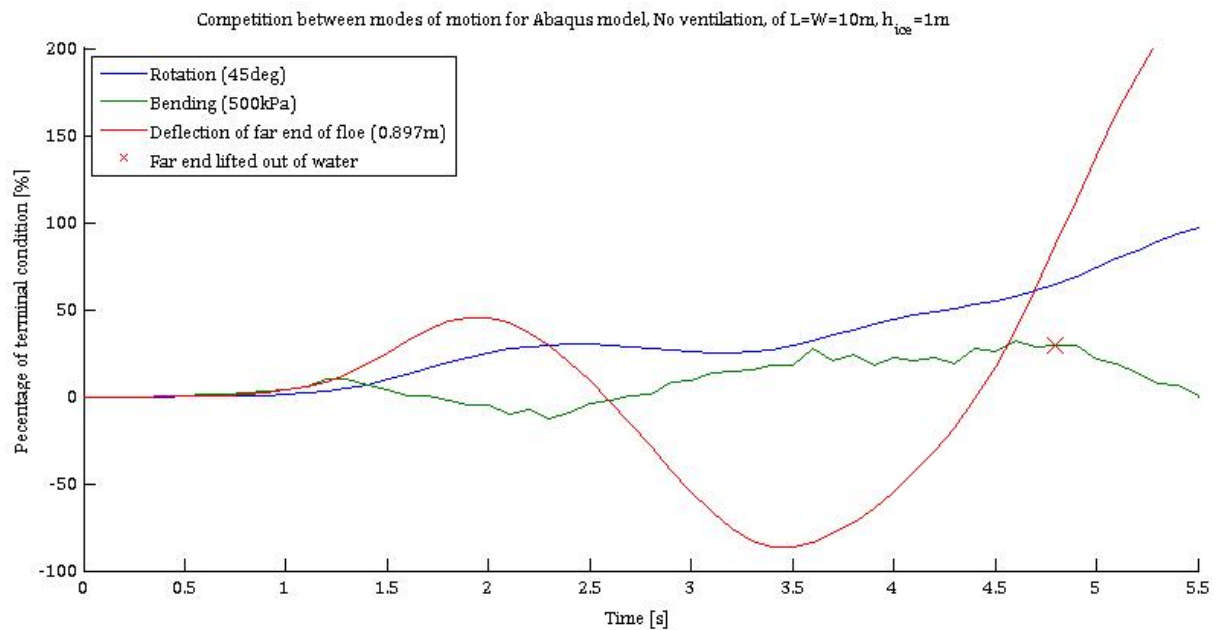


Figure 6-24 Competition between rotation and bending for ship-ice interaction in 3D model with $v_s=1.5\text{m/s}$

Examining the case of no ventilation further, Figure 6-25 both provide insight to the stress development process and the stress distribution in the floe. Neglecting the singularities present at the boundary condition at the far end of the floe, the distribution shows little dependency on the gravity forces one should expect to be present on the part of the floe lifted out of the water. This could be due to the support from the hinge at the far end of the floe, serving as a mechanism relieving the floe from bending moments.

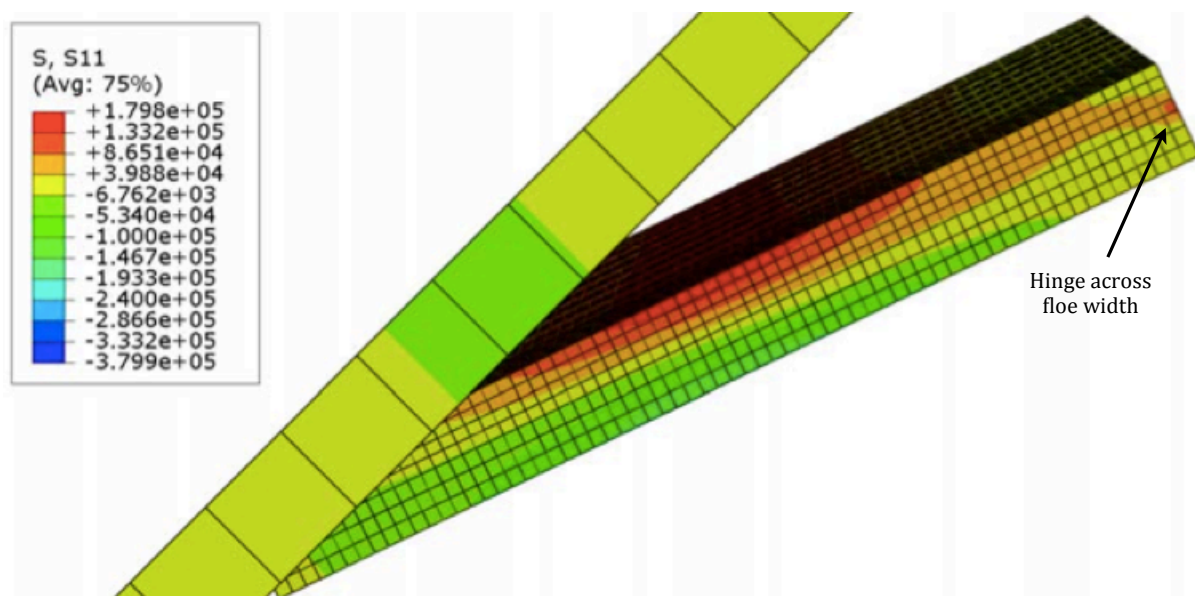


Figure 6-25 Maximum stress at the moment the far end of the floe lifts out of the water for $v_s=1.5\text{m/s}$

6.3.3 Comparison with theoretical 2D ice rotation module

Recent research performed by Lu et al. (2013) resulted in a theoretical model for level ice interaction with sloping structures. The results obtained by utilizing the *2D ice rotation module* described in their paper could, be compared to the results observed in the 3D finite element calculations presented in Section 6.3.2.

The approach of Lu et al. (2013) is to a large degree based on the assumptions Valanto (2001) used in his model, treating the ice floe (or ice beam as they name it) as a rigid body during rotation, due to the assumed small elastic deformations. Thereafter, they use the same static balance principle to calculate the stresses in the floe during rotation.

Regarding ventilation, their results indicate bending moments along the ice beam to be an order of magnitude larger for the semi-backfilled case of half ventilation, compared with the case of no ventilation. The reason for this finding could be explained by their static balance approach, only requiring equilibrium of vertical forces, thereby implying a significantly larger part of the floe to be lifted out of the water. Increasing the lifted length (d) in the semi-ventilated case 3 times the length of the case of no ventilation corresponds well to 10 times the moment, as this is dependent on d^2 . For the submerged part of the floe, the load intensity would depend on $(\rho_w - \rho_i)$ and $(\rho_w - \frac{1}{2}\rho_i)$ accordingly, hence also explaining the ratio of approximately 5, as found in Figure 6-26. From a theoretical point of view it's therefore appropriate to claim that the assumption fully ventilated interaction conditions would be more conservative than the opposite.

Although the results obtained by Lu et al. (2013) seems appropriate, several of them were not possible to reproduce in the 3D ice-structure impact analysis. As described in Figure 6-23, the floe reached its terminal velocity before it was lifted out of the water. The main reason was that only isolated floes were treated. Lu et al. (2013), did not treat isolated floes. Imposing an additional constraint on the floe, retaining movement in x-direction for the far end of the floe, should make the results comparable.

As seen in Figure 6-26, Lu et al. (2013) found a peak of the bending moment at the water-air contact point for the end of the floe that gets lifted out of the water ($d-L_1$ transition point, Figure 6-27). Due to the seemingly appropriate theoretical foundation, the stresses were also expected to behave similarly in the 3D numerical model. This was, however, not the case. As described in the discussion above Figure 6-25, this might be due to the error of introducing the rigid boundary condition in x-direction for the far end of the floe. Due to not accounting for equilibrium of horizontal forces, this force could seem to be forgotten in the moment calculation. Hence, the desirable validation of the calculation of stresses based on the rigid beam assumption would be infeasible.

Still, the 3D model doesn't necessarily disprove the validity of the *2D ice rotation module*. As the 3D model assumes that the ship is moving and that the ice floe is initially at rest, the model of Lu et al. (2013) assumes that the sloping wall structure is fixed, while the floe is the moving instance. Hence one could imagine that the floe would be able to rotate and submerge sufficient momenta of the floe is present at the point of interaction.

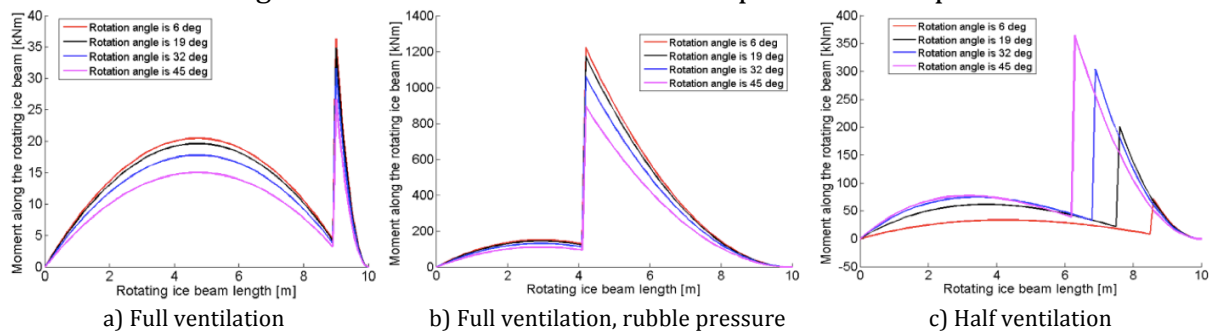


Figure 6-26 Moment distribution during the ice beam rotation process (Lu et al, 2013)

6.4 Discussion and comparison of decoupled and coupled approach

In order to develop a proper criterion for unbreakable floes, caution must be taken in order to maintain on the conservative side when making assumptions (Figure 6-1). In the light of the discussion in Section 6.2 and Section 6.3, the following should therefore be the basis for development of the final criterion:

- *Loading of the full edge* of the floe would always be the more conservative approach when faced with the choices of Figure 6-4. The loads an ice floe is capable of resisting is limited by its compressive strength – hence a larger loading area will produce larger forces in the floe.
- *Full ventilation* is a more conservative assumption than partly or no ventilation
- *The flexural stress of the floe* is at maximum at the point where the far end of the floe lifts out of the water. Determining the unbreakable-criterion as whether the floe could resist the forces required for $y_b > y_{b,lim}$, would hence be conservative

As seen, by comparison of the approaches of decoupling (Section 6.2) and coupling (Section 6.3) of the modes of response, the first is too conservative for bending. However, decoupling of the surge component seems to provide good results. One important observation from the decoupled events is that the stresses are likely to be at it's maximum when the floe leaves the water. This could be utilized in order to define the criterion for unbreakable floes.

Solving Eq 6-12 for $y_{b,lim}$ (Eq 6-17) and applying to Eq 6-15 and Eq 6-16 gives the flexural stress along an edge-loaded floe as follows:

$$\sigma_{b,max}(x) = 3k \frac{y_{b,lim}}{Wh_{ice}^2 \lambda^2} \frac{\sinh(\lambda L) \sin(\lambda x) \sinh(\lambda x') - \sin(\lambda L) \sinh(\lambda x) \sin(\lambda x')}{\sinh(\lambda L) \cos(\lambda L) - \sin(\lambda L) \cosh(\lambda L)} \quad \text{Eq 6-33}$$

Iteration could then be used to find the corresponding length and thickness of the floe that would provide $\sigma_{b,max} = \sigma_f$. Elaborating on the thoughts of Lu et al. (2013), and with reference made to the process of rotation described by Valanto (2001), the possibility of secondary breaking as the far end of the floe elevates above water level and gets loaded by its self-weight, should be investigated (Figure 6-27).

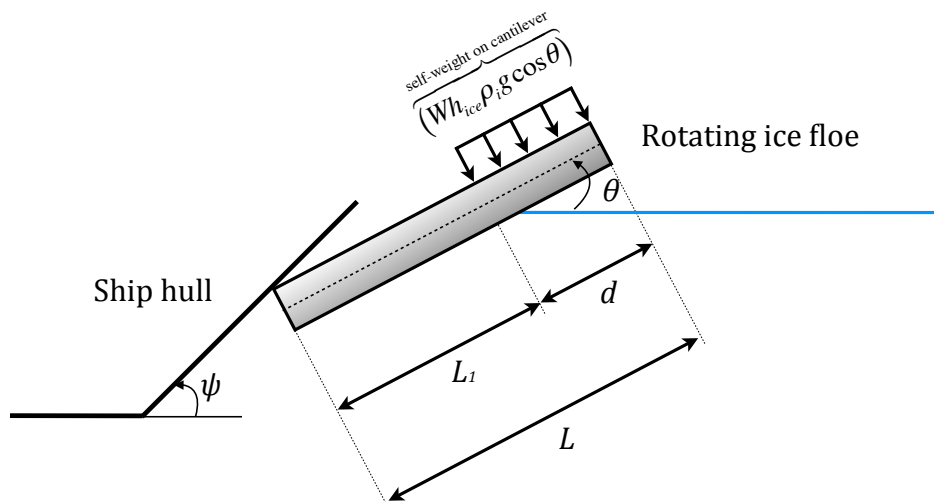


Figure 6-27 Load on cantilever part of floe lifted above the waterline (after Lu et al. (2013))

Generally, the elevated part of the floe could be considered as a uniformly loaded cantilever (as defined in Lu et al. 2013), with length equal to $d=L-L_1$ (Eq 6-27). Iteration is then performed in order to obtain the maximum length of the floe that would not give secondary breaking for a given length, as described in Eq 6-34 and Figure 6-28. Be aware that this is a conservative estimation, since axial load in the floe due to confinement and self-weight is neglected. Including this load would lower the flexural stresses.

$$\left. \begin{aligned} M_{\max}(\theta) &= \frac{\overbrace{(Wh_{ice}\rho_i g \cos\theta)}^{\text{self-weight on cantilever}} \cdot d(\theta)^2}{2} \\ \sigma_{\max} &= \frac{6M_{\max}}{bh_{ice}^2} = \sigma_f \end{aligned} \right\} \Rightarrow d_{cr}(\theta) = \sqrt{\frac{\sigma_f}{3\rho_i g \cos(\theta)}} h_{ice} \quad \text{Eq 6-34}$$

Combining Eq 6-27 and Eq 6-34, one obtains the relationships for the expected (d) and critical (d_{cr}) cantilever length during the process of rotation. Figure 6-28 shows that the critical length, for which one would expect secondary breaking to occur before rotation is completed, is approximately $L=W=7.3$ m for a floe of $h_{ice}=0.5$ m.

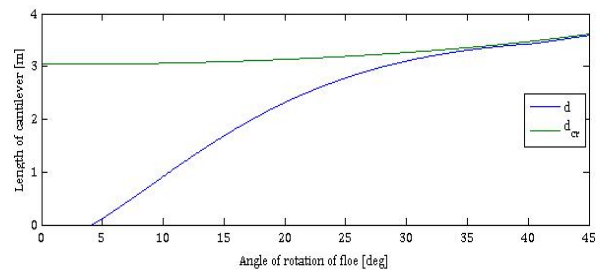


Figure 6-28 Limit stadium for secondary breaking of rotating floe of $L=W=7.3$ m, $h_{ice}=0.5$ m

Combining the limits given above provides the limit in Figure 6-29 for which floes that could be considered as unbreakable (Figure 6-29). Note the point of transition at $h_{ice}=1$ m, where the limit for lifting the floe out of the water becomes governing for the criterion opposed to the secondary breaking, which is governing for thinner floes.

Worth mentioning is that the phenomenon of secondary cantilever breaking – to the authors knowledge – not have been observed in nature. Hence could the introduction of secondary breaking, as a limiting condition, be an overly conservative approach.

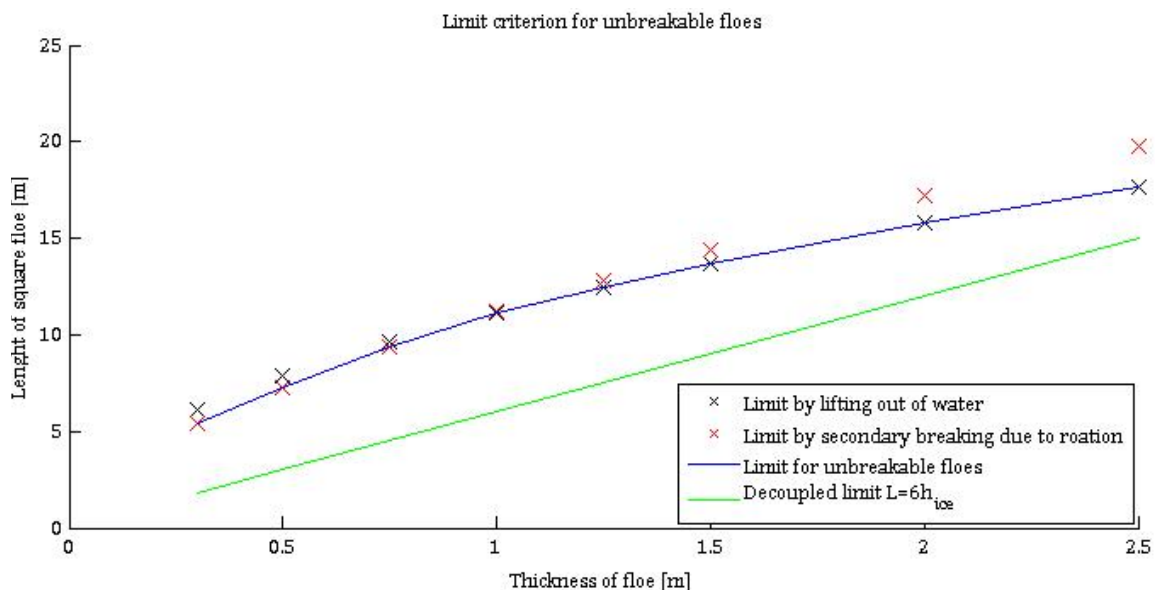


Figure 6-29 Limit for unbreakable ice floes. All floes below the blue line could be considered unbreakable

The effect of surge could be incorporated in the criterion in order to increase the length for which a floe could be considered as unbreakable. This, due to the possibility of the floe reaching its terminal velocity, $v_{floe}=v_s$, before bending failure would occur. For instance, a floe of 1.5m thickness, hit by a ship of $v_s=1\text{m/s}$, could have dimensions of $L=W=15.8\text{m}$ (iterations based on APPENDIX A) and still reach its terminal velocity before having its far end lifted out of the water or being subjected to bending failure.

One of the main assumptions in this chapter is that a floater is moving towards a floe initially at rest. However, if the criterion developed is simply a function of floe geometry, neglecting inertia, the results could just as well be transferred to the case of a geo-fixed floater or a ship on dynamic positioning encountering drifting sea ice. Hence, the approach of including velocity effects through the surge mode should not be pursued in order to make the criterion more robust, as long as dynamic effects are omitted. The consequence of such assumption would be that one could argue that this limit would only be applicable for the case of longitudinally confined floes, as it only treats the competition between rotation and bending. Still, the reason for non-occurrence of rotation during the unconfined case is that the forces are not able to build up to the level required for rotation before terminal velocity is reached. Hence, a floe that would be able to resist rotation will always be able to resist the forces required for obtaining terminal velocity as well.

The purpose of the development of the unbreakable-criterion is to be able to instantaneously determine whether an ice floe is breakable instantaneously when ship-ice contact occurs. Therefore, the possibility of deriving an analytical expression is not pursued; curve fitting is found more appropriate. The expression in Eq 6-35 shows good fit with the limit for unbreakable floes as shown in Figure 6-29, with all residuals less than 2%. The equation is adjusted in order to have all residuals on the conservative side.

$$L_{\text{lim}} = \sqrt{130h_{\text{ice}} - 11}, \quad 0.3\text{m} \leq h_{\text{ice}} \leq 2.5\text{m} \quad \text{Eq 6-35}$$

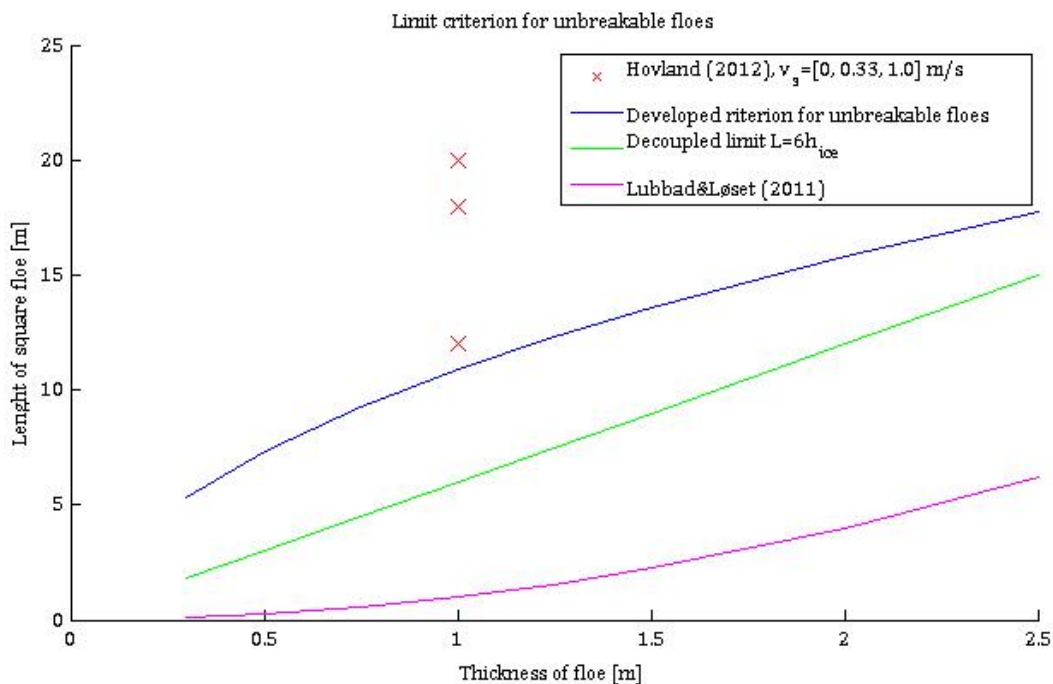


Figure 6-30 Comparison of developed criterion with the other approaches present in the literature

Figure 6-30 intends to compare the currently developed criterion with previous approaches. The main finding is the comforting placement below the quasi-static approach of Hovland (2012), while still being substantially less conservative than the initial approach of Lubbad and Løset (2011) and the decoupled limit. Not shown is that the criterion also is within the expected limit of the breaking length of a semi-infinite floe, $3h_{ice} < L_b < 10h_{ice}$, as stated in ISO19906 (A.8.2.6.2).

Breakable floes require calculation of intra-floe stresses in order to determine which of the modes of failure (Figure 3-4) the floe would be subjected to. When treatment as unbreakable is feasible, only rigid body motion of the floe – which requires far less computational power – needs to be considered. Hence, the main benefit of this newly developed criterion is the ability to reduce the computational expense, while at the same time providing the conservatism necessary to ensure that no breakable floes are treated as unbreakable.

6.5 Summary and proposed criterion

This chapter describes the process to obtain a criterion for unbreakable ice floes. The criterion was obtained by utilizing two different approaches. First a “decoupled motions”-approach, based on analytical solutions for floe rotation (Valanto, 2011), bending of beams (Hetenyi, 1946) and simple equations of motion, was first pursued. The decoupled approach resulted in the unbreakable-limit as of Eq 6-30. Thereafter a semi-coupled and a fully coupled approach (Section 6.3), based on results from an Abaqus model, proved that for floes shorter than the limit for secondary breaking (Figure 6-29), the bending stresses in a floe is at it’s maximum when the far end of the floe gets lifted out of the water. Finally, the obtained knowledge was assembled to a criterion defined by the length (L) to thickness (h_{ice}) ratio of the floes.

Although the criterion is based on isolated floes with one edge fully loaded, the previous discussions and verifications through *Abaqus*, proved this criterion also to be useful for non-isolated floes with loading covering less than one full edge (as would be the case for most ship-ice interaction scenarios). Further, only square floes have been discussed in the previous sections. This, however, is of less importance to the applicability of the criterion. As long as the length parameter (measured normal from the hull interaction point) is within the limits defined by Figure 6-31, the representative width of the floe could be less than the width without introducing any error. In case of $W > L$, fully loaded floe edge (Figure 6-4) needs to be present in order for the developed criterion to be valid.

The proposed solution is conservative, but in order for the criterion to be robust this is a necessity. Compared to the previously proposed criterion by Lubbad and Løset (2011), this still represents a substantial improvement, as the area of the unbreakable floes is allowed to be more than 100 times larger. Hence the updated criterion could decrease the computational cost substantially. Figure 6-31 depicts the decision mechanism for the updated criterion.

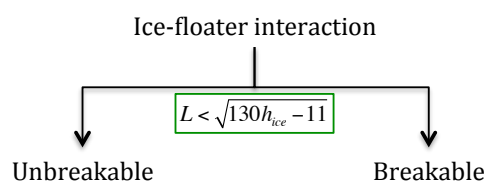


Figure 6-31 Criterion for determination of unbreakable ice floes

The major area of improvement for the criterion is to develop a dependency on the flexural strength, which in this case was assumed to be $\sigma_f=500\text{kPa}$. The other important assumptions of the criterion, hence dependencies to be investigated further, are:

- Homogenous ice with parameters as of Table 2-2
- Central ship-ice floe impact
- Hull inclination angle of $\psi=45^\circ$ with buttock angle of 180° (fully loaded edge)
- Lost mass of floe due to crushing of floe edges is neglected
- Dynamic effects and the potential improvement of the criterion by including the interaction impact velocity are excluded
- The floe would be unbreakable if the maximum force required to rotate the floe is less than the force corresponding to the flexural strength during bending
- Floes are treated as unbreakable if they are capable of both
 - Resisting the force required to lift its far end out of the water
 - Resist secondary breaking momentum of cantilever part during rotation

7 Splitting as a load releasing mechanism in ice

The introduction of this thesis states the lack of knowledge on splitting, and the relevance of further examination of this particular mode of failure for ice. This chapter therefore evaluates the previously developed approaches to treat splitting, through use of the nonlinear *Cohesive Element Method* in *Abaqus 6.12-1*.

Validating the old LFM-approaches for prediction of splitting, with new theory and computational power through cohesive elements, would develop valuable insights to the phenomenon of splitting as a load release mechanism in ice. Regarding the discussions of Chapter 6, one should be aware that the previous LFM-approaches only treats ice-structure impact for non-inclined cylinders ($\psi=90^\circ$). Hence, only in-plane forces are considered. Ice bending failure or rotation is therefore not relevant for this comparison.

7.1 Model setup

The loading and boundary conditions was applied to replicate the loading conditions representative for Bhat (1988) and Sodhi and Chin (1995), which both treated splitting of rectangular floes by means of LFM. As seen in Figure 7-1 and Figure 7-2, this implies applying the splitting force (P_{sc}) as a pressure on the edges of a pre-cut crack and applying hinges to the far end of each part of the floe to be split. The depth and width of the cut was arbitrarily chosen to be 0.15m, hence corresponding to $\beta=0.5$ of Bhat (1988) and $d=0.30$ in the model setup of Sodhi and Chin (1995), as seen in Figure 4-14. The same distance was used between the hinges, since this was found preferable to avoid introduction of distorted elements during the meshing procedure.

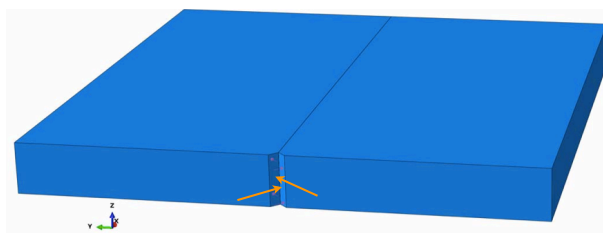


Figure 7-1 Pressure loading on pre-cut crack surface

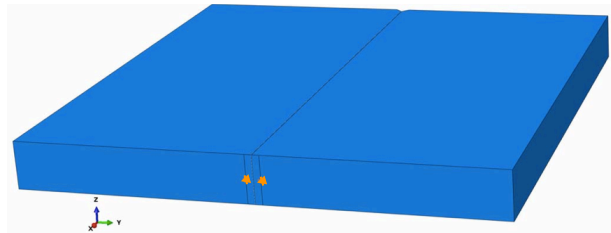


Figure 7-2 Hinges at far end of floe, $U_1=U_2=U_3=0$

Surface-based tied constraints were used to connect the bulk material and the cohesive zone. This was done in order to be able to apply a finer mesh to the cohesive zone than the bulk material, as described to be beneficial in the *Abaqus 6.12 Analysis User's manual 32.5.3*. For the bulk mesh, C3D8R-elements of common size 0.1m (Figure 7-3) were chosen. A simple mesh dependency test of the bulk material proved this choice to be adequate for the splitting phenomenon to be observed. The implementation of the cohesive method in the splitting analysis was done by inserting an infinitesimally thin layer of cohesive elements along the centreline of the floe.

Brick elements of type COH3D8 were used to model the cohesive zone. Further, the stacking direction was defined to align the thickness direction of the cohesive elements in the global y-direction. The node coordinates of the cohesive instance were then adjusted in order to obtain zero element thickness.

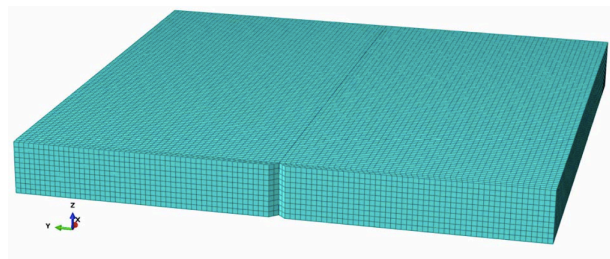


Figure 7-3 Mesh for examination of splitting

Due to the expected failure along the line of the cohesive elements, the bulk material was considered linear-elastic throughout the analysis. The bulk element material parameters were taken from Table 2-2. Based on the discussions of Chapter 2 and 4, the tensile strength was chosen to represent the cohesive failure stress.

Equal cohesive stiffness was applied in all directions, and the *initial thickness*-option for the cohesive section was specified as unity. Eq 4-21 then proves that the cohesive stiffness would be directly comparable to Young's modulus. The rate-independent K_{nn} , as shown in Figure 7-4, was chosen to be 10 times the stiffness of the bulk material. The logic behind this choice was to prevent the cohesive zone from introducing global softening, and to ensure brittle behaviour.

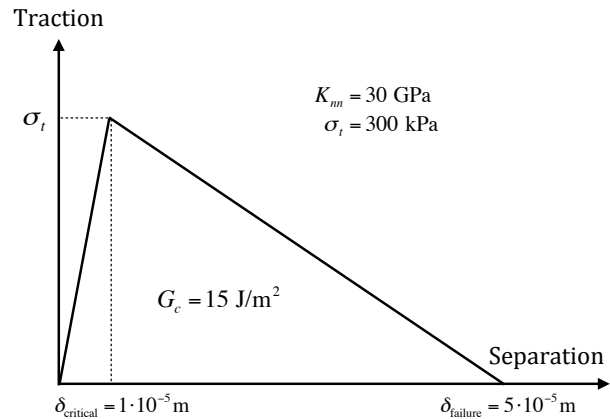


Figure 7-4 Illustration of the cohesive traction-separation relationship for $G_c=15\text{J/m}^2$, $\sigma_t=300\text{ kPa}$ (δ -axis not in scale)

Abaqus 6.12-1 Explicit was chosen for the analysis. The reason for not applying an implicit method, was the desire of obtaining information on the time dependent crack growth. Konuk et al. (2009b) emphasise that the time increment should be chosen small enough to ensure that the cohesive elements require several steps before they fail. The default time increment in *Abaqus* takes care of this for all the following analyses. Since these time increments are diminishingly small, the double precision option was used in order to minimize round-off errors. Further, Konuk et al. (2009b) suggests that a sampling rate of at least 100 Hz should be used. Based on the mesh dependency study, a sampling rate of 1000 Hz was chosen in order to capture the rapid propagation that characterizes the splitting process examined in this chapter.

When performing the validation, one could chose between load-controlled or displacement-controlled deformation of the floe. There are pros and cons with each method. The first would be able to determine the realistic degradation of the cohesive zone, while the latter avoids the expected instability as crack extends towards its critical length. For load-control, small numerical instabilities could cause large errors. Therefore, displacement-controlled deformation was used for the main comparison, whereafter a load-controlled case study was performed.

In order to compare the results obtained by the cohesive element method in *Abaqus* with the LEFM-approach of Bhat (1988), the applied load and reaction forces needs to be translated to the equivalent horizontal load in surge direction. Figure 7-5 shows the critical applied impact force during the *Abaqus* analysis (P_{SC}) and the equivalent impact force (P_{IMPACT}). The latter corresponds to P^* in Eq 4-10. For $\beta=0.5$, $P_{IMPACT}=\sqrt{2}P_{SC}$. No dynamic effects are included.

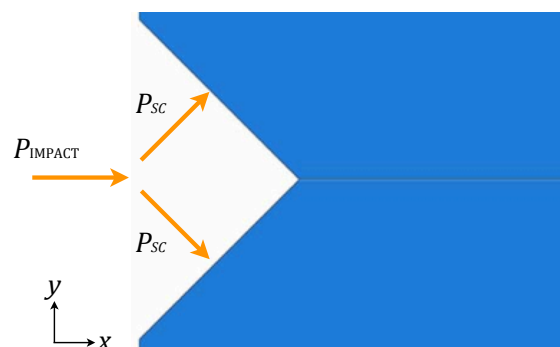


Figure 7-5 Relationship between the analysis applied force and corresponding Bhat (1988) impact force

Further, for comparison with the previous LEFM-approaches, a reference fracture toughness needs to be applied to the splitting load equations of Section 4.4. By Eq 4-20, it's obvious that the fracture toughness not necessarily can be taken as the preferred values in the papers of Bhat (1988), Bhat et al. (1991) and Sodhi and Chin (1995). As discussed in Subsection 4.4.7, the fracture toughness is directly related to the energy release rate. While the standard fracture toughness value of $K_{IC}=115 \text{ kPa}\sqrt{\text{m}}$ belongs to the school of Timco, Dempsey is the one behind the fracture energy level of 15 J/m^2 . It would therefore not be consistent to mix these values. Comparable values, based on Young's modulus of 3 GPa , are shown in Table 7-1. Since Dempsey et al. (2012) presents the fracture energy (G_c) obtained from *in field* experiments, this set of values are chosen for the first evaluation of the LEFM approaches. Still it's important to notice that Eq 4-20 is derived under the assumptions of LEFM, while Dempsey's derivation of the fracture energy was based on a nonlinear approach. As discussed in Chapter 4, LEFM requires a small fracture process zone compared to the specimen size, which not necessarily is in concurrence with the experiments of Dempsey et al. (1999). The *assumed* consistent values are therefore more the result of engineering approximation than an objective truth.

Table 7-1 Corresponding values of fracture toughness and fracture energy. Values by Eq 4-20 are denoted with *.

	Fracture toughness	Fracture energy
Timco	$K_{IC}=115 \text{ kPa}\sqrt{\text{m}}$	$G_c=3.93 \text{ J/m}^2^*$
Dempsey	$K_{IC}=225 \text{ kPa}\sqrt{\text{m}}^*$	$G_c=15 \text{ J/m}^2$

Mesh sensitivity is a common problem in simulations with cohesive elements, as stated by Lu et al. (2012a) among others. Therefore, a mesh sensitivity study was performed in order to make sure that the chosen mesh for the analyses would obtain energy convergence. The test was performed by displacement-controlled deformation, and the results are presented in Figure 7-6. Based on these observations, square cohesive elements, with a mesh density of 20 elements per meter in both directions in the cohesive plane, were chosen to represent the fracture process zone for the further numerical investigations.

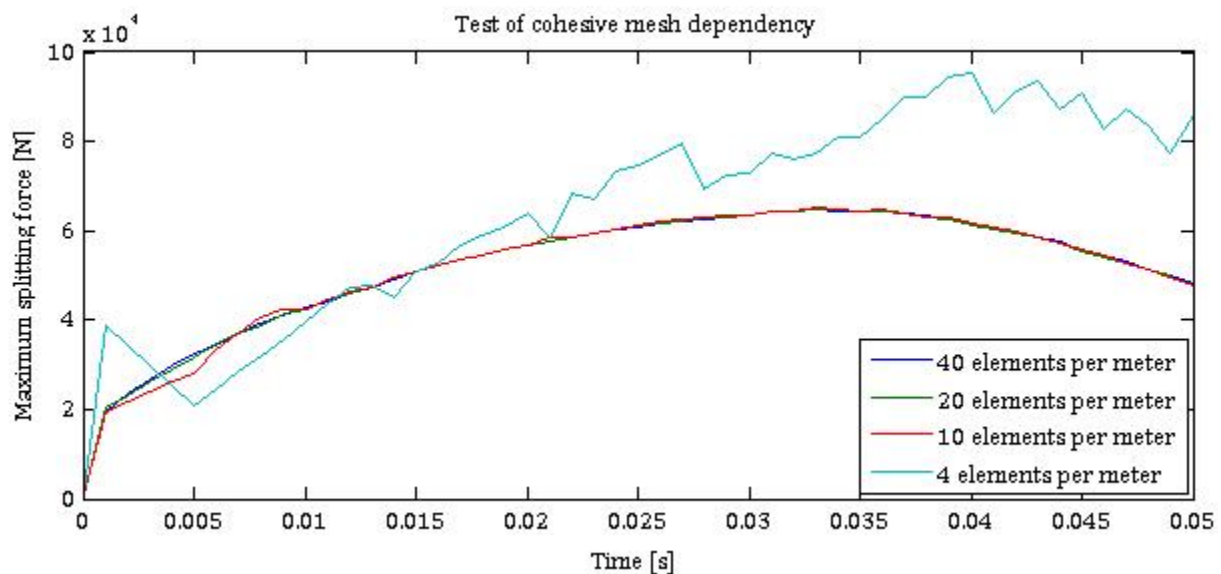


Figure 7-6 Mesh dependency for the cohesive zone. Forces measured at nodes in the centre of the pre-cut crack. Performed with displacement controlled deformation with constant crack mouth opening velocity of 0.01 m/s on a floe of $L=W=10 \text{ m}$, $h_{ice}=1 \text{ m}$. Elements per meter given for both directions in the cohesive plane (square elements).

7.2 Results and discussion

Three different numerical experiments were performed. One displacement-controlled analysis of the geometric influence on the floe resistance towards splitting; Two load-controlled analyses on crack propagation and the crack velocity during rapid fracture. The results are continuously discussed as they are presented.

7.2.1 Geometric influence on the ice floe resistance towards splitting

In order to provide insight to the phenomenon of splitting, and for comparison with the previously developed LFM-approaches, an initial study was performed on a selection of square floes. For determination of the maximum splitting load capacity it would be beneficial to avoid the instability often associated with load controlled deformation. Therefore, displacement controlled deformation conditions were chosen. A compared-to-the sampling rate sufficiently small constant crack mouth opening velocity of 0.01m/s was applied over the same pre-cut crack surface as depicted in Figure 7-5. The only nonzero component of the displacement field was in the global y-direction.

The observant reader will see the discrepancy between the results reported in Table 7-2 and the loads for the mesh dependency analysis (Figure 7-6). The reasons are two: Firstly, the mesh dependency load does not represent the total load, but a representative selection of nodal forces; Secondly, the observed lateral resistance during the crack propagation is back-calculated with Eq 4-9, in order to obtain values comparable with the predicted impact loads (Eq 4-10) of Bhat (1988). The force evolution with time for the different floe sizes is shown in Figure 7-7.

Table 7-2 Maximum load (kN), for displacement-controlled splitting. Comparable results of Bhat (1988) are given in parenthesis for comparison, for $G_c=15 \text{ J/m}^2$, $\sigma_t=300 \text{ kPa}$, $K_{IC}=225 \text{ kPa}\sqrt{\text{m}}$ and $\beta=0.5$.

	$L=W=5 \text{ m}$		$L=W=10 \text{ m}$		$L=W=15 \text{ m}$		$L=W=20 \text{ m}$	
$h_{ice}=1.0 \text{ m}$	170	(190)	230	(270)	270	(330)	340	(380)
$h_{ice}=2.0 \text{ m}$	330	(380)	460	(540)	580	(660)	680	(770)

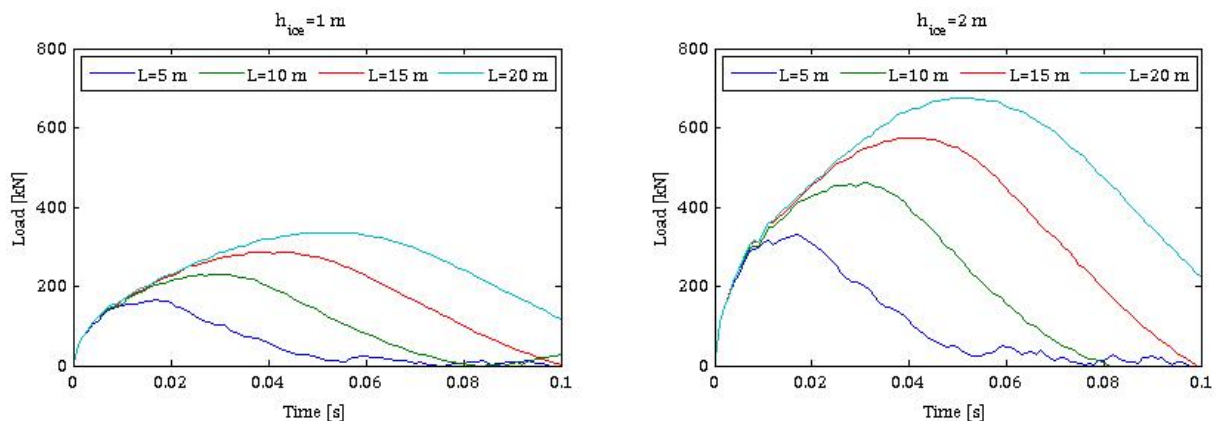


Figure 7-7 Force evolution for displacement controlled deformation with crack mouth opening of 0.01 m/s. For $G_c=15 \text{ J/m}^2$, $\sigma_t=300 \text{ kPa}$.

From Table 7-2 it's obvious that no perfect match between the cohesive approach and the LFM-approach of Bhat (1988) was obtained. This, even though consistent use of fracture energy (G_c) and fracture toughness (K_{IC}) was applied (Table 7-1). Still, they are only 15% off target, and there are at least two important factors that influence this discrepancy. Firstly, the tensile strength (σ_t) used in the cohesive element analysis is not adjusted in order to be consistent with G_c and K_{IC} , since no such general transformation

rule – to the author’s knowledge – exists. Increased tensile capacity would naturally provide larger (but also more brittle) resistance towards splitting for the same G_c . Secondly, the modulus of elasticity is an important part of Eq 4-20. Different choice of elastic modulus would alter the corresponding fracture toughness. For the cohesive element approach by Lu et al. (2012b), the elastic modulus of the bulk material was chosen as 0.35 GPa (also used in Lubbad and Løset, 2011). If this value is assumed, $G_c=15 \text{ J/m}^2$ would correspond to $K_{IC}=77 \text{ kPa}\sqrt{\text{m}}$, for which the comparison in Table 7-2 would look completely different. Hereby the difficulty in obtaining consistent and comparable results for fracture of ice is illuminated.

Although not perfect, obtaining results of the same order for small-scale ice floes is promising. Mulmule and Dempsey (1999) claimed that for ice floes larger than $L=W=30 \text{ m}$, the size of the fracture process zone (FPZ) would essentially be the same as for a large floe of 80 m, hence would be constant. One conclusion that could be made out of this is that the CZM-approach would converge towards LEFM for larger floes, as the FPZ length-to-floe length ratio would decrease. Therefore, eight more simulations were performed to test this assumption (Figure 7-9). Due to computational expense, and the limited time available, the largest floes were not tested for $h_{ice}=2 \text{ m}$.

For computational efficiency, the mesh for the floes larger than 20 m was in general made coarser (Figure 7-8). Still, it was made sure that the mesh in the vicinity of the crack had the same fineness as described for Figure 7-3.

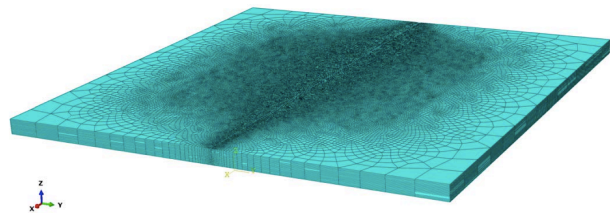


Figure 7-8 Varying mesh density for larger floes

As evident from Figure 7-9, the expected convergence was confirmed. Still, this was obtained for $\sigma_t=300 \text{ kPa}$, which was chosen on basis of the discussions of Chapter 2 rather than as a consequence of the chosen G_c and calculated K_{IC} , since this relationship does not exist. The reasons for the concurrence might be that the choice of tensile strength, elastic modulus and fracture energy for the cohesive model all together provide conditions equivalent to $K_{IC}=225 \text{ kPa}\sqrt{\text{m}}$.

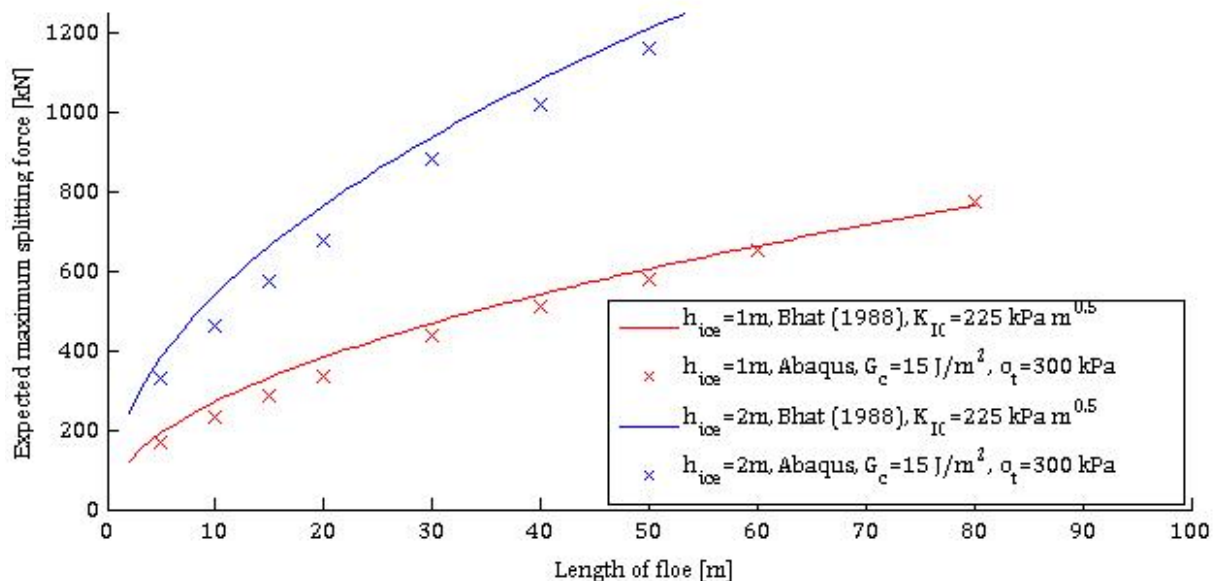


Figure 7-9 Comparison between Bhat (1988) and the Cohesive Element Approach for compatible parameters

Disregarding the potential inconsistent σ_t and the discrepancies in the results, one important general conclusion is still made. The above-presented results provide proof that the splitting load depends linearly on the ice thickness (h_{ice}), while the length (L) influences through \sqrt{L} . This is as predicted by both Bhat (1988) and Bažant (2000), hence serving as confirmation of that the model applied provides reasonable results, and that one is able to obtain comparable results for the linear and nonlinear fracture mechanics approach.

Although left to future research, a small test was performed in order to provide some insight to the influence the tensile strength (σ_t) has on the resistance towards splitting (P^*). For a constant fracture energy of $G_c=15 \text{ J/m}^2$, doubling and more-than-tripling σ_t , disproved the linear (order of 1) relationship one might intuitively expect. As seen in Table 7-3, the dependency compares approximately to an order of $-1/4$. It should, however, be noted that the limited data from this test is far from sufficient to conclude on the correct dependency. Still, the important observation is that the tensile strength is of minor importance to the total resistance towards splitting. These observations are in favour of the results presented in Figure 7-9. Since the results there – at least for the smaller floes – are 10-15% below the predictions of Bhat (1988), the (potentially more consistent) increase in tensile strength could cancel out the deviance.

Table 7-3 Comparison for different choices of tensile strength, $G_c=15 \text{ J/m}^2$. $L=W=10 \text{ m}$, $h_{ice}=1 \text{ m}$.

	$\sigma_t=300 \text{ kPa}$	$\sigma_t=600 \text{ kPa}$	$\sigma_t=1000 \text{ kPa}$
Impact load (P^*)	230 kN	283 kN (+23 %)	322 kN (+40 %)

The most important factor for the nonlinear $P^*-\sigma_t$ relationship, is the close dependency between CZM and the fracture energy release rate. As evident by Figure 7-4, $\delta_{failure}$ would decrease with increasing σ_t and constant G_c , providing more brittle behaviour. Constant G_c implies that the resistance towards energy applied to the crack remains the same regardless of σ_t . Understanding the combined influence of the elastic modulus, fracture energy, tensile strength and fracture toughness would therefore be important for improving the understanding of splitting in ice. Obtaining this relationship is beyond the scope of this thesis, but this topic should definitely be subject to further research.

Bhat (1988) developed a relationship between the floe aspect ratio and the splitting resistance (Figure 4-15). The results by Bhat (1988) were only presented with the superimposed effect of inertia included. As discussed in Chapter 4, the inertia would tend to close the crack due to horizontal bending stresses, hence increasing the splitting resistance substantially. Superposition is not applicable for nonlinear theory, and the limited time did not permit an extensive impact study. However, the concurrence between LEFM and CZM found in Figure 7-10 provides the possibility to see the CZM-results in Figure 7-10 as the pure tensile stress component of the total, inertia driven, splitting force. The latter aspect ratio dependency is assumed related to the horizontal bending stiffness of the floe.

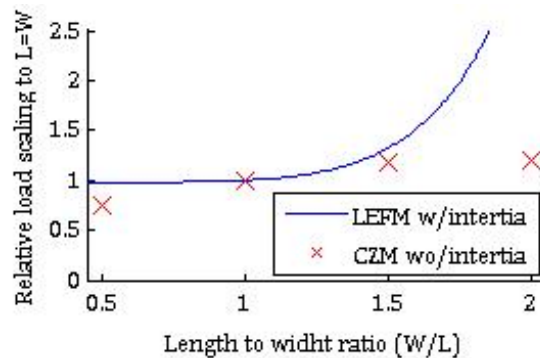


Figure 7-10 Comparison between the reported length-to-width ratio of Bhat (1988) and observations with CZM

7.2.2 Crack propagation and velocity

Two case studies for splitting of a reference square floe, of $L=W=10\text{m}$ and $h_{ice}=1\text{m}$, was investigated by a load-controlled analysis. The load in Table 7-4 corresponds to the total force exerted on each pre-cut crack surface of each side of the floe (P_{SC}), and was applied instantaneously in the following analyses. As seen, is the critical P^* larger for the load controlled analysis. The reason for this is the same as for the difference in the solutions of Bhat (1988) with and without the inertia effect. A closing moment is induced by the x -component of P_{SC} due to the boundary conditions (non-central hinges), increasing the capacity towards splitting (compare Eq 4-10 and Eq 4-11). This, however, has minor importance for the illustrative purpose of this subsection.

For the crack propagation analysis, an interesting observation was that increased loads only gave minor increase for the crack length-to-floe length ratio (α), as long as the applied load was less than the predicted splitting resistance of Table 7-2. For loads larger than, or in the vicinity of this load, rapid propagation occurred. Compared to the displacement-controlled analysis for the same floe, the observed capacity here is somewhat lower. The reason for this is the above-mentioned instabilities associated with load-controlled analysis, and the unstable nature of the crack (c) as it extends to its critical length. For Abaqus output plots, reference is made to APPENDIX E.

Table 7-4 Results for $L=W=10\text{m}$ $h_{ice}=1\text{m}$. Tested for $\beta=0.5$, $d=0.30\text{m}$, ref. Figure 4-14.

Applied load P^* (P_{SC})	Deleted element columns	Alpha ($\alpha=c/L$)	Time to stable crack
240 (170) kN	5	0.040	0.007
250 (180) kN	7	0.050	0.043
270 (190) kN	12	0.075	0.088
280 (200) kN	16	0.077	0.077
300 (210) kN	23	0.130	0.182
310 (220) kN	all	1.000	0.132
350 (250) kN	all	1.000	0.066

Bhat (1988), Bhat et al. (1991) and Sodhi and Chin (1995) all described the occurrence of rapid propagation once the crack exceeds 5-20% of the floe length. For the case of only tensile loading, Bhat (1988) specified the critical crack length ratio to be 15%, hence being in line with the results shown in Figure 7-11.

Figure 7-11 depicts the evolution of degradation in the cohesive elements for a given load of $P_{SC}=220\text{ kN}$. Crack growth acceleration was observed as the crack extended past its critical length for stable propagation. This was expected, as the torque will increase with increased crack opening. Further, it's interesting to observe that the stable range of the crack growth observed by use of nonlinear theory coincides with the previous predictions by LEFM.

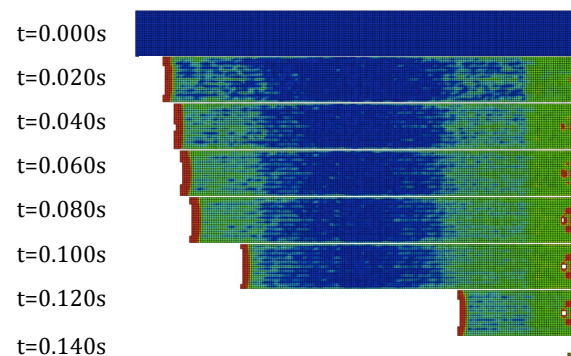


Figure 7-11 Crack propagation illustrated by element degradation plot, for $P_{SC}=220\text{ kN}$, $L=W=10\text{m}$, $h_{ice}=1\text{m}$

Regarding the crack propagation velocity, neither of the previous approaches to splitting load estimations available in the literature provides any information on how fast the crack propagates. The model developed for this chapter does. Table 7-4 shows that the crack propagation velocity increases with increased load (see $P_{sc}=220$ kN and $P_{sc}=250$ kN). This is reasonable, as the increased load would imply more energy applied to the fracture process zone for each incremental increase in deformation. Further, by calculating rough averages based on Figure 7-11, it's possible to estimate the crack propagation velocity. The first 0.10 s of the analysis the crack velocity is fairly constant at 20 m/s, before it accelerates to approx. 400 m/s. By looking more thoroughly into the 1000Hz output plot from the simulation, the estimate of half a kilometre per second crack propagation velocity was confirmed. One should still recognize that this test was performed on assumed homogenous ice, without thermal cracks or other localized defects embedded in the ice model. *In field* crack propagation is therefore likely to be even more rapid. Hence, a crack velocity of 666 m/s as suggested by Bhat (1988) or even as high as the dilatational speed of sound in ice is not unlikely (Subsection 4.4.1).

7.2.3 Suggested areas of improvements for the cohesive finite element model

The main area of improvement of the model presented in this chapter would be to perform a parametric study on the tensile strength in order to obtain better correlation between the approaches of LFM and CEM. Although perfect match between the results were not obtained, the linear relationship between them suggests that there should be found concurrence between the results for the appropriate choice of fracture toughness, elastic parameters, fracture energy and tensile strength. By applying such a relationship, one would be able to conclude on a more solid basis that the methods coincide. Further investigations on the influence these parameters have on each other should be performed, and is likely to provide a sound theoretical foundation that links all these values together.

All tests in this chapter are performed for $\beta=0.5$ and conditions corresponding to vertical hull of the impacting structure ($\psi=90^\circ$). In order to examine the competing phenomenon between splitting and other failure mechanisms for ice floes of various geometries, a complete impact CEM analysis should be performed. Such analysis would also provide insight on the potential load reduction to be obtained by splitting. A viable approach could then be to utilize the impact model described in Subsection 6.3.2. By implementing the cohesive zone as described this chapter, understanding of the influence the ship hull, friction and other modes of failure have on splitting as a load releasing mechanism for a floater in ice could be enhanced. Dynamic effects were of less importance for the validation purposes of this chapter. Still, these effects might prove to be important for the numerical impact tests, and should therefore considered for further studies.

All the previous LFM-approaches assume that the ship-ice impact will occur central on the ice floe. As discussed in Chapter 6, central impact is not likely to be the standard interaction scenario for *in field* operations. The Cohesive model, on the other hand, could be used to treat non-central impacts, if more than one cohesive zone is embedded in the bulk material, like the models of Konuk et al. (2009) and Lu et al. (2012b). This should be a topic for future research.

Ice present in the Arctic would, as discussed in Chapter 2, not be homogenous due to its formation and later developed thermal cracks. Presence of such cracks might be the reason for the observed splitting of large ice caps at much lower force than the required load predicted by the results of this chapter. Shreyer et al. (2006) obtained the closing stress for a thermal crack to be in the order of 15-25 kPa. Although calculated for ice caps of several orders larger than the floes considered in this thesis, one could by utilizing the conclusions of Schulson and Duval (2009) use these values in combination with the splitting model of this chapter to predict failure loads for weakened zones of the ice for smaller floes as well. The thermal cracks could for instance be distributed randomly in a modelled ice cover, such as the one in the real-time simulator of Lubbad and Løset (2011).

Regarding the consistent values of fracture toughness (K_{IC}) and fracture energy release rate (G_c), the analyses performed in this chapter is based on the $G_c=15$ J/m² by Dempsey. A topic for later research could be to examine this relationship with the more commonly accepted fracture toughness of $K_{IC}=115$ kPa√m and its corresponding fracture energy release rate in order to observe if the same concurrence would occur. More full-scale tests to verify the fracture energy release rate (G_c) of Dempsey et al. (1999) would also be beneficial. The reliability of a material property value, which is solely based on a single test, is highly questionable.

More time could also have been spent on optimizing the mesh. Even though energy convergence was obtained for the method outlined in the *Abaqus user manual*, the available time did not permit a more thorough examination of other meshing procedures, like the “shared nodes”-approach. For further research, such methods should be compared with the one presented in this chapter.

If these improvements are understood and implemented, the model could be used to examine ship-ice interactions for various floe geometries and non-central impacts in order to quantify load reduction potential for splitting compared to other modes of failure.

7.3 Conclusions

Valuable information on splitting of ice was obtained by using a nonlinear fracture mechanics approach through the cohesive element method (CEM) to verify the LFM-relationships derived by Bhat (1988). By obtaining the consistent fracture toughness corresponding to the fracture energy release rate obtained by Dempsey et al. (1999), the results from LFM and CEM was found to converge for larger floes in accordance with the predictions of Mulmule and Dempsey (1999). The geometric dependency exerted on ice thickness and floe length on the splitting resistance stated by Bhat was confirmed.

Time to progressive failure, and hence the propagation velocity has to the author's knowledge not been previously analysed for splitting in ice. This chapter illustrates the possibility to observe these quantities by the means of the cohesive element method. The crack growth velocity after the crack length exceeded its critical value was found to be in the order of several hundred meters per second, which is in accordance with what reported by Bhat (1988) and Lubbad et al. (2012). Regarding the validity of the model, this is comforting.

The above outlined approach says little about the fracture process that occurs when an ice floe interacts with a sloping structure that introduce bending stresses as the floe deflects. It's not unlikely that radial cracking could produce massive fracture of the floe if the crack-to-floe length (α) ratio exceeds the critical α before a circumferential crack form. The critical crack length for which splitting of the entire floe would occur seems, from the results obtained in this chapter, to be approximately 10-15% of the floe length. Considering that the typical breaking length (distance to circumferential crack) for ice is 3-10 times the ice thickness (ISO19906), one could roughly estimate that splitting is likely for floes shorter than 20-100 times the floe thickness.

Limitations of the previous LEFM-approaches make them applicable only for cases of plane forces. The most important finding of the previous section is therefore the concurrence between LEFM and CEM, which provides confidence that cohesive elements would represent crack growth in a suitable manor. Hence it would be possible to perform, utilize and rely on, CEM-simulations for other loading cases than purely in-plane loading conditions.

For use in the numerical real-time simulator of Lubbad and Løset (2011), this would be of importance. One possible implementation of splitting could be the definition of a maximum horizontal contact force component, for which splitting of the floe would occur. Due to the concurrence between the simple equations of Bhat (1988) and the more advanced cohesive element simulation, the necessity of calculating the internal stresses in the floe would be redundant if the ship-ice contact pressure exceeds the defined limit. The dependency on bending failure is still to be investigated.

8 Summary, conclusions and recommendations for further work

The theory developed in this thesis serves as a contribution to the understanding of load releasing mechanisms of ice in general, and further development of the numerical real-time simulator for ship-ice interactions of Lubbad and Løset (2011) in particular.

8.1 Breakable or unbreakable ice floes

An improved criterion to decide whether an ice floe should be treated as breakable or unbreakable has been developed. Both a decoupled analytical and a coupled finite element approach was applied to the problem. While both resulted in conservative criteria, the latter both proved problems of inconsistency in the former. Additionally, it represented a less conservative criterion, while still guaranteeing no breakable floes to be treated as unbreakable. The coupled approach was therefore decisive to the development of the final geometric relationship for which floes to be treated as unbreakable.

The new criterion corresponds well to the available literature, and places naturally in the upper range of the assumed breaking lengths of ice floes defined in ISO19906. Compared to previous approaches, the one presented in this thesis represents a significant improvement in terms of the size of an ice floe that safely could be treated as unbreakable. Still, the criterion is developed in a manor that ensures the conservative assumptions needed not to treat breakable floes as unbreakable.

Even though the criterion represents a significant improvement, there are several aspects that aren't treated in this thesis that would be relevant to consider for further research. The most important areas for further work on this criterion would be thorough examination on:

- The effect of varying flexural strength of the ice
- The inclination of the ship hull and various geometric shapes of the ice floes
- The dependency of dynamic effects in relation to the velocity dependency

8.2 Splitting as a load releasing mechanism

Nonlinear elastic fracture mechanics, through use of the *Cohesive Element Method* (CEM), was used to validate the previously developed linear theories to determine the resistance towards splitting for rectangular ice floes. Similar results were obtained for comparison between the methods for consistent choice of fracture toughness and fracture energy release rate.

The difference in obtained results by the methods was found to converge as the floe size increased, as predicted by Mulmule and Dempsey (1999). For engineering applications, this implies that the computationally inexpensive LEFM-relationships derived by Bhat (1988), Bhat et al. (1991) and Sodhi and Chin (1995) could be used as maximum horizontal loads the structure will encounter during a ship-ice interaction scenario with isolated floes. In addition this provides confidence that CEM could be used to analyse impact situations and crack initiation processes too complex to model by *Linear Elastic Fracture Mechanics* (LEFM). The LEFM-limitation of only considering one crack can hence also be overcome by use of CEM.

Crack propagation during splitting of a level ice floe was investigated. For the critical crack length, at which rapid propagation would occur, correlation was found between

the new nonlinear fracture mechanics approach and the previous predictions from existing LEFM-theory. Splitting caused by the tensile field developed when ice impacts a vertical structure was the case of consideration. Still, if combined with the available knowledge on the radial cracking that occur during interaction with sloping structures, development of a criterion for when splitting is likely to occur is feasible.

Despite the observed match between linear and nonlinear theory, more research on the fracture energy release rate is necessary in order for the results obtained by CEM to be reliable. Designing structures based on predicted ice failure by a mode for which the material parameter is based on only one test, is not likely to be feasible regarding economic risk, environmental risk and political risk.

Arctic offshore field development in ice-infested areas is dependent of conservative design load criteria in order to guarantee safe operations. Splitting has traditionally been associated with reduced loads compared to other modes of failure. Thorough understanding of splitting has therefore not been seen as a prerequisite for enabling exploration and exploitation of the hydrocarbon resources present in the high north. If properly understood, splitting could prove to be important for optimization of ice management to reduce the loads encountered from ice-structure impacts. By improving the ice management procedures the risk of structural failure would be minimized. If ice management is used actively in the design procedure, deeper understanding of splitting could also prove to enable safe field development in areas where the current state of knowledge on failure of ice limits the range of feasible concepts. Focus on splitting as a load releasing mechanism for a floater in ice is therefore expected to be an important topic for Arctic offshore research.

The main areas of improvement for the approach towards splitting considered in this thesis will be to:

- Obtain better understanding on how fracture energy release rate, tensile strength, elastic modulus and fracture toughness relate to each other
- Understand the influence dynamic effects has on the phenomenon of splitting
- Examine how the confining pressure from adjacent floes influence the tendency of and load reducing capacity for splitting

9 References

9.1 Research papers and books

- Ashby, M. F. (1989): "Materials selection in conceptual design". Mater. Sci. Technol., Vol. 5, pp. 517–525.
- Assur, A. (1958): "Composition of sea ice and its tensile strength". In Arctic Sea Ice, U.S. National Academy of Sciences, National Research Council, Pub. 598, pp. 106-138.
- Barrenblatt, G.I. (1959): "On equilibrium cracks formed on a brittle fracture". Dokl USSR Acad Sci. 127:47–50.
- Barenblatt, G.I. (1959): "The formation of equilibrium cracks during brittle fracture. General ideas and hypotheses. Axially-symmetric cracks". Journal of Applied Mathematics and Mechanics, Vol. 23, pp. 622-636.
- Bhat, S. (1988): "Analysis of Splitting of Ice Floes During Summer Impact". Cold Regions Science and Technology. Vol.15, pp. 53-63.
- Baratta, Francis I. (1984): "When is a Beam a Plate?", Communications of the American Ceramic Society, C-86.
- Bažant, Z.P. and J. Planas (1998): "Fracture and size effect in concrete and other quasi-brittle materials". CRC Press.
- Bažant, Z.P. (2000): "Size effect". International Journal of Solids and Structures, Vol. 37, Issues 1–2, pp. 69-80.
- Bird, K.J., Charpentier, R.R., Gautier, D.L, Houseknecht, D.W., Klett, T.R., Pitman, J.K., Moore, T.E., Schenk, C.J., Tennyson, M.E. and Wandrey, C.J. (2008): "Circum-Arctic resource appraisal: Estimates of undiscovered oil and gas north of the Arctic Circle". U.S. Geological Survey Fact Sheet 2008-3049, 4 p. Version 1.0, July 23 2008.
- Cook, R.D., Malkus, D.S., Plesha, M.E. (2002): "Concepts and applications of finite element analysis 4th edition". John Wiley & Sons Inc. ISBN 978-0-471-35605-9
- Cornec, A., Scheider, I., Schwalbe, K-H. (2003): "On the practical application of the cohesive model". Engineering Fracture Mechanics, Vol. 70, Issue 14, pp. 1963-1987.
- Dempsey, J.P., Adamson, R.M., Mulmule, S.V. (1999): "Scale effects on the in-situ tensile strength and fracture of ice. Part II: first-year sea ice". Resolute, N.W.T. International Journal of Fracture 95, 347–366.
- Dempsey, J.P., Xie, Y., Adamson, R.M., Farmer, D.M. (2012): "Fracture of a ridged multi-year Arctic sea ice floe"
- Dugdale D.S. (1960): "Yielding of steel sheets containing slits". Journal of Mechanics and Physics of Solids, Vol. 8, pp. 100–104.

Eik, K. (2011): "Sea-ice management and its impact on the design of offshore structures". *Cold Regions Science and Technology*, Vol. 65 (2), pp. 172-183.

Elices, M., Guinea G.V., Gómez, J., Planas, J. (2002): "The cohesive zone model: advantages, limitations and challenges". *Engineering Fracture Mechanics*, Vol. 69 (2), pp. 137-163.

Evans, R.J., Parmarter, R.R. (1985): "Ice forces due to impact loading on a sloping structure." *Civil Engineering in the Arctic Offshore: Proceedings of the Conference Arctic '85*, pp. 220-229.

Frankenstein, G.E., Garner, R. (1967): "Equations for determining the brine volume of sea ice from -0.5 to -22.9 °C". *Journal of Glaciology* 6 (48), 943-944.

Frederking, R., Barker, A. (2002): "Friction of sea ice on steel for condition of varying speeds". *Proceedings of the 12th International Offshore and Polar Engineering Conference*, pp. 766-771. Kitakyushu, Japan.

Gammon, P. H., H. Kiefte, M. J. Clouter and W. W. Denner (1983): "Elastic constants of artificial ice and natural ice samples by Brillouin spectroscopy". *Journal of Glaciology* Vol. 29, pp. 433-460.

Geißler, G., Kaliske, M. (2010): "Time-dependent cohesive zone modeling for discrete fracture simulation, *Engineering Fracture Mechanics*, Vol. 77 (1), pp. 153-169.

Gillet-Chaulet, F., Gagliardini, O., Meyssonier, J., Zwinger, T., Ruokolainen, J., (2006): "Flow-induced anisotropy in polar ice and related ice-sheet flow modeling". *Journal of Non-Newtonian Fluid Mechanics*, Vol. 134, pp. 33-43.

Gold, L. W. (1977): "Engineering properties of freshwater ice". *Journal of Glaciology* Vol. 19 (81), pp. 197-212.

Griffith, A.A. (1921): "The Phenomena of Rupture and Flow in Solids". *Philosophical Transactions of the Royal Society of London. Series A, Containing Papers of a Mathematical or Physical Character*, Vol. 221, pp. 163-198.

Hallam, S.D. (1986): "The role of fracture in limiting ice forces". *Proc. IAHR Ice Symp., Iowa City, Iowa, II*: 287-319.

Hovland, A.C. (2012): "ICE MANAGEMENT - how to document reduced actions from managed ice on floating downward conical sloping structures". Master thesis, Norwegian University of Science and Technology. Trondheim.

Hill, R., (1950): "Theory of Plasticity". University Press, Oxford.

Hillerborg, A., Modéer, M., Petersson, P.E. (1976): "Analysis of crack formation and crack growth in concrete by means of fracture mechanics and finite elements". *Cement and Concrete Research*, Vol. 6, pp. 773-782.

Hurdle, B. G. "The Nordic Seas," Springer-Verlag, New York, 1986.

- Irwin, G.R. (1957): "Analysis of stresses and strains near the end of a crack traversing a plate". *Journal of Applied Mechanics*, Vol. 24, pp. 361–364.
- ISO 19906 (2010): "Petroleum and natural gas industries — Arctic offshore structures". International Organization for Standardization.
- Kennedy, F. E., Schulson, E. M., Jones, D. (2000): "Friction of ice on ice at low sliding velocities". *Philosophical Magazine A*, Vol. 80, No. 5, pp. 1093–1110.
- Kerr, A.D. (1996): "Bearing capacity of floating ice covers subjected to static, moving and oscillatory loads". *Applied Mechanics Reviews*, Vol. 49, No 11, pp. 463-476.
- Konuk, I., Gürtner, A., Yu, S. (2009a): "Study of Dynamic Ice and Cylindrical Structure Interaction by the Cohesive Element Method". *Proceedings of the ASME 2012 20th International Conference on Port and Ocean engineering under Arctic conditions, POAC2009*.
- Konuk, I., Gürtner, A. and Yu, S. (2009b): A cohesive element framework for the analysis of ice- structure interaction problems: Part II – implementation, *OMAE 2009*.
- Kotras, T.V., Baird, A.V. and Naegle, J.N. (1983): "Predicting Ship Performance in Level Ice". *SNAME Transactions*, Vol. 91, pp. 329-349.
- Kovacs, A. (1997): "The bulk salinity of Arctic and Antarctic sea ice versus thickness". *Proc. 16th Int. Conf. Offshore Mechanics and Arctic Engineering*, Yokohama, 13-18 April 1997, Vol. IV, pp. 271-281.
- Kuutti, J., Kolari, K., Marjavaara, P. (2013): "Simulation of ice crushing experiments with cohesive surface methodology". *Cold Regions Science and Technology*, Vol. 92, pp. 17-28.
- Lindseth, S.H. (2012a): "Governing Criteria for Splitting of Level Ice Floes". Report in TKT4511, Norwegian University of Science and Technology. Trondheim.
- Lindseth, S.H. (2012b): "Elasticity in Ice – Litterature Review". Report in AT327, The University Centre at Svalbard. Trondheim.
- Lu, W., Lubbad, R., Løset, S., Høyland, K. (2012a): "Cohesive Zone Method Based Simulations of Ice Wedge Bending: a Comparative Study of Element Erosion, CEM, DEM and XFEM". 21st IAHR International Symposium on Ice, Dalian, China.
- Lu, W., Løset, S., Lubbad, R. (2012b): "Simulating ice-sloping structure interactions with the cohesive element method". *Proceedings of the ASME 2012 31st International Conference on Ocean, Offshore and Arctic Engineering OMAE2012 Volume 6*.
- Lu, W., Lubbad, R., Serre, N., Løset, S. (2013): "A theoretical model investigation of ice and wide sloping structure interactions". *Proceedings of the 22nd International Conference on Port and Ocean Engineering under Arctic Conditions*.
- Lubbad, R. (2011): "Some Aspects of Arctic Offshore Floating Structures". Doctoral thesis at NTNU 2011:9. Norwegian University of Science and Technology, Faculty of Science and Engineering, Department of Civil and Transport Engineering. Trondheim.

Lubbad, R., Løset, S. (2011): "A numerical model for real-time simulation of ship-ice interaction". *Cold Regions Science and Technology*, Vol. 65, pp. 111–127.

Lubbad, R., Løset, S., Lu, W. (2012): "Oden Arctic Technology Cruise 2012 (OATRC 2012): Data Report". SAMCoT_WP5_2012_02, 235 p.

Lubbad, R. (2013): Personal communication based on experience from KV Svalbard and Oden, such as Lubbad et al. (2012). 18.04.2013

Løset, S., K. Shkhinek and K. V. Høyland (1998): "Ice Physics and Mechanics". NTNU, Department of Structural Engineering, Trondheim, 125 p.

Løset, S; Shkhinek, K. N., Gudmestad, O. T., Høyland, K. V. (2006): "Actions from Ice on Arctic Offshore and Coastal Structures". St. Petersburg: Lan

Løset, S. (2012a): Lecture: "Structure and formation of ice". AT-327 (UNIS), 09.10.2012.

Løset, S. (2012b): Lecture: "Ice Mechanics I – Rheology". AT-327 (UNIS), 10.10.2012.

Løset, S. (2012c): Personal communication, 13.11.2012. Improved version of Fig.A.8-3 in ISO19906 (2010).

Løset, S. (2012d): Lecture: "Origin, drift and deterioration of icebergs" AT-327 (UNIS), 12.10.2012.

Løset, S. (2012e): Lecture: "Ice management in Arctic Offshore Operations and Field Developments" AT-327 (UNIS), 15.10.2012.

Metrikin, I., Lu, W., Lubbad, R., Løset, S., Kashafutdinov, M. (2012a): "Numerical simulation of a floater in a broken-ice field – Part I: Model Description". *Proceedings of the ASME 2012 31st International Conference on Ocean, Offshore and Arctic Engineering OMAE2012 Volume 6*.

Metrikin, I., Borzov, A., Lubbad, R., Løset, S. (2012b): "Numerical simulation of a floater in a broken-ice field – Part II: Comparative study of physics engines". *Proceedings of the ASME 2012 31st International Conference on Ocean, Offshore and Arctic Engineering OMAE2012 Volume 6*.

Michel, B., Toussaint, N. (1977): "Mechanisms and theory of indentation of ice plates". *Journal of Glaciology* Vol. 19 (Ž81), pp. 285– 300.

Murat, J.R., Lainey, L.M. (1982): "Some experimental observations on the Poisson's ratio of sea ice." *Cold Regions Science and Technology* 6, pp. 105–113.

Mulmule, S.V. and Dempsey, J.P. (1998): "A Viscoelastic Crack Model for the Fracture of Sea Ice". *Mechanics of Time-Dependent Materials*, Vol. 1, No.8, pp. 331-356.

Mulmule, S.V. and Dempsey, J.P. (1999): "Scale effects in sea ice fracture". *Mechanics of Cohesive-Frictional Materials*, Vol. 4, pp. 505-524.

Nixon, W. A. and E. M. Schulson (1988): "Fracture toughness of ice over a range of grain sizes". *J. Offshore Mech. Arctic Eng.*, 110, pp. 192–196.

- Nixon W.A., Weber, L.J. (1993): "Fatigue Crack Propagation in Fresh Water Ice". U.S. Army Research Office. Iowa.
- INTECSEA and Offshore Magazine (2012): "2012 Survey of Arctic & Cold Region Technology for Offshore Field Development". Poster 103, Offshore 2012.
- Poznyak, I.I., Ionov, B.P (1981): "The division of icebreaker resistance into components". Proceedings of the 6th Ship Technology and Research (STAR) Symposium, SNAME, pp. 249-252. Ottawa.
- Que, N.S., Tin-Loi, F. (2002): "Numerical evaluation of cohesive fracture parameters from a wedge splitting test". Engineering Fracture Mechanics, Vol. 69, pp. 1269-1286.
- Regjeringen (2011): "The High North". Mld.St.7 2011-2012. White paper from the Norwegian Government.
- Renshaw, C.E., Schulson, E. M. (2001): "Universal behavior in compressive failure of brittle materials". Nature, Vol. 412, pp. 897-900.
- Rist, M.A., Sammonds, P.R., Oerter, H., Doake, C.S.M. (2002): "Fracture of Antarctic shelf ice". Journal of geophysical research, Vol. 107. ECV 2 1-13.
- Rossmannith, H.P. (1997): "The struggle for recognition of engineering fracture mechanics". In: H.P. Rossmannith (Ed.), Fracture Research in Retrospect, A.A. Balkema, Rotterdam, Netherlands, 1997, pp. 37-94.
- Sanderson, T. O. J. (1988): "Ice Mechanics – Risks to offshore structures". BP Petroleum Development Ltd, London. Graham and Trotman, London.
- Schulson, E. M. (1990): "The Brittle Compressive Fracture of Ice". Acta Metall. Mater. Vol. 38, No. 10, pp. 1963-1976.
- Schulson, E. M. and Duval P. (2009): "Creep and Fracture of Ice". Cambridge University Press, New York.
- Schulson, E.M. (2012): Lecture: "Fracture toughness of ice". Given at NTNU, 29.10.2012.
- Schwarz, J. and Weeks, W. F. (1977): "Engineering properties of ice", Journal of Glaciology, Vol. 19, No. 81, pp. 49-530.
- Sinha, N. K. (1978): "Rheology of columnar-grained ice". Exp. Mech., 18, 464-470.
- Sinha, N. K. (1983): "Creep Model of Ice for Monotonically Increasing Stress". Cold Regions Science ad Technology, Vol. 8, pp. 25-33.
- Sinha, N. K. (1989): "Elasticity of Natural Types of Polycrystalline Ice". Cold Regions Science ad Technology, Vol. 17, pp. 127-135.
- SNL (2013): "Arktis". Store norske leksikon, 28.02.2013. From: <http://snl.no/Arktis>

Strub-Klein, L., Høyland, K. V. (2012): "Spatial and temporal distributions of level ice properties Experiments and thermo-mechanical analysis". *Cold Regions Science and Technology*, Vol. 71, pp. 11-22.

Sun, C.T. and Jin Z.-H. (2012): "Fracture Mechanics". Academic Press, Boston. ISBN 9780123850010

Tatinclaux, J.C., Hirayama, K.I. (1982): "Determination of the flexural strength and elastic modulus of ice from in situ cantilever-beam tests". *Cold Regions Science and Technology*, Vol. 6, (1), pp. 37-47.

Timco and Frederking (1990, 1991?)

Timco, G.W., Frederking, R.M.W. (1996): "A review of sea ice density". *Cold Regions Science and Technology*, Vol. 24 (1), pp. 1-6.

Timco G. W., Weeks, W. F. (2010): "A review of engineering properties of sea ice". *Cold Regions Science and Technology*, Vol. 60, pp. 107-129.

Valanto, P. (2001): "The resistance of ships in level ice". *SNAME Transactions* vol. 109, pp. 53-83.

Weeks, W.F., Ackley, S.F. (1982): "The Growth, Structure, and Properties of Sea Ice". COLD REGIONS RESEARCH AND ENGINEERING LAB HANOVER NH.

Weeks, W.F., Assur, A., 1967: "The mechanical properties of sea ice". U.S. Army CRREL Monograph II-C3, Hanover, NH, USA.

9.2 Pictures from other sources

Front page photo http://media.snl.no/system/images/499/standard_arktis_israak.jpg

Figure 3-1 a) http://www.lukoil.ru/back/gallery_image.asp?id=1368

Figure 3-1 b) <http://www.shell.com/global/future-energy/meeting-demand/arctic/shell-in-the-arctic.html>

Figure 3-1 c) <http://www.akersolutions.com/en/Global-menu/Projects/technology-segment/Engineering/Floater-designs/White-Rose-FPSO-Meeting-the-harsh-environment-on-the-Grand-Banks/>

Figure 3-1 d) <http://www.tu.no/olje-gass/2009/02/06/sevan-klar-for-arktis>

Figure 3-1 e) <http://www.tu.no/olje-gass/2008/11/11/her-vil-ingen-bore>

Figure 3-1 f) <http://www.offshore-technology.com/projects/shtokman/>

Figure 3-2 <http://www.gso.uri.edu/~dcsmith/page1/page25/assets/Oden%20from%20above.JPG>

Figure 3-3 http://barentsobserver.com/sites/barentsobserver.com/files/styles/grid_8/public/main/articles/tanker.mikhailulyanov28admsh_0.jpg

APPENDIX A Matlab code for unbreakable criterion

Common for the code presented in this appendix is that the main concept of calculation is shown. Several different approaches for plotting of the results were tried, but only those used for development of the criterion itself is shown.

```
%%%%%%%%%%%%%%%%%%%%%%%%%%%%%%%%%%%%%%%%%%%%%%%%%%%%%%%%%%%%%%%%%%%%%%%%%%
%Input variables for rotation, surge, deflection
%version/date: 15.04.2013 inp
%%%%%%%%%%%%%%%%%%%%%%%%%%%%%%%%%%%%%%%%%%%%%%%%%%%%%%%%%%%%%%%%%%%%%%%%%%
h=1.00;           %Thickness of ice floe [m]
L=6;             %Length of floe [m]
W=L;             %Width of floe [m]
g=9.81;          %Acceleration of gravity [m/s2]

rho_i=900;        %Density of sea ice [kg/m3]
rho_w=1025;       %Density of sea water [kg/m3]

my=0.05;         %Ice-ship coefficient of friction
my0=0.50;        %Ice-ice coefficient of friction
Cd=1.00;         %Drag coefficient
Cs=1e-3;         %Skin friction coefficient

E=3e9;           %Young's modulus [Pa]
ny=0.33;         %Poisson's ratio
sig_c=1000e3;    %Compressive strength of ice [Pa]
sig_f=500e3;     %Flexural strength of ice [Pa]
psi=25/180*pi;   %Angle of inclination of ship at design water level (DWL)

r=10;            %Radius of conical structure (ship)
vs=0.65;         %Velocity of ship [m/s] (1m/s=1.94384knots)
%end inp
%%%%%%%%%%%%%%%%%%%%%%%%%%%%%%%%%%%%%%%%%%%%%%%%%%%%%%%%%%%%%%%%%%%%%%%%%%
%%%%%%%%%%%%%%%%%%%%%%%%%%%%%%%%%%%%%%%%%%%%%%%%%%%%%%%%%%%%%%%%%%%%%%%%%%

%%%%%%%%%%%%%%%%%%%%%%%%%%%%%%%%%%%%%%%%%%%%%%%%%%%%%%%%%%%%%%%%%%%%%%%%%%
%Plotting assistant
%version/date: 15.04.2013 plotting
%%%%%%%%%%%%%%%%%%%%%%%%%%%%%%%%%%%%%%%%%%%%%%%%%%%%%%%%%%%%%%%%%%%%%%%%%%
clc
clf
% figure
hold on
surge_time_conical
deflection_time_conical
rotation_time
hold off

st=sprintf('Floe, W=L=%g m, h_{ice}=%g m, V_s=%g m/s',L,h,vs);
title(st)
xlabel('Time [s]')
ylabel('Equivalent horizontal force [MN]')
s1=sprintf('Surge');
s2=sprintf('Deflection');
s3=sprintf('Rotation');
legend(s1,s2,s3,'location','southeast')
axis([0 15 0 1])
%end plotting
%%%%%%%%%%%%%%%%%%%%%%%%%%%%%%%%%%%%%%%%%%%%%%%%%%%%%%%%%%%%%%%%%%%%%%%%%%
%%%%%%%%%%%%%%%%%%%%%%%%%%%%%%%%%%%%%%%%%%%%%%%%%%%%%%%%%%%%%%%%%%%%%%%%%%
```

```

%%%%%%%%%%%%%%%%%%%%%%%%%%%%%%%%%%%%%%%%%%%%%%%%%%%%%%%%%%%%%%%%%%%%%%%%
%Force calculations for surge of floe
%version/date: 08.04.2013 surge_time_conical
%%%%%%%%%%%%%%%%%%%%%%%%%%%%%%%%%%%%%%%%%%%%%%%%%%%%%%%%%%%%%%%%%%%%%%%%
clc
clear all
%Import variables from imp.m
inp

% h=0.5:0.5:1.5; %Height override [m]
% L=5:5:100; %Length override [m]
nh=length(h); %Determining steps
nL=length(L); %Determining steps
h=h';
L=L';
W=L;

time=1;
steps=100000;
dt=time/steps;

t_q=zeros(steps,nL,nh);
u_q=zeros(steps,nL,nh);
du_q=zeros(steps,nL,nh);
ddu_q=zeros(steps,nL,nh);
Fh_q=zeros(steps,nL,nh);
t_max=zeros(nh,nL);

for j=1:nh
    for k=1:nL
        vfc=tan(psi)*h(j); %Full crushing length [m]
        m_i=W(k)*L(k)*h(j)*rho_i; %Mass of ice floe [kg]
        us=zeros(steps,1); %Surge movement of ship
        u=zeros(steps,1); %Surge movement of ice
        du=zeros(steps,1); %Surge velocity of ice
        ddu=zeros(steps,1); %Surge acceleration of ice
        vc=zeros(steps,1); %Crushing length in ice
        Fh=zeros(steps,1); %Horizontal component of ship-ice interaction

force
        Fs=zeros(steps,1); %Skin friction
        Fd=zeros(steps,1); %Drag force
        t=zeros(steps,1); %Time vector

        for i=2:steps
            t(i)=(i)*dt;
            us(i)=vs*(i*dt);
            vc(i)=us(i)-u(i-1);
            WL=(2*sqrt(r^2-(r-vc(i))^2)); %Conical (2*sqrt(r^2-(r-
vc(i))^2))
            if WL>W(k)
                WL=W(k);
            end
            if vc(i)<0
                vc(i)=0;
            end
            if vc(i)<vfc
                Fh(i)=vc(i)*WL*sig_c*tan(psi); %Assumed full contact
            else
                Fh(i)=h(j)*WL*sig_c; %Assumed full contact
            end
        end
    end
end

```



```
        if vc(i)<vc(i-1)
            break
        end
%         Fd(i)=Cd*W(k)*rho_i*h(j)*(du(i))^2;
%         Fs(i)=Cs*rho_w*L(k)*W(k)*du(i);
%         ddu(i)=(Fh(i)-Fs(i)-Fd(i))/m_i;
        ddu(i)=Fh(i)/m_i;
        du(i+1)=du(i)+dt*ddu(i);
        u(i+1)=u(i)+dt*du(i);
    end
    t_max(j,k)=t(i);
    for q=i:steps
        t(q)=(q)*dt;
        du(q)=du(i);
        u(q+1)=u(q)+dt*du(q);
    end
    t_q(:,k,j)=t(1:steps,1);
    u_q(:,k,j)=u(1:steps,1);
    du_q(:,k,j)=du(1:steps,1);
    ddu_q(:,k,j)=ddu(1:steps,1);
    Fh_q(:,k,j)=Fh(1:steps,1);
end
end

max(Fh)
max(du)

%Plot
ps=plot(t,(Fh/1e6));
set(ps,'color','red')

%end surge_time_conical
%%%%%%%%%%%%%%%%%%%%%%%%%%%%%%%%%%%%%%%%%%%%%%%%%%%%%%%%%%%%%%%%%%%%%%%%
%%%%%%%%%%%%%%%%%%%%%%%%%%%%%%%%%%%%%%%%%%%%%%%%%%%%%%%%%%%%%%%%%%%%%%%%
```

```

%%%%%%%%%%%%%%%%%%%%%%%%%%%%%%%%%%%%%%%%%%%%%%%%%%%%%%%%%%%%%%%%%%%%%%%%
%Force calculations for deflection of floe
%version/date: 15.04.2013 deflection_time_conical
%%%%%%%%%%%%%%%%%%%%%%%%%%%%%%%%%%%%%%%%%%%%%%%%%%%%%%%%%%%%%%%%%%%%%%%%

clc
clear all

%Import variables from imp.m
inp

%Initialize vectors
% h=0.5:0.5:1.5; %Height override [m]
% L=5:5:100; %Length override [m]
nh=length(h); %Determining steps
nL=length(L); %Determining steps
h=h';
L=L';
W=L;

qstep=100; %Discretization steps of beam, stress vector
time=6; %Time domain [s]
dt=0.0001; %Time increment [s]
t=0:dt:time; %Time vector
istep=length(t); %Discretization steps of time vector

ms=zeros(nL,1);
t_max=zeros(nh,nL);
M=zeros(qstep);
sig=zeros(qstep,1);
sig_max=zeros(istep,1);
ts=zeros(istep,1);
Fh_v=zeros(istep,1);

%Calculation
K=rho_w*g; %Foundation modulus for Winkler foundation
C=(cos(psi)-my*sin(psi))/(sin(psi)+my*cos(psi));

for j=1:nh
    vfc=tan(psi)*h(j); %Full crushing length [m]
    for k=1:nL
        K=W(j)*rho_w*g;
        l=(3*rho_w*g/(E*h(j)^3))^(1/4);
        s=sin(l*L(k));
        sh=sinh(l*L(k));
        c=cos(l*L(k));
        ch=cosh(l*L(k));
        vc=zeros(istep,1);
        sig_max=0;
        for i=1:istep
            vc(i)=vs*t(i); %Crushing length
            if vc(i)>vfc
                break
            end
            WL=(2*sqrt(r^2-(r-vc(i))^2));%Conical (2*sqrt(r^2-(r-vc(i))^2))
            if WL>W(k)
                WL=W(k);
            end
            Fv=C*WL*sig_c*tan(psi)*vc(i);%Assumed full contact
            M=zeros(qstep,1);
            sig=zeros(qstep,1);
        end
    end
end

```

```

    for q=1:qstep
        x=(q/qstep)*L(k);
        xm=(1-q/qstep)*L(k);
        M(q)=(Fv/l)*(sh*sin(l*x)*sinh(l*xm)-
s*sinh(l*x)*sin(l*xm))/(sh^2-s^2);
        sig(q)=6*M(q)/(W(k)*h(j)^2);
    end
    msig=max(sig);
    if msig>sig_f
        break
    end
    ya=(2*Fv*l/K)*(sh*ch-s*c)/(sh^2-s^2);
    yb=(2*Fv*l/K)*(sh*c-s*ch)/(sh^2-s^2);
    if abs(yb)>(rho_i/rho_w)*h(j);
        break
    end
    ts(i,1)=i*dt;
    sig_max(i)=msig;
    Fh_v(i,1)=Fv/C;
end
rest=i;
for i=rest:istep
    Fh_v(i,1)=Fv/C;
    ts(i,1)=i*dt;
end
ms(k)=max(sig_max);
t_max(j,k)=max(ts);
%     plot(ts,sig_max)
%     hold on
end
end

pd=plot(ts,Fh_v/1e6);
set(pd,'color','blue')
%end deflection_time_conical
%%%%%%%%%%%%%%%%%%%%%%%%%%%%%%%%%%%%%%%%%%%%%%%%%%%%%%%%%%%%%%%%%%%%%%%%
%%%%%%%%%%%%%%%%%%%%%%%%%%%%%%%%%%%%%%%%%%%%%%%%%%%%%%%%%%%%%%%%%%%%%%%%

```

```

%%%%%%%%%%%%%%%%%%%%%%%%%%%%%%%%%%%%%%%%%%%%%%%%%%%%%%%%%%%%%%%%%%%%%%%%
%Valanto force calculations of rotating floe
%version/date: 15.04.2013 rotation_time
%%%%%%%%%%%%%%%%%%%%%%%%%%%%%%%%%%%%%%%%%%%%%%%%%%%%%%%%%%%%%%%%%%%%%%%%

clc
clear all
% clf

%Import variables from imp.m
inp

% h=1;
% L=6;
nh=length(h); %Determining steps
nL=length(L); %Determining steps
h=h';
L=L';
W=L;

dteta=0.001; %Incremental stepwise increase in angle of rotation
teta0=1e-6; %Start angle (non-zero due to instability)
teta=teta0:dteta:psi; %Angle of rotation of the floe
steps=length(teta);

t=zeros(steps,nL,nh);
t_max=zeros(nh,nL);

Cmt=zeros(steps,1);
deg=zeros(steps,1);
F1_h=zeros(steps,1);

for i=1:steps
    Cmt(i)=1/(1-my*tan(psi-teta(i)));
end

for j=1:nh
    for k=1:nL
        %Initialization of vectors
        L1t=zeros(steps,3);
        L1=zeros(steps,1);
        Us=zeros(steps,1); %Movement of ship in horizontal direction
        % Ventilation length (L1)
        WL=W(k); %Representative loading width
        for i=1:steps
            a=tan(teta(i));
            b=3*h(j);
            c=0;
            d=-3*L(k)^2*(rho_i/rho_w)*h(j);
            L1t(i,:)=roots([a b c d]);
            L1z=L1t(i,:);
            L1(i)=max(L1z(L1z == real(L1z)));
            t(i,k,j)=(sin(teta(i))/tan(psi)+1-cos(teta(i)))*L1(i)/vs;
            F1=W(k)*(-
(1/(6*L(k)))*L1(i)^3*rho_w*g*sin(teta(i))+((L1(i)^2)/2)*rho_w*g*sin(teta(i)
)-(L(k)-L1(i))^2/(2*L(k))*rho_i*g*h(j)*cos(teta(i))+(L1(i)/L(k))*(L(k)-
L1(i)/2)*(rho_w-rho_i)*g*h(j)*cos(teta(i)))*Cmt(i);
            F1_max=(sig_c*WL)/(sin(psi)+my*cos(psi))*h(j);
            F1_h(i)=F1*(sin(psi)+my*cos(psi));
            if F1>F1_max
                break

```

```
        end
    end
    rest=i;
    for i=rest:steps
        t(i,k,j)=t(rest,k,j);
    end
    t_max(j,k)=t(i,k,j);
end
end
for i=1:steps
    deg(i)=teta(i)*180/pi;
end

%Plot
% figure
pd=plot(t,F1_h/1e6);
set(pd, 'color', 'green')

%end rotation_time
%%%%%%%%%%%%%%%%%%%%%%%%%%%%%%%%%%%%%%%%%%%%%%%%%%%%%%%%%%%%%%%%%%%%%%%%
%%%%%%%%%%%%%%%%%%%%%%%%%%%%%%%%%%%%%%%%%%%%%%%%%%%%%%%%%%%%%%%%%%%%%%%%
```

```

%%%%%%%%%%%%%%%%%%%%%%%%%%%%%%%%%%%%%%%%%%%%%%%%%%%%%%%%%%%%%%%%%%%%%%%%
%Valanto force calculations of rotating floe
%version/date: 05.04.2013 rotation_initial_and_main
%%%%%%%%%%%%%%%%%%%%%%%%%%%%%%%%%%%%%%%%%%%%%%%%%%%%%%%%%%%%%%%%%%%%%%%%
clc
clear all
%Import variables from imp.m
inp

dteta=0.001;           %Incremental stepwise increase in angle of rotation
teta0=0.0001;         %Start angle (non-zero due to instability)
teta=teta0:dteta:psi; %Angle of rotation of the floe
steps=length(teta);

%Initialization of vectors
L0=zeros(steps,1);
L1t=zeros(steps,3);
L1=zeros(steps,1);
F=zeros(steps,1);
F0=zeros(steps,1);
F1=zeros(steps,1);
Fk=zeros(steps,1);
Cm=zeros(steps,1);
Cpt=zeros(steps,1);
Cmt=zeros(steps,1);
Us=zeros(steps,1); %Movement of ship in horizontal direction

%General expressions and coefficients
Fdp=1.5*(rho_w-rho_i)*g*h*L*(sin(psi)-my*cos(psi));
for i=1:steps
    Cm(i)=sin(teta(i))-my*cos(teta(i));
    Cpt(i)=cos(teta(i))*(my+tan(psi-teta(i)));
    Cmt(i)=1/(1-my*tan(psi-teta(i)));
    deg(i)=teta(i)/pi*180;
end

%% Initial floe rotation
for i=1:steps
    L0_t=L-(1-(rho_i/rho_w))*(h/tan(teta(i)));
    if L0_t<0
        L0(i)=0;
    else
        L0(i)=L0_t;
    end
    F0(i)=((1/(3*L))*(L-L0(i))^3*(rho_w-
rho_i)*g*sin(teta(i))+(L0(i)^2/(2*L))*(L-
L0(i)/3)*rho_w*g*sin(teta(i))+(L0(i)/L)*(L-L0(i)/2)*(rho_w-
rho_i)*g*h*cos(teta(i))+Fdp*sin(psi-teta(i)))*Cmt(i);
end

%% Main floe rotation
for i=1:steps
    a=(1-Cm(i)*Cpt(i)*Cmt(i))*tan(teta(i));
    b=3*(h*(1-Cm(i)*Cpt(i)*Cmt(i))+L*Cm(i)*Cpt(i)*Cmt(i))*tan(teta(i));
    c=6*L*Cm(i)*h*(Cpt(i)*Cmt(i)+sin(teta(i)));
    d=-
3*L^2*(rho_i/rho_w)*h*((1+Cm(i)*Cpt(i)*Cmt(i))+2*Cm(i)*sin(teta(i)))+6*L*Cm
(i)*Fdp/(rho_w*g)*(Cpt(i)*Cmt(i)*sin(psi-teta(i))/cos(teta(i))+cos(psi-
teta(i)));
    L1t(i,:)=roots([a b c d]);
    L1z=L1t(i,:);
end

```

```

L1(i)=max(L1z(L1z == real(L1z)));
F1(i)=(-
(1/(6*L))*L1(i)^3*rho_w*g*sin(teta(i))+((L1(i)^2)/2)*rho_w*g*sin(teta(i))-
(L-L1(i))^2/(2*L)*rho_i*g*h*cos(teta(i))+L1(i)/L*(L-L1(i)/2)*(rho_w-
rho_i)*h*cos(teta(i))+Fdp*sin(psi-teta(i))*Cmt(i);
Fk=F1(i)*(my+tan(psi-teta(i)))-(L-
L1(i))*rho_i*g*h*sin(teta(i))+L1(i)*(rho_w-
rho_i)*g*h*sin(teta(i))+Fdp*cos(psi-teta(i));
if Fk<0
    Cm(i)=0;
    a=(1-Cm(i)*Cpt(i)*Cmt(i))*tan(teta(i));
    b=3*(h*(1-Cm(i)*Cpt(i)*Cmt(i))+L*Cm(i)*Cpt(i)*Cmt(i)*tan(teta(i)));
    c=6*L*Cm(i)*h*(Cpt(i)*Cmt(i)+sin(teta(i)));
    d=-
3*L^2*(rho_i/rho_w)*h*((1+Cm(i)*Cpt(i)*Cmt(i))+2*Cm(i)*sin(teta(i)))+6*L*Cm
(i)*Fdp/(rho_w*g)*(Cpt(i)*Cmt(i)*sin(psi-teta(i))/cos(teta(i))+cos(psi-
teta(i)));
    L1t(i,:)=roots([a b c d]);
    L1z=L1t(i,:);
    L1(i)=max(L1z(L1z == real(L1z)));
    F1(i)=(-
(1/(6*L))*L1(i)^3*rho_w*g*sin(teta(i))+((L1(i)^2)/2)*rho_w*g*sin(teta(i))-
(L-L1(i))^2/(2*L)*rho_i*g*h*cos(teta(i))+L1(i)/L*(L-L1(i)/2)*(rho_w-
rho_i)*g*h*cos(teta(i))+Fdp*sin(psi-teta(i))*Cmt(i);
end
end

%% Results
for i=1:steps
Us(i)=(sin(teta(i))/tan(psi)+1-cos(teta(i)))*L1(i);
End

subplot(2,1,1)
plot(deg,L0,deg,L1)
xlabel('Rotation [deg]')
ylabel('Length of L_0 and L_1 [m]')
title('Length of ventilated side of the floe centre of rotation')
hleg1=legend('L_0','L_1','location','southeast');
subplot(2,1,2)
plot(deg,F0,deg,F1)
xlabel('Rotation [deg]')
ylabel('Force [N]')
title('Ship-ice contact force from initial an main phase of rotation')
hleg2=legend('Initial','Main','location','east');

%end rotation_initial_and_main
%%%%%%%%%%%%%%%%%%%%%%%%%%%%%%%%%%%%%%%%%%%%%%%%%%%%%%%%%%%%%%%%%%%%%%%%

```

APPENDIX B Abaqus user subroutine for non-uniform pressure

The Fortran code below depicts the Abaqus subroutine VDLOAD applied for applying the non-uniformly distributed pressure due to the buoyancy of the submerged part of the floe. It includes also the weight of the floe as it lifts out of the water. Important to notice is the following:

- The coordinates of the base of the floe modelled must be at $z=0$ initiation
- The direction of the gravity is surface normal
- Ventilation is removed by uncommenting the “No ventilation”-code

```
      subroutine vdload (
C Read only (unmodifiable)variables -
      1 nblock, ndim, stepTime, totalTime,
      2 amplitude, curCoords, velocity, dirCos, jltyp, sname,
C Write only (modifiable) variable -
      1 value )
C
      include 'vaba_param.inc'
C
      dimension curCoords(nblock,ndim), velocity(nblock,ndim),
      1 dirCos(nblock,ndim,ndim), value(nblock),Gravity(nblock),
      2 Buoyancy(nblock),Drag(nblock),elastic_foundation(nblock)
      character*80 sname
C
      parameter (roui=920.0,rouw=1025.0,g=9.81,
      1 zero=0.0,thickness=1.0,hd=0.897)
C
      do km = 1, nblock
C tt=-0.5*sign(1.0,velocity(km,3))
C Drag(km)=tt*rouw*velocity(km,3)*velocity(km,3)
      elastic_foundation(km)=zero
      gravity(km)=zero
C Full ventilation
      if (curCoords(km,3).le.hd) then
        elastic_foundation(km)=-1.0*((rouw)*g*(curCoords(km,3)))
      end if
C No ventilation (uncomment if no ventilation should be applied)
C if (curCoords(km,3).le.(hd-thickness)) then
C elastic_foundation(km)=-1.0*(rouw-roui)*g*thickness
C end if
C Gravity
      if (curCoords(km,3).gt.hd) then
        gravity(km)=-1.0*(roui)*g*thickness*dirCos(km,3,3)
      end if
      VALUE(km)=elastic_foundation(km)+gravity(km)
      end do
      return
      end
```


APPENDIX C Matlab code for iterations for unbreakable criterion

The following files were used for calculation of the limiting lengths of the square floes for the unbreakable criterion: stresscalc.m and dcrit.m

```
%Critical length for cantilever part of rotating floe
%version/date: 05.05.2013 stresscalc.m
%%%%%%%%%%%%%%%%%%%%%%%%%%%%%%%%%%%%%%%%%%%%%%%%%%%%%%%%%%%%%%%%%%%%%%%%
% Calculation of stresses in floe
clc
clf
clear all
% close all
hb= [0.3 0.5 0.75 1.0 1.25 1.5 2.0 2.5];
Lsigf= [6.102 7.885 9.661 11.158 12.476 13.668 15.784 17.649];
qpr=1;
%Input variables
L=Lsigf(qpr); %Floe length[m]
W=L; %Floe width [m]
h=hb(qpr); %Floe thickness [m]
g=9.81; %Acceleration of gravity [m/s2]
rho_i=920; %Density of sea ice [kg/m3]
rho_w=1025; %Density of sea water [kg/m3]
E=3e9; %Young's modulus [Pa]
ny=0.33; %Poisson's ratio
sig_c=1000e3; %Compressive strength of ice [Pa]
sig_f=500e3; %Flexural strength of ice [Pa]
%Define discretization
qstep=100;
%Initialize constants
K=W*rho_w*g;
l=(3*rho_w*g/(E*h^3))^(1/4);
lambda=l;
s=sin(l*L);
sh=sinh(l*L);
c=cos(l*L);
ch=cosh(l*L);
yb=(rho_i/rho_w)*h;
Fv=(yb*K)/(2*l)*(sh^2-s^2)/(sh*c-s*ch);
%Calculate stresses along beam
for q=1:qstep
    x(q)=(q/qstep)*L;
    xm=(1-q/qstep)*L;
    M(q)=-(Fv/l)*(sh*sin(l*x(q))*sinh(l*xm)-s*sinh(l*x(q))*sin(l*xm))...
        /(sh^2-s^2);
    sig(q)=6*M(q)/(W*h^2);
end
msig=max(sig);
msig/sig_f*100
yb=(2*Fv*l/K)*(sh*c-s*ch)/(sh^2-s^2)
hb(qpr)
Lsigf(qpr)
%Define line for flexural capacity
tx=0:L:L;
ty=[sig_f sig_f];
%Plot stress curve
plot(x,sig,tx,ty)
xlabel('coordinate along floe x-axis [m]')
ylabel('Flexural stress [Pa]')
axis([0 L 0 6e5])
%%% end stresscalc.m
%%%%%%%%%%%%%%%%%%%%%%%%%%%%%%%%%%%%%%%%%%%%%%%%%%%%%%%%%%%%%%%%%%%%%%%%
```

```

%%%%%%%%%%%%%%%%%%%%%%%%%%%%%%%%%%%%%%%%%%%%%%%%%%%%%%%%%%%%%%%%%%%%%%%%
%Critical length for cantilever part of rotating floe
%version/date: 05.05.2013 dcrit.m
%%%%%%%%%%%%%%%%%%%%%%%%%%%%%%%%%%%%%%%%%%%%%%%%%%%%%%%%%%%%%%%%%%%%%%%%
clc
clear all
hb= [0.3 0.5 0.75 1.0 1.25 1.5 2.0 2.5];
Lrot= [5.39 7.34 9.40 11.21 12.85 14.40 17.19 19.80];
Lcrb= [3.0387 4.2973 5.2631 6.0773 6.7946]
%Import variables from imp.m
L=19.80; %Floe length[m]
W=L; %Floe width [m]
h=2.5; %Floe thickness [m]
g=9.81; %Acceleration of gravity [m/s2]
rho_i=920; %Density of sea ice [kg/m3]
rho_w=1025; %Density of sea water [kg/m3]
E=3e9; %Young's modulus [Pa]
ny=0.33; %Poisson's ratio
sig_c=1000e3; %Compressive strength of ice [Pa]
sig_f=500e3; %Flexural strength of ice [Pa]
psi=45/180*3.14;%Ship hull inclination angle
my=0.05;
my0=0.5;
dteta=0.001; %Incremental stepwise increase in angle of rotation
teta0=0.0001; %Start angle (non-zero due to instability)
teta=teta0:dteta:psi; %Angle of rotation of the floe
steps=length(teta);
%Initialization of vectors
L0=zeros(steps,1);
L1t=zeros(steps,3);
L1=zeros(steps,1);
% dcr=zeros(steps,1);
F=zeros(steps,1);
F0=zeros(steps,1);
F1=zeros(steps,1);
Fk=zeros(steps,1);
Cm=zeros(steps,1);
Cpt=zeros(steps,1);
Cmt=zeros(steps,1);
Us=zeros(steps,1); %Movement of ship in horizontal direction
%General expressions and coefficients
Fdp=1.5*(rho_w-rho_i)*g*h*L*(sin(psi)-my*cos(psi));
for i=1:steps
    Cm(i)=sin(teta(i))-my0*cos(teta(i));
    Cpt(i)=cos(teta(i))*(my+tan(psi-teta(i)));
    Cmt(i)=1/(1-my*tan(psi-teta(i)));
    deg(i)=teta(i)/pi*180;
end
%% Initial floe rotation
for i=1:steps
    L0_t=L-(1-(rho_i/rho_w))*(h/tan(teta(i)));
    if L0_t<0
        L0(i)=0;
    else
        L0(i)=L0_t;
    end
    F0(i)=((1/(3*L))*(L-L0(i))^3*(rho_w-rho_i)*g*sin(teta(i))+...
        (L0(i)^2/(2*L))*(L-L0(i)/3)*rho_w*g*sin(teta(i))+(L0(i)/L)*...
        (L-L0(i)/2)*(rho_w-rho_i)*g*h*cos(teta(i))...
        +Fdp*sin(psi-teta(i)))*Cmt(i);
end

```

```

%% Main floe rotation
for i=1:steps
    a=(1-Cm(i)*Cpt(i)*Cmt(i))*tan(teta(i));
    b=3*(h*(1-Cm(i)*Cpt(i)*Cmt(i))+L*Cm(i)*Cpt(i)*Cmt(i)*tan(teta(i)));
    c=6*L*Cm(i)*h*(Cpt(i)*Cmt(i)+sin(teta(i)));
    d=-3*L^2*(rho_i/rho_w)*h*((1+Cm(i)*Cpt(i)*Cmt(i))+2*Cm(i)...
        *sin(teta(i)))+6*L*Cm(i)*Fdp/(rho_w*g)*(Cpt(i)...
        *Cmt(i)*sin(psi-teta(i))/cos(teta(i))+cos(psi-teta(i)));
    L1t(i,:)=roots([a b c d]);
    L1z=L1t(i,:);
    L1(i)=max(L1z(L1z == real(L1z)));
    F1(i)=(-(1/(6*L))*L1(i)^3*rho_w*g*sin(teta(i))+...
        ((L1(i)^2)/2)*rho_w*g*sin(teta(i))-(L-L1(i))^2/(2*L)...
        *rho_i*g*h*cos(teta(i))+(L1(i)/L)*(L-L1(i)/2)*...
        (rho_w-rho_i)*h*cos(teta(i))+Fdp*sin(psi-teta(i)))*Cmt(i);
    Fk=F1(i)*(my+tan(psi-teta(i)))-(L-L1(i))*rho_i*g*h*sin(teta(i))...
        +L1(i)*(rho_w-rho_i)*g*h*sin(teta(i))+Fdp*cos(psi-teta(i));
    if Fk<0
        Cm(i)=0;
        a=(1-Cm(i)*Cpt(i)*Cmt(i))*tan(teta(i));
        b=3*(h*(1-Cm(i)*Cpt(i)*Cmt(i))+L*Cm(i)*Cpt(i)*Cmt(i)*tan(teta(i)));
        c=6*L*Cm(i)*h*(Cpt(i)*Cmt(i)+sin(teta(i)));
        d=-3*L^2*(rho_i/rho_w)*h*((1+Cm(i)*Cpt(i)*Cmt(i))...
            +2*Cm(i)*sin(teta(i)))+6*L*Cm(i)*Fdp/(rho_w*g)*...
            (Cpt(i)*Cmt(i)*sin(psi-teta(i))/cos(teta(i))...
            +cos(psi-teta(i)));
        L1t(i,:)=roots([a b c d]);
        L1z=L1t(i,:);
        L1(i)=max(L1z(L1z == real(L1z)));
        F1(i)=(-(1/(6*L))*L1(i)^3*rho_w*g*sin(teta(i))...
            +((L1(i)^2)/2)*rho_w*g*sin(teta(i))-(L-L1(i))^2/(2*L)...
            *rho_i*g*h*cos(teta(i))+(L1(i)/L)*(L-L1(i)/2)*(rho_w-rho_i)...
            *g*h*cos(teta(i))+Fdp*sin(psi-teta(i)))*Cmt(i);
    end
    dcr(i)=sqrt(sig_f*h/(3*rho_i*g*cos(teta(i))));
end
%% Results
for i=1:steps
    Us(i)=(sin(teta(i))/tan(psi)+1-cos(teta(i)))*L1(i);
end
i=1;
while L1(i)>L0(i)
    F(i)=F0(i);
    i=i+1;
end
while i<steps
    F(i)=F1(i);
    i=i+1;
end
F(steps)=F1(steps);
d=L-L1;
for i=1:steps
    if d(i)<0
        d(i)=0;
    end
end
end
plot(deg,d,deg,dcr)
xlabel('Angle of rotation of floe [deg]')
ylabel('Length of cantilever [m]')
legend('d', 'd_{cr}', 'location', 'east')

```

APPENDIX D Matlab code for beam type behaviour of floe

```

%%%%%%%%%%%%%%%%%%%%%%%%%%%%%%%%%%%%%%%%%%%%%%%%%%%%%%%%%%%%%%%%%%%%%%%%
%Input variables for rotation, surge, deflection
%version/date: 08.04.2013 inp
%%%%%%%%%%%%%%%%%%%%%%%%%%%%%%%%%%%%%%%%%%%%%%%%%%%%%%%%%%%%%%%%%%%%%%%%

clc

% h=1.00;           %Thickness of ice floe [m]
% L=100;           %Length of floe [m]
% W=L;            %Width of floe [m]

g=9.81;           %Acceleration of gravity [m/s2]
rho_i=900;        %Density of sea ice [kg/m3]
rho_w=1025;       %Density of sea water [kg/m3]
psi=45/180*pi;   %Angle of inclination of ship at design water level (DWL)
my=0.05;         %Ice-ship coefficient of friction
my0=0.50;        %Ice-ice coefficient of friction
E=3e9;           %Young's modulus [Pa]
ny=0.33;         %Poisson's ratio
sig_c=1000e3;    %Compressive strength of ice [Pa]
sig_f=500e3;     %Flexural strength of ice [Pa]

r=10;            %Radius of conical structure (ship)

%end inp
%%%%%%%%%%%%%%%%%%%%%%%%%%%%%%%%%%%%%%%%%%%%%%%%%%%%%%%%%%%%%%%%%%%%%%%%

%%%%%%%%%%%%%%%%%%%%%%%%%%%%%%%%%%%%%%%%%%%%%%%%%%%%%%%%%%%%%%%%%%%%%%%%
%Deflection pattern of edge loaded beam (Hetenyi, 1946)
%version/date: 19.04.2013 beam_deflection
%%%%%%%%%%%%%%%%%%%%%%%%%%%%%%%%%%%%%%%%%%%%%%%%%%%%%%%%%%%%%%%%%%%%%%%%

clc
clear all

%Import variables from imp.m
inp
h=0.50;          %Thickness of ice floe [m]
L=3;
% L=10:10:100;   %Length of floe [m]
W=1;            %Beam width

%Initialize vectors
nh=length(h);   %Determining steps
nL=length(L);   %Determining steps
h=h';
L=L';

qstep=1000;     %Discretization steps of beam, stress vector
M=zeros(qstep);
sig=zeros(qstep,1);

%Calculation
K=rho_w*g;      %Foundation modulus for Winkler foundation
C=(cos(psi)-my*sin(psi))/(sin(psi)+my*cos(psi));

Fv=10e3;

```

```

for j=1:nh
    vfc=tan(psi)*h(j); %Full crushing length [m]
    for k=1:nL
        K=W(j)*rho_w*g;
        l=(3*rho_w*g/(E*h(j)^3))^(1/4);
        s=sin(l*L(k));
        sh=sinh(l*L(k));
        c=cos(l*L(k));
        ch=cosh(l*L(k));
        M=zeros(qstep,1);
        sig=zeros(qstep,1);
        for q=1:qstep
            x(q)=(q/qstep)*L(k);
            xm=(1-q/qstep)*L(k);
            M(q)=(Fv/l)*(sh*sin(l*x(q))*sinh(l*xm)-
s*sinh(l*x(q))*sin(l*xm))/(sh^2-s^2);
            sig(q)=6*M(q)/(W*h(j)^2);
        end
        sigmax(j,k)=max(sig);
        ya(j,k)=(2*Fv*l/K)*(sh*ch-s*c)/(sh^2-s^2);
        yb(j,k)=(2*Fv*l/K)*(sh*c-s*ch)/(sh^2-s^2);
    end
end

for i=1:qstep
    if sig(i)==max(sig)
        break
    end
end
sigmax/1000
x(i)

str=sprintf('Flexural stresses along %g m beam for F_v=%g kN',L,Fv/1000);
plot(x,sig/1000)
title(str)
xlabel('x-coordinate of beam [m]')
ylabel('Flexural stress in beam [kPa]')

%end beam_deflection
%%%%%%%%%%%%%%%%%%%%%%%%%%%%%%%%%%%%%%%%%%%%%%%%%%%%%%%%%%%%%%%%%%%%%%%%

```

APPENDIX E Cohesive element crack propagation for $L=W=10\text{m}$, $h_{ice}=1\text{m}$

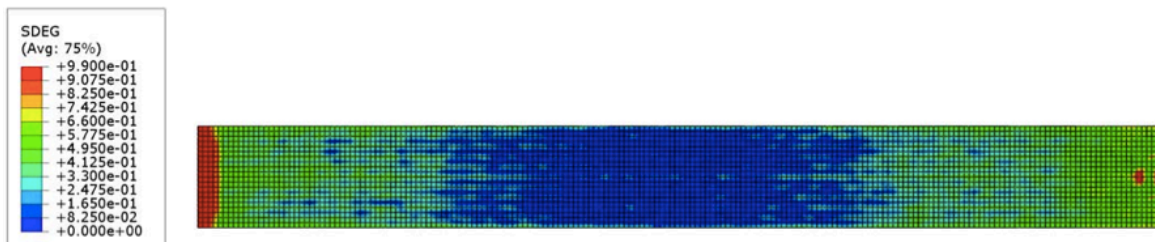
The figures present in this appendix shows the degradation of the cohesive elements for varying magnitude of the applied load (P_{Sc}) for the results shown in Table 7-4.



z
x

ODB: LEFM-L10h1-170.odb Abaqus/Explicit 6.12-1 Mon May 27 10:23:16 Vest-Europa (sommertid) 2013
Step: Step-1
Increment 270: Step Time = 7.0152E-03
Primary Var: SDEG
Deformed Var: U Deformation Scale Factor: +1.000e+00

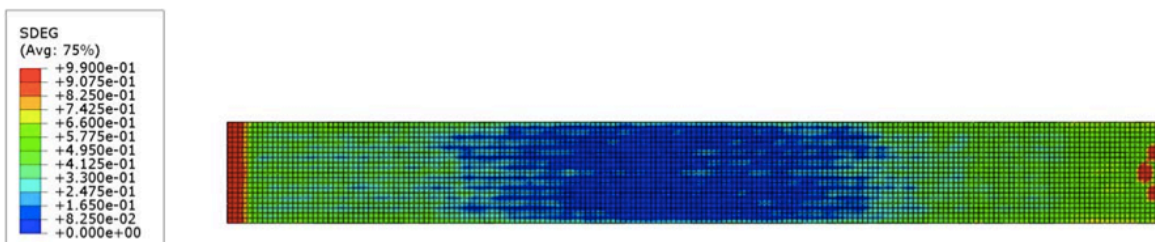
Stable crack at $t=0.007$ s, for $P_{Sc}=170$ kN



z
x

ODB: LEFM-L10h1-180.odb Abaqus/Explicit 6.12-1 Mon May 27 10:03:54 Vest-Europa (sommertid) 2013
Step: Step-1
Increment 1650: Step Time = 4.3005E-02
Primary Var: SDEG
Deformed Var: U Deformation Scale Factor: +1.000e+00

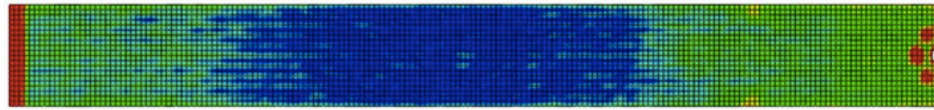
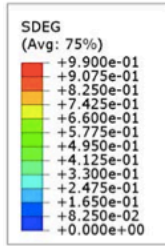
Stable crack at $t=0.043$ s, for $P_{Sc}=180$ kN



z
x

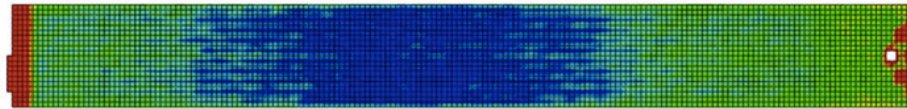
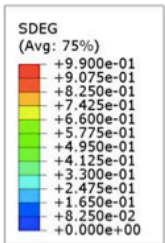
ODB: LEFM-L10h1-190.odb Abaqus/Explicit 6.12-1 Mon May 27 09:48:30 Vest-Europa (sommertid) 2013
Step: Step-1
Increment 3376: Step Time = 8.8017E-02
Primary Var: SDEG
Deformed Var: U Deformation Scale Factor: +1.000e+00

Stable crack at $t=0.088$ s, for $P_{Sc}=190$ kN



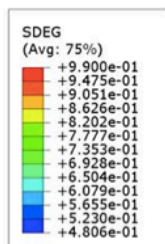
ODB: LEFM-L10h1-200.odb Abaqus/Explicit 6.12-1 Sun May 26 19:15:16 Vest-Europa (sommertid) 2013
Step: Step-1
Increment 2954: Step Time = 7.7012E-02
Primary Var: SDEG
Deformed Var: U Deformation Scale Factor: +1.000e+00

Stable crack at $t=0.077$ s, for $P_{sc}=200$ kN



ODB: LEFM-L10h1-210.odb Abaqus/Explicit 6.12-1 Mon May 27 07:40:27 Vest-Europa (sommertid) 2013
Step: Step-1
Increment 4986: Step Time = 0.1300
Primary Var: SDEG
Deformed Var: U Deformation Scale Factor: +1.000e+00

Stable crack at $t=0.130$ s, for $P_{sc}=210$ kN



ODB: LEFM-L10h1-220.odb Abaqus/Explicit 6.12-1 Sun May 26 19:51:55 Vest-Europa (sommertid) 2013
Step: Step-1
Increment 5102: Step Time = 0.1330
Primary Var: SDEG
Deformed Var: U Deformation Scale Factor: +1.000e+00

Complete splitting at $t=0.133$ s, for $P_{sc}=180$ kN